Extensive review about industrial and laboratory dynamic filtration modules: Scientific production, configurations and performances

Ming Cheng, Xiaomin Xie, Philippe Schmitz, Luc Fillaudeau

EXTENSIVE REVIEW ABOUT INDUSTRIAL AND LABORATORY DYNAMIC FILTRATION MODULES: SCIENTIFIC PRODUCTION, CONFIGURATIONS AND PERFORMANCES

CHENG Ming[1*], XIE Xiaomin[2,3], SCHMITZ Philippe[1,4] and FILLAUDEAU Luc[1,4*]

[1]TBI, Université de Toulouse, CNRS UMR5504, INRA UMR792, INSA, 135, avenue de Rangueil, 31077, Toulouse, France

[2]Guangdong Midea White Home Appliance Technology Innovation Centre Co. Ltd. Foshan 528311, China

[3]Institute of Environmental & Ecological Engineering, School of Environmental Science of Engineering, Guangdong University of Technology, Guangzhou 510006, China

[4]FERMAT, Université de Toulouse, CNRS, INPT, INSA, UPS, 4 Allee Emile Monso, 31432 Toulouse, France

Abstract: By maintaining a high shear rate, dynamic filtration (DF) provides excellent performances in controlling fouling and improving flux during filtration. Many DF devices comprising a mechanical movement generated by the rotation, oscillation and/or vibration of one element have been developed. Based on the bibliometric analysis, new applications and technologies related to DF have become the new research hotspots. Major applications were reported in food processing, water treatment and bioprocess engineering. With a precise definition of the concepts of oscillation and vibration, 55 DF modules have been classified into 15 different types according to movement and shape (filtration cell, membrane, impeller, disk…). But it appears that it remains a great challenge to complete the knowledge on the flow of fluid inside DF modules because of their complex geometries. Global, semi-local and local investigation of hydrodynamics have been detailed. They not only make it possible to estimate performances but also to help to calculate energy consumption according to operating conditions. This review presents the main characteristics of DF devices and existing applications. These empirical results are already beneficial for the selection of DF devices for a dedicated application. However, a better understanding of local and temporal variations in pressure and shear stress is still necessary to refine the choice of a device and the operating conditions. The overarching aims propose to report the main criteria that will help engineers select the DF module or identify the scientific and/or technological bottlenecks about hydrodynamics or applications.

Keywords: Dynamic filtration; Bibliography analysis; Hydrodynamics; Shear rate; Power consumption

Corresponding author at: Toulouse Biotechnology Institute, Bio & Chemical Engineering (TBI), Université de Toulouse, CNRS, INRAE, INSA, 135 avenue de Rangueil, 31077 Toulouse CEDEX 04, France

E-mail: cheng@insa-toulouse.fr (CHENG Ming); luc.fillaudeau@insa-toulouse.fr (Fillaudeau Luc)

Highlights:

- Bibliography overview of dynamic filtration (application, research items, trends and stakeholders)
- Classification and specification of laboratory and industrial dynamic filtration modules
- Global, local and instantaneous characterizations of fluid flow
- Main criteria to select dynamic filtration modules (critical conditions, performances, power).

Table of contents

1. Introduction 14

1.1 Conventional dead-end filtration and cross-flow filtration 14

1.2 Dynamic filtration 15

2. Scientific production related to dynamic filtration 17

2.1 Quantitative analysis 17

2.1.1 Scope of journals and research areas 18

2.1.2 Research institutions and scientific cooperation 19

2.1.3 Identification of research items 20

2.2 Qualitative analysis 22

2.2.1 Water treatment 23

2.2.2 Food processing 24

2.2.3 Bioprocess engineering 24

3. Specifications of Laboratory and Industrial Dynamic Filtration Modules 26

3.1 Classification of dynamic filtration modules 26

3.2 Rotating systems 32

3.2.1 Rotating membrane modules 32

3.2.2 Rotating mechanical device module 36

3.2.3 Rotating disk and membrane module 40

3.3 Oscillating system 41

3.3.1 Oscillating filtration cell modules 41

3.3.2 Oscillating membrane module 43

3.3.3 Oscillating spacers module 45

3.4 Oscillating and vibrating system 45

4. Characterization of fluid flow in dynamic filtration 48

4.1 Global approaches 48

4.1.1 Dimensionless analysis 48

4.1.2 Friction and power consumption curves 51

4.2 Semi-local approaches 52

4.2.1 Radial pressure and core velocity coefficient 52

4.2.2 Shear rate and shear stress 56

4.3 Local approaches 60
4.3.1 Local velocity and shear stress 60
4.4 Computational Fluid Dynamics (CFD) 61
5. Discussion 63
5.1 Energy demand associated with DF module 63
5.1.1 Mechanical power 64
5.1.2 Pumping power 64
5.1.3 Specific energy demand 65
5.2 Specifications and decision tree for DF application 67
6. Conclusion 70
7. Acknowledgement 71

List of figures

Fig. 1 Comparison between Dead-end filtration (DEF), Cross-flow filtration (CFF) and dynamic filtration (DF). 15
Fig. 2 Number of publications and citations per year (Source: Core Collection-WoS (Thomson-Reuter), period: 1991 to 2020) 18
Fig. 3 Institutions cooperation network 20
Fig. 4 Keywords co-occurrence network 20
Fig. 5 Distribution map of keywords and nodes time-zone associated with DF 22
Fig. 6 Application fields and filtration type associated with dynamic filtration 23
Fig. 7 Friction curve established with RVF lab-scale module [193] 52
Fig. 8 Power consumption curve established with RVF lab-scale module [193] 52
Fig. 9 Determination of hydrodynamic performances, evolution of the radial pressure distribution versus the radius and the rotational speed [193] 53
Fig. 10 Evolution of core velocity coefficient, $K\theta$ as a function of gap-to-radius ratio, z/Rm. Values are reported from literature for DF modules using confined rotating impeller close to the membrane and established under laminar or turbulent regimes [195] 55
Fig. 11 Filtration modes, (a). Single-pass continuous filtration (b). Continuous filtration with partial retentate recycle (Feed & Bleed) 64
Fig. 12 Main criteria and knowledge gap in DF application 68

List of tables

Table. 1 Top 5 most productive journals considering the number of articles and citations (source: WoS)...18
Table. 2 Top 9 most productive institutions (source: WoS) 19
Table. 3 Clusters of research hotspots 21
Table. 4 Top 10 keywords with the strongest citation bursts 21
Table. 5 Classification of DF modules according to the movement and shape 26
Table. 6 Classification and specification of DF modules (d: membrane diameter, S: membrane surface area, N/F: maximum rotating, vibrating and/or oscillating speed/ frequency, A: amplitude, displacement or vibrating angle, TMP: maximum operating transmembrane pressure)....27
Table. 7 Dimensionless numbers used to describe hydrodynamic within Dynamic Filtration device (d: diameter, u: velocity, Q: flowrate, r: radius, d_h: hydraulic diameter, r_h: hydraulic radius, d_o: outer diameter; d_i: inner diameter, u_z, axial flow velocity, N: mixing rate, d_m: rotor diameter, k: core velocity coefficient, ω: angular velocity, h: rotor height, α: inclination angle of conical rotor, s: characteristic length scale, F: oscillating/ vibrating frequency, H: vertical distance)....48
Table. 8 Four flow pattern in rotating system....49
Table. 9 Core velocity coefficient of different DF filters 55
Table. 10 Shear rate of four flow regimes in a rotation system....57
Table. 11 Specific energy demand in different modules 66
Table. 12 Resume of available data about hydrodynamics and applications with the different type of DF module (n.a: not available)....68

Equations

Eq. 1 48
Eq. 2 48
Eq. 3 48
Eq. 4 48
Eq. 5 48
Eq. 6 49
Eq. 7 49
Eq. 8 49
Eq. 9 49
Eq. 10 51
Eq. 11 51
Eq. 12 51
Eq. 13 51
Eq. 14 52
Eq. 15 53
Eq. 16 53
Eq. 17 53
Eq. 18 53
Eq. 19 57
Eq. 20 57
Eq. 21 57
Eq. 22 57
Eq. 23 57
Eq. 24 57
Eq. 25 57
Eq. 26 57
Eq. 27 57
Eq. 28 57
Eq. 29 58
Eq. 30 58
Eq. 31 58
Eq. 32 58
Eq. 33 58
Eq. 34 58
Eq. 35 58
Eq. 36 58

Eq. 37 59
Eq. 38 59
Eq. 39 59
Eq. 40 59
Eq. 41 59
Eq. 42 59
Eq. 43 59
Eq. 44 63
Eq. 45 64
Eq. 46 64
Eq. 47 65
Eq. 48 65
Eq. 49 65
Eq. 50 66

192

Nomenclature

Abbreviation		
AVM	axial vibration membrane	
BDF	biodruck-filter	
BOD	biological oxygen demand	
BSA	bovine serum albumin	
CAPEX	capital expenditure	
CFD	computational fluid dynamics	
CFF	cross-flow filtration	
COD	chemical oxygen demand	
CP	concentration polarization	
CR	cross rotational	
CRD	compact rotating disc filter	
CRDM	retentate recycling process	
CSAF	controlled shear affinity filtration	
CSF	controlled shear filtration	
CTF	Couette-Taylor flow	
DCF	dynamic cross-flow filter	
DCF	dynamic cross-flow filtration	
DEF	dead-end filtration	
DF	dynamic filtration	
DMF	dynamic membrane filter	
DRDM	retentate non-recycling process	
FMX	anti-fouling membrane unit	
HF	hollow fibre	
HSR-MS	high shear rotary membrane system	
IREC	Catalonia Institute for Energy Research	
ISBM	intermeshed spinning basket membrane	
LDV	laser doppler velocimetry	
LLR	Log-likelihood Ratio	
MBR	membrane bioreactors	
MF	microfiltration	
MMV	magnetically induced membrane vibration	
MSD	multi-shaft disk	
MSDF	modular span disk filtration	
MTV	molecular tagging velocimetry	
NF	nanofiltration	
OFSM	oscillatory flat surface membrane	
OPEX	operational expenditure	

PAAS	poly acrylic acid sodium	
PIV	particle image velocimetry	
PMA	copolymer of maleic acid and acrylic acid	
PMMA	polymethyl methacrylate	
PTV	particle tracking velocimetry	
RCF	rotating cross-flow	
RDM	rotating disk module	
RD-M	rotating disk-membrane	
RD-M	rotating disk-membrane	
R-HFM	rotating hollow fibre membrane	
RO	reverse osmosis	
RVF	rotating and vibrating filtration	
SBM	spinning basket membrane	
SBR	styrene butadiene rubber	
SS	single stirred	
SSDF	signal shaft disk filter	
TMP	transmembrane pressure	
UF	ultrafiltration	
UHT	ultra-high temperature processing	
URV	Rovira Virgili University	
USVM	uniform shearing vibration membrane	
UTC	University of Technology of Compiègne	
VCF	volume concentration factor	
VERO	vibration enhanced reverse osmosis	
VHM	vibrating hollow fibre microfiltration	
VMBR	vibrating membrane bioreactor	
VMF	vibrating membrane filtration	
VRM	vacuum rotation membrane	
VSEP	vibratory shear enhanced processing	
WoS	web of science	
Latin letter		
A	amplitude	m
a, b	numerical constants	/
D	diffusion coefficient	m^2/s
d	diameter	m
d_h	hydraulic diameter	m
d_i	inner diameter	m
d_m	rotor diameter	m

d_o	outer diameter	m
Da	Darcy number	/
E	Specific energy demand	kWh/m^3
Ek	Ekman number	/
F	oscillating/ vibrating frequency	Hz
f	velocity factor, friction factor	/
H	vertical distance	m
h	rotor height	m
I	tension	A
J	Flux	m/s
Jss	steady-state flux	m/s
k	core velocity coefficient	/
k_m	transfer coefficient	/
L	channel length	m
L_p	permeability	$m/(s \cdot Pa)$
N	mixing rate	Hz
N_p	Power number	/
P	power consumption	W
P_M	mechanical power	W
P_P	pumping power	W
P_T	total power	W
P_{in}	inlet pressure	Pa
P_{out}	outlet pressure	Pa
P_p	permeate pressure	Pa
Δp	pressure drop	Pa
ΔP	transmembrane pressure	Pa
ΔP_{ag}	additional pressure	Pa
Q	flowrate	m^3/s
Q_c	circulation flowrate	m^3/s
Q_f	feeding flowrate	m^3/s
Q_p	permeate flowrate	m^3/s
Q_r	retentate flowrate	m^3/s
r	radius	m
R_h	hydraulic resistance	m^{-1}
R_m	rotor radius	m
r_h	hydraulic radius	m

r_i	inner radius	m
r_o	outer radius	m
Re	Reynolds number	/
Re_a	Reynolds number for axial flow in annulus	/
Re_m	Reynolds number for mixing	/
Re_Q	Reynolds number in the tube	/
Re_r	Reynolds number in rotating system	/
Re_s	Reynolds number for rotating cone	/
Re_v	Reynolds number in oscillating/ vibrating system	/
S	membrane surface area	m^2
s	characteristic length scale	m
Sh	Sherwood number	/
Sc	Schmidt number	/
T	period	Hz
t	time	s
Δt	time interval	s
Ta	Taylor number	/
U	current	V
u	velocity	m/s
u_z	axial flow velocity	m/s
v	kinematic viscosity	m^2/s
v_0	amplitude of velocity	m
y	gap	m
z	gap between rotor and membrane, or between two cylinders	m
Greek letter		
α	inclination angle	°
γ	shear rate	s^{-1}
γ_R	shear rate at rotor surface	s^{-1}
γ_S	shear rate at membrane surface	s^{-1}
δ	limiting layer thickness	m
μ	dynamic viscosity	Pa.s
μ_p	permeate viscosity	Pa.s
ρ	density	kg/m^3
τ	shear stress	Pa
ω	angular velocity	rad/s

η	mechanical efficiency	/

193

194

1. INTRODUCTION

Membrane separation technology has become widely used in the bioprocess and food processing industry (dairy, juice, wine, water) [1, 2]. Among three-phase reactors, membrane bioreactors (MBR) appeared in the 70s and were primarily applied in the biotechnology field: white biotechnology, pharmaceutical and food industries [2-4]. However, membrane processes are yet to identify as an industrial alternative by users. The choice of membrane process is a multi-criteria and fundamental approach including diversities of (i) mass transfer processes (from electro-dialysis up to microfiltration), (ii) the geometry of module (plane, filter-press, tubular, spiral wound, hollow fibre), (iii) the nature of membrane (mean pore diameter and associated distribution/chemical nature: organic, mineral, metal, composite) and (iv) the operating mode (dead-end, cross-flow or dynamic filtration) and technology dedicated to fouling limitation (co-current, back-filtration, back-shock, back-flush,…). The overarching aim is to improve qualitative and quantitative performances of separation processes, in other terms, their intensification and efficiency in biological, chemical, and food processes. Retention could be described by mechanical and/or physico-chemical retention, but the mechanisms of retention result from a complex balance between the local hydrodynamic conditions, the product, the nature and the membrane cut-off.

1.1 Conventional dead-end filtration and cross-flow filtration

In conventional dead-end filtration (DEF) (Fig. 1), the feeding flux is perpendicular to the permeation, and the fouling will accumulate at the membrane surface. Transmembrane pressure (TMP) increases with the formation of the cake layer, resulting in lower filtration efficiency. Cross-flow filtration (CFF), also known as tangential flow filtration, was typically designed to reduce the impact of fouling by applying a tangential feeding flow passing over the membrane and remove some of the deposits from the surface. Increasing feeding flowrate is one of the conventional ways to enhance performances in CFF. However, energy consumption rapidly increases with pumping power, which is proportional to the cube of flowrate in a turbulent flow regime [5].

A large number of hydrodynamic techniques has been proposed to limit or manage fouling by modifying dead-end and cross-flow filtration modules to improve the performances. The main technologies are introduced below:

- The periodic shutdown of transmembrane pressure [6, 7];
- Co-current operation (homogeneity of TMP along with the diaphragm) [8];
- Reversal of the permeation flow (backflush) [9];
- The back-shock process (periodic inversion of the permeate flow, effective backflush time of less than 0.1 s) [10];
- Cleaning by generating non-stationarity in the tangential flow: generation of Dean or Taylor vortices [11-13], installation of static turbulence promoters such as baffled channel or stamped membrane [14, 15], pulsed flow [16], generation of two-phase flow (gas-liquid, liquid-solid) [17], ultrasound [18].

Although the impressive results to control fouling with these methods, the performance limitation of previous configurations and operating modes lead engineers and researchers to propose an alternative named Dynamic filtration (DF).

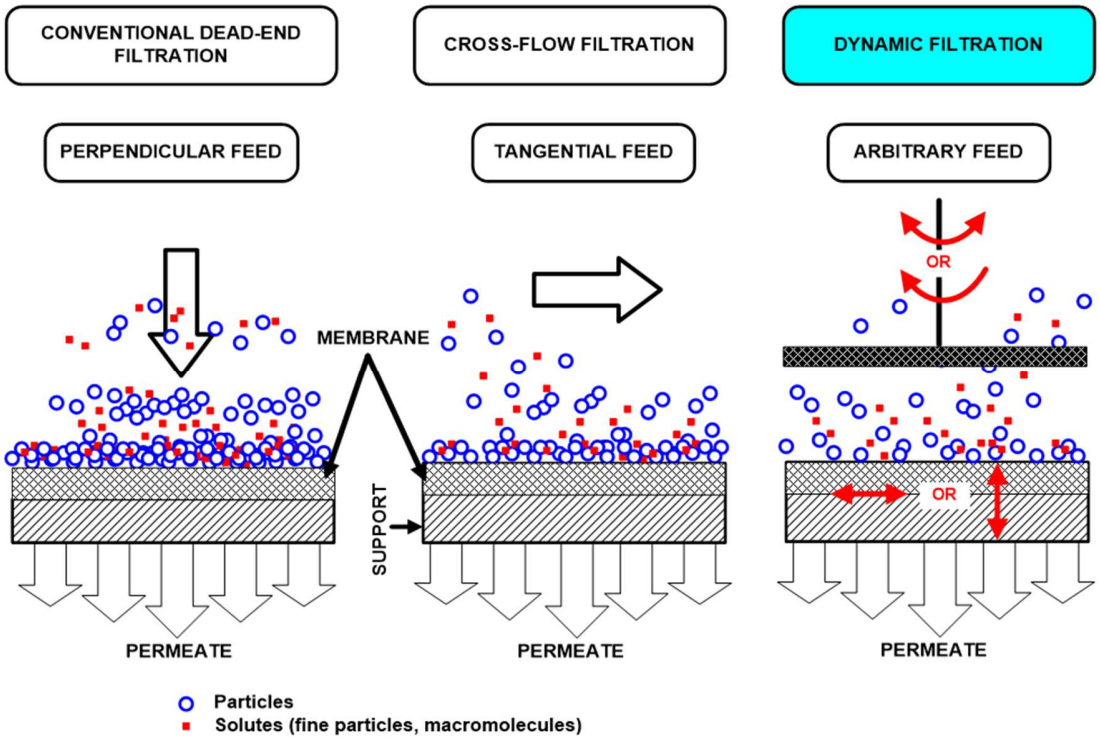

Fig. 1 Comparison between Dead-end filtration (DEF), Cross-flow filtration (CFF) and dynamic filtration (DF).

1.2 Dynamic filtration

Dynamic Filtration, also named Shear Enhanced Filtration, appears as a promising and alternative way compared to DEF and CFF. DF is characterized by the mechanical movement of devices to create high shear stress at the membrane surface result in uncoupling between local shear rate and TMP from feeding flowrate. As shown in Fig. 1, the permeate flux is not limited by the feeding flowrate but determined by local hydrodynamic conditions. The rotating disk/impeller/cylinder or membrane, oscillating and vibrating device or membrane, or other mechanical motion can generate locally high shear rates approximately up to 3×10^5 s^{-1} without large feeding flow rates [19]. Taking advantage of this technology, DF performs its outstanding behaviours in permeability and productivity, which leads to an effective and economical process, and those major expected advantages are [20, 21]:

- Enhanced local shear rates (magnitude and time fluctuation) at the membrane surface;
- Application of low TMP;
- Reduction of fouling magnitude, which generates higher permeate flux and requires lower filtration area;

- Reduction of loop dead volume;
- Significant energy-saving (Power/ Permeate flux or Energy/ Permeate volume).

Many studies [22-24] have shown an improvement in efficiency and fouling control with DF. However, additional motion modules will also generate a series of defects. The drawbacks of DF modules mainly attribute to their mechanical and hydrodynamics complexities:

- Technical limitations:
  - The complex mechanical configuration of devices may generate higher capital and operational investment, especially when scaling up;
  - The increase in the filtration area for scaling-up can be difficult.
- Hydrodynamic limitations:
  - Characterization of internal flow pattern is difficult (global performances and space-time resolution of velocity and pressure fields);
  - Local high shear stress may generate energy dissipation and subsequent local thermal increase.

For process engineers, the balance between advantages and drawbacks should be established for industrial applications through rational criteria, generally derived from lab-scale investigations. These strategies include estimating local and global parameters, theoretical models and computational fluid dynamics (CFD) simulation, practical filtration performances and energy consumption. More and more new devices and investigations are emerging to deal with these issues.

In 1994, Mikulasek [25] reviewed the typical methods to reduce concentration polarization and membrane fouling thanks to chemical, physical and hydrodynamic methods. The dynamic effects of rotating and oscillating to promote instabilities of flow were detailed. The anti-fouling mechanisms in rotating filtration were summarized by Lee and Lueptow (2004) [26], and they also described the recent efforts to apply rotating filtration to reverse osmosis (RO). Jaffrin (2008, 2012) [20, 27, 28] and Ding et al. (2014, 2015) [21, 29] summarized the industrial dynamic filtration modules with rotating and oscillating. The hydrodynamics inside the filtration cell was specialised concerning the shear rate and radial pressure. The empirical equation $J = a\gamma^b$ linked the permeate flux (J) and mean shear rate (γ) with two constants, a and b. Outputs from a review of available data from studies of rotating and vibrating membrane filters, as well as vibrating hollow fibre membranes, providing a direct correlation between performances (flux) and local hydrodynamics (shear rate) [30]. However, confusion remains between the mean and maximum shear rates. Meanwhile, there is still no clear classification of dynamic filtration devices.

In this review, the bibliometric analysis was conducted to confirm the research trends about DF modules over the years and summarized its application field and filtration type. Due to the diversity of DF devices, the industrial or lab-scale modules were classified into 15 types according to the mechanical movement form and shape. The use of the available information related to internal hydrodynamics of DF allows the prediction of local performance and power consumption. They were combined with practical application requirements to guide the selection of appropriate industrial equipment.

2. SCIENTIFIC PRODUCTION RELATED TO DYNAMIC FILTRATION

The database interrogation was carried out to review scientific publications and to gain insight into research hotspots. The scientific database Web of Science (WoS) Core Collection (Thomson-Reuter) was used to identify relevant articles concerning "dynamic filtration" and with the following methodology.

- Database: Web of Science Core Collection
- Profiles: (dynamic filtration) AND (membrane) AND (high shear OR shear enhanced OR rota* OR vibra* OR oscilla*)
- Field: Topic (Title, Abstract, Keywords)
- Period: 1975 to 2020 (Updated: February 30, 2020).

Citespace [31] is one of the most commonly used tools in the visual exploration of scientific literature. It was adopted as a research tool for quantitative analysis, while qualitative analysis was associated with its application fields and filtration types to identify the investigated scientific problematics. The working database was established by filtering the related publications about dynamic filtration from WoS.

2.1 Quantitative analysis

Out of 251 extracted articles, 150 publications are related to "dynamic filtration" including research articles (142, 94.7%), proceedings papers (22, 14.7%), reviews (6, 4.0%), and book chapter (2, 1.3%). Fig. 2 shows the number of papers per year from 1991 to 2020. During the period 1975-1990, no article was found in WoS. The average number of publications per year is 1.8±0.8 between 1991 and 2001, and increased rapidly to 11.8±3.4 during 2002-2019, even up to 16 in 2018. The number of citations almost grows exponentially and is strongly correlated with the publication rate. 2544 citations between 2002 and 2019 equivalent to 19.6 citations/articles ratio. This basic figure indicates an increasing research activity, scientific and industrial interests in DF.

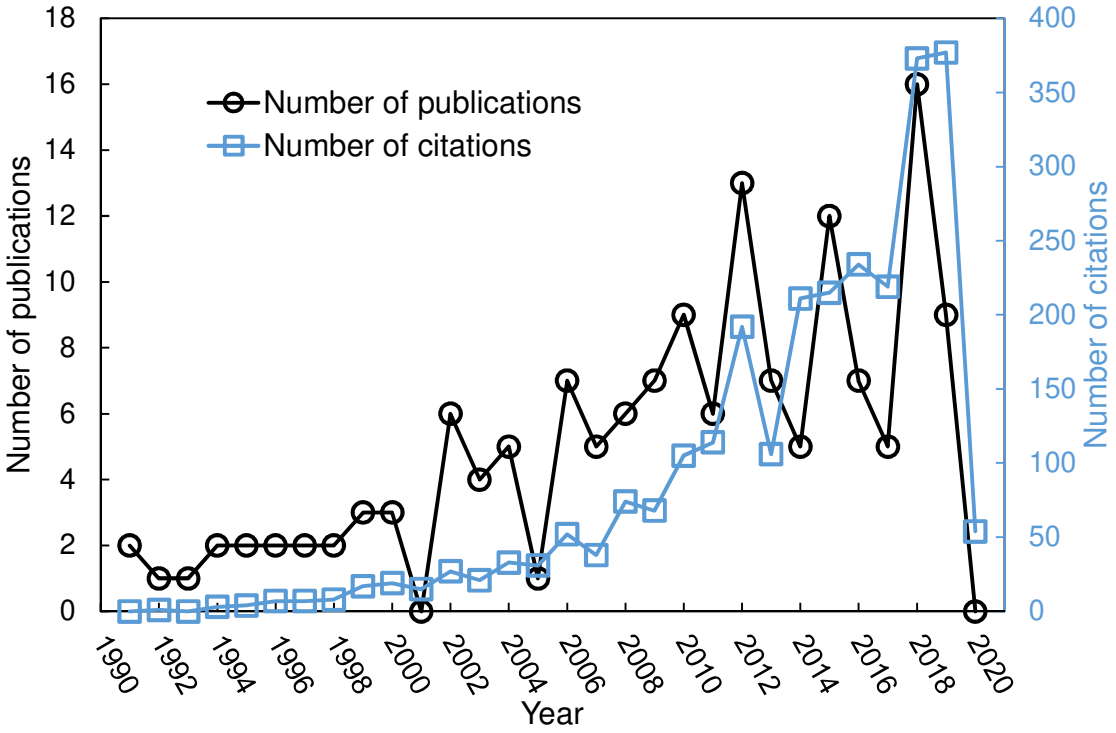

Fig. 2 Number of publications and citations per year (Source: Core Collection-WoS (Thomson-Reuter), period: 1991 to 2020)

2.1.1 Scope of journals and research areas

Five research areas represent almost 90% of articles. Engineering (in general) account for 78.7% of total publications, which include 118 articles, whereas Polymer Science and Water Resources rank second and third places with only 31 (20.7%) and 28 (18.7%) articles, respectively. Biotechnology & Applied Microbiology, Chemistry and Environmental Science & Ecology also account for a significant proportion. Besides, DF modules have been reported in the other 11 categories, such as Food Science Technology, Agriculture, Mechanics, Physics, Energy & Fuels, etc.

According to the Citation report for 150 selected results, the articles related to DF were published by 26 journals among 23 WoS subject categories. The five most productive journals with the number of articles and categories of journals are shown in Table. 1. Total articles and citations rate in each journal follows the same trend with a dominant position for the Journal of Membrane Science.

Table. 1 Top 5 most productive journals considering the number of articles and citations (source: WoS)

Journal	TA (P)	TC (P)	Category
JOURNAL OF MEMBRANE SCIENCE	31 (20.7)	1143 (43.5)	ENGINEERING; POLYMER SCIENCE
DESALINATION	20 (13.3)	298 (11.4)	ENGINEERING; WATER RESOURCES
SEPARATION AND PURIFICATION TECHNOLOGY	14 (79.3)	203 (7.7)	ENGINEERING

Journal	TA (P)	TC (P)	Category
BIOTECHNOLOGY AND BIOENGINEERING	7 (4.7)	165 (6.3)	BIOTECHNOLOGY & APPLIED MICROBIOLOGY
CHEMICAL ENGINEERING RESEARCH DESIGN	6 (4.0)	32 (1.2)	ENGINEERING

**TA: Total article; TC: Total citation; P: percentage (%)*

2.1.2 Research institutions and scientific cooperation

Table. 2 shows the top 9 most productive institutions with the same indicators. The leading institution is University of Technology of Compiègne, UTC (France), which published the most articles accounting for 30.0% of the total, and almost half of them were in cooperation. Afterward, Rovira Virgili University, URV (Spain), Jadavpur and Calcutta University (India) and Nagoya University (Japan) published relatively few articles, but they all exceed five. Then followed by IREC (Spain) and Tamkang University (China).

Table. 2 Top 9 most productive institutions (source: WoS)

Institution	TA(P)
UNIV TECHNOL COMPIEGNE	45 (30.0)
UNIV ROVIRA VIRGILI	9 (6.0)
JADAVPUR UNIV	8 (5.3)
UNIV CALCUTTA	7 (4.7)
NAGOYA UNIV	6 (4.0)
IREC	5 (3.3)
TAMKANG UNIV	5 (3.3)
DALIAN UNIV TECHNOL	4 (2.7)
UNIV TOULOUSE	4 (2.7)

**TA: Total article; P: percentage (%)*

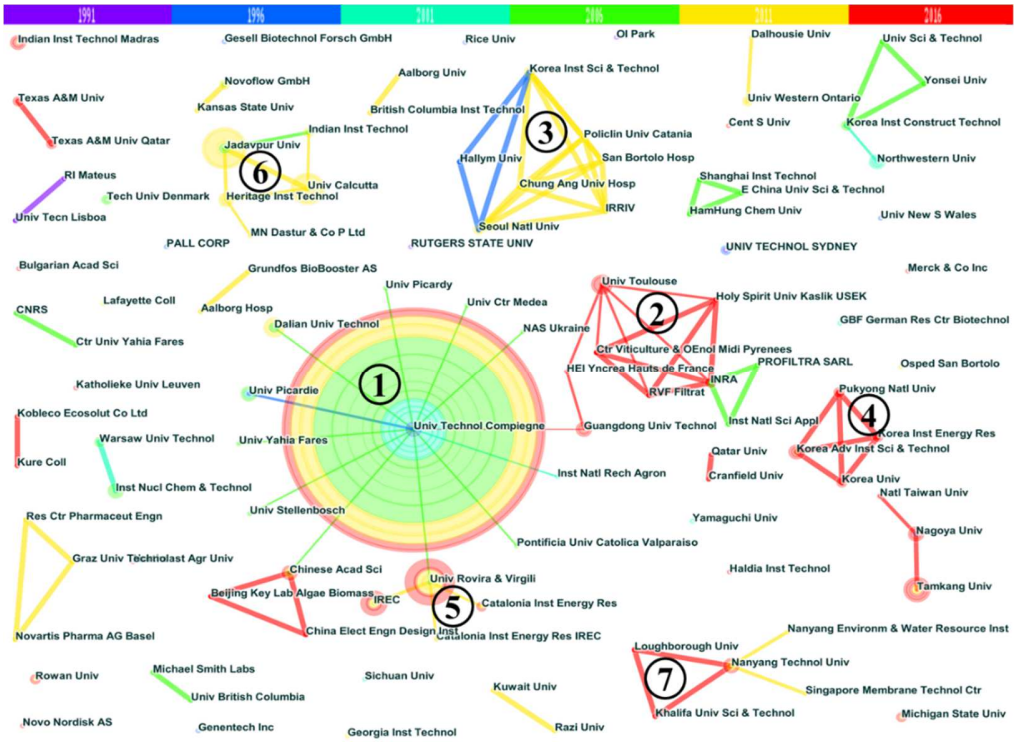

Fig. 3 Institutions cooperation network

113 institutions (academics or private companies) and 99 collaborative links were illustrated by the cooperation network (Fig. 3). The size of the nodes represents the scientific activity, and the links inform the cooperation between the academic institutions and/ or private companies. As for the major network, the dominant position is led by UTC (France) from the 7 most massive clusters, which published 45 articles and linked with other 12 institutions, but mainly concentrated in 2000 to 2010. Another major one emerged at University of Toulouse. It has 5 collaborators, among 4 of them are connected. Furthermore, the bilateral national cooperations in India, Korea, and China, the international collaborations between Tamkang University (China) and Nagoya University (Japan), URV (Spain) and UTC (France) indicate the high degree of cooperation. In Fig. 3, the colour informs about the production year. Most productive institutions come from China, France and Korea in the last four years.

2.1.3 Identification of research items

Generally, the keywords are associated with the core content of the publications; the higher frequency of occurrence in specific fields reflects the research hotspots. Fig. 4 lists the co-occurrence network of high-frequency keywords (count≥3, representing more than 75% of total keywords) related to DF. Most of these keywords correspond to filtration types (microfiltration, ultrafiltration, nanofiltration and reverse osmosis), DF modules (rotating membrane, perforated disk, overlapping ceramic membrane, …), treated fluids (microalgae, dairy wastewater, biofuel, chicory juice, emulsion…), performances (permeate flux, critical flux, threshold flux, shear stress/ rate…).and CFD simulation.

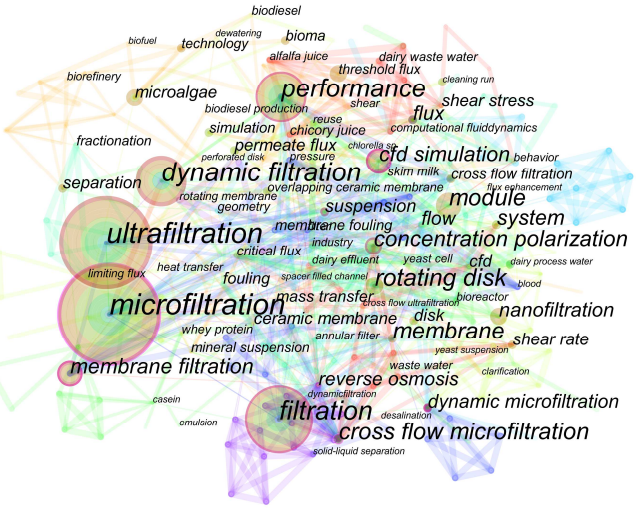

Fig. 4 Keywords co-occurrence network

Based on keyword co-occurrence analysis, network relationships were simplified into a relatively small number of clusters. Table. 3 lists 12 clusters with the top 5 terms by using Log-likelihood Ratio (LLR). The majority of the keywords are cross-linked and can be summarized in 4 dominants:

- DF technologies, such as rotating disk, vibratory disk, rotating membrane filter, shear enhanced filtration and vibration;
- Applications including yeast cells, dairy effluent, microalgae, alpha-lactalbumin, etc.;
- Hydrodynamics and performances associated with flux behaviour, turbulent flow, shear stress, concentration polarization and mass transfer;
- Simulations (dynamic simulation).

Table. 3 Clusters of research hotspots

Cluster ID	Size	Top Terms (LLR)
0	44	particle size, clean-bed, membrane separations, yeast cells, ferric hydroxide
1	37	rotating disk, dairy effluent, nanofiltration, vibratory disk, ceramic membranes
2	36	flux behaviour, alfalfa juice, dynamic cross-flow filtration, turbulent flow, rotating membrane filter
3	28	concentration polarization, number, concentration polarization (cp), mass transfer, vibration enhanced reverse osmosis (vero)
4	24	microalgae, dynamic membrane filtration, perforated disk, shear stress, dewatering
5	20	shear enhanced filtration, beta-lactoglobulin, milk fractionation, alpha-lactalbumin and beta-lactoglobulin transmissions, alpha-lactalbumin
6	15	dynamic simulation, back transport flux, rotating disk uf membrane, cell pore-plugging model, mathematical modelling
7	14	algae dewatering, ceramic microfilter, vibrating membrane system, algae microfiltration, membrane dewatering impact factor
8	13	ceramic membrane, solid-liquid separation, rotary filter, filtration, membrane
9	12	ultrafiltration module, dean vortice, fluidized bed, co2 transfer, variable secondary flow
10	8	bundle configuration, hollow fibres, vibration, analytical solution, shear rate

11	7	vibratory disk, particle size, dynamic cross-flow filtration, ceramic membranes, dynamic simulation

Table. 4 presents the top 10 keywords citation bursts about DF between 1991 and 2019. It is noticeable that all keywords alternate between technologies, applications and performances. Dynamic filtration ranked the first position with strength was bursting from 2000 to 2005. Meantime, skim milk, ultrafiltration, performance and crossflow microfiltration also stood as the hot pots before 2010. Afterward, the scientific interest evolves from the description of fouling mechanisms (concentration polarization, permeate flux and threshold flux) to new applications (microalgae) and technological developments.

Table. 4 Top 10 keywords with the strongest citation bursts

Keywords	Year	Strength	Begin	End	1991 - 2019
dynamic filtration	1991	4.2973	2000	2005	
skim milk	1991	2.5107	2004	2009	
ultrafiltration	1991	3.1852	2004	2009	
performance	1991	2.7155	2008	2010	
cross flow microfiltration	1991	2.4962	2009	2010	
concentration polarization	1991	2.5581	2011	2012	
permeate flux	1991	3.0425	2011	2013	
microalgae	1991	2.9145	2014	2019	
technology	1991	2.3293	2015	2019	
threshold flux	1991	3.0737	2015	2017	

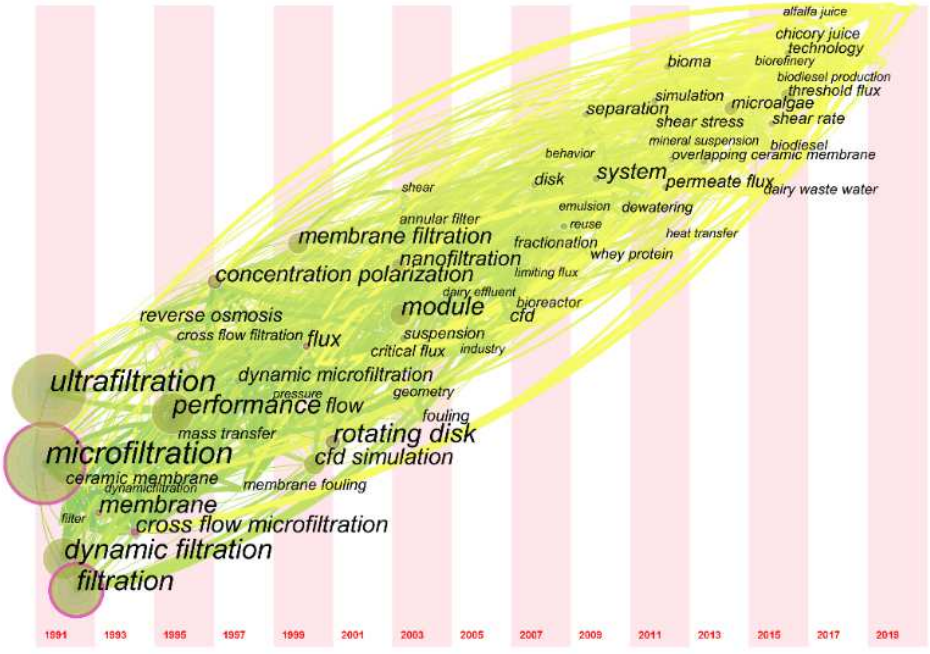

Fig. 5 Distribution map of keywords and nodes time-zone associated with DF

The time-zone visualization (Fig. 5) distributes keywords in chronological order and co-occurrence relations help to clear the research trend over a given period. For each node, the keywords indicate the early emerging interest, and the size informs about the cumulated number of publications. Since 1990, filtration type, module geometries, fluids, flux behaviours and fouling have been investigated. Some of them are still research hotspots. Over the last 5 years, attention was paid to the emerging applications (microalgae, juice and biofuel) and alternative technologies.

2.2 Qualitative analysis

Fig. 6 reports the main domain of DF applications and membrane separation types identified from 150 publications. DF is used in three main domains: Water treatment, Food processing and Bioprocess engineering.

According to the types of fluid, microfiltration (MF) and ultrafiltration (UF) were widely applied for separating fine particles from liquids, while nanofiltration (NF) and reverse osmosis were commonly used for removing dissolved constituents. As present in Fig. 6**,** MF (67 articles) and UF (63 articles) stands as the most frequent processes compared with NF (11 articles) and RO (8 articles). In MF, the articles mainly concerned large suspended solids removal such as biotic suspension (cell harvest, yeast suspension, microalgae suspensions), mineral suspension, sludge dewatering and model suspension. In UF, DF modules were tested with skim milk, soymilk, juice, surfactant solution, BSA suspension, and oily emulsions. Besides, DF treatment of wastewater from food processing presented a high-efficiency removal of chemical oxygen demand (COD) and biological oxygen demand (BOD). NF and RO are mostly used for a deeper treatment of separation, such as dissolved metals and salts removal, and drinking water purification.

In all processes (MF, UF, NF and RO), most membrane materials were organics (94 out of 119). In contrast, inorganic membranes (34) such as ceramic membranes and metal oxide membranes were mainly used in MF processes.

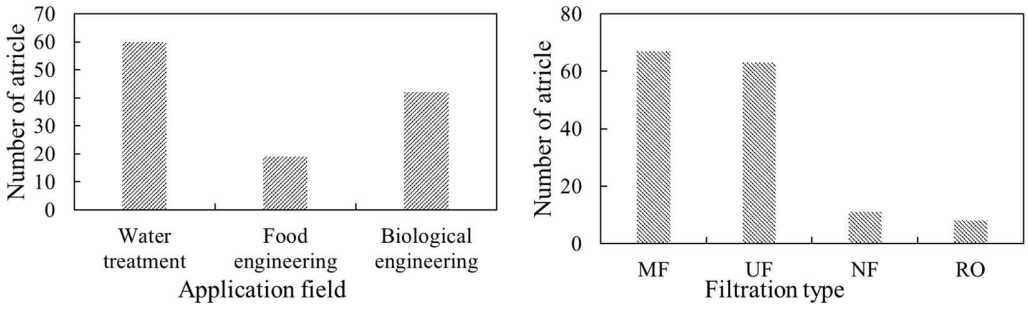

Fig. 6 Application fields and filtration type associated with dynamic filtration

2.2.1 Water treatment

In water treatment (60 articles), researchers investigated DF to treat industrial and municipal wastewater and rarely drinking water. Experimental fluids were mostly synthetic model fluids and suspensions, whereas others used wastewater from the treatment plants (paper mill [32, 33], detergent [34] and food industries [35, 36], sludge from anaerobic membrane reactor [37, 38]. Due to the complex composition of industrial

wastewater, simple solutions, emulsions and solid-liquid suspensions were preferred as test fluids. Simple solutions were used to mitigate toxic pollutants (halogenated organic compounds [39, 40], 2-MIB and geosmin [41], polyvinyl alcohol [42], heavy metal ions [43, 44] and sodium dodecylbenzene sulfonate [45, 46]), artificial seawater (NaCl, KCl, $MgCl_2$, $CaCl_2$, and $MgSO_4$) [47, 48], viscous solutions (polyethylene glycol-6000 [49-51], carboxymethyl cellulose [52], ethanol [53]), soluble salts ($CaSO_4$ [54], NaCl [55]), model wastewater in dairy process [56-62] and space mission [63]. For emulsion, oil/water mixtures with surfactants were considered [64-70]. Solid-liquid suspensions with dispersed particles as model effluent included bentonite [71], polymethyl methacrylate (PMMA) [72-74], styrene butadiene rubber (SBR) latex [75], polystyrene latex [76], $CaCO_3$ [77-81], SiO_2 [82-85], Al_2O_3 [86], ZnO, $Fe(OH)_3$ [87, 88] and hollow glass microspheres [89].

The permeation/retention bottlenecks were scrutinized versus operating conditions (effluent, concentration, temperature, TMP) and device configurations (geometry of DF modules, shear rate, membrane nature and cut-off). Most of the works reported qualitative performances (flux, steady-state flux, hydronic resistance, concentration factor, volume reduction ratio, rejection rate, concentration polarization) to establish the empirical correlations (flux versus shear rate/ shear stress). Computational fluid dynamics [47, 55, 61, 73, 84, 89] was used to simulate local and global performances (shear rate/ shear stress, flux) within the filtration cell and membrane surface. Only one article used PIV (particle image velocimetry) [71] to examine the local hydrodynamics and compared it with the filtration performances.

2.2.2 Food processing

In food processing (19 articles), DF was applied in liquid food production (dairy, brewing and extract juice). 12 articles (63%) were related to the concentrations of milk protein from casein micelle [19, 90-96] and separation of α-lactalbumin and β-lactoglobulin [97-100]. The fluids commonly came from commercial UHT skim milk and low heat powder milk. Defatted soy milk was also used to recover trypsin inhibitor and soy milk protein [101]. Microfiltration in brewing (rough and clarified beer) [102] and wine-making (crude simulated and filtered wine) [103] was investigated with DF. Retention/permeation performances were reported in terms of product quality and cost-effectiveness. Juices of sugar beets [104], *Alfalfa* [105, 106] and *Jerusalem Artichoke* [107] contain a large number of nutritional compounds, such as sugar, leaf protein and inulin, which have been separated, purified and/or concentrated by ultrafiltration with DF.

All works are associated with technical locks about product concentration and quality. Performances versus volume reduction ratio and modelling of hydraulic resistance stand as major scientific questions. To increase filtration efficiency, optimizations of operating conditions and modifications of DF geometrical configurations are handsome strategies. The filtration performances do not only focus on the permeate flux but also permeate quality (purification and separation rate). These analyses mainly rely on the permeate/retentate turbidity, coloration or conductivity, and the concentration or °Brix of target products. It should be mentioned that membrane selectivity (membrane materials, structure and cut-off) is a critical issue for some particular compositions.

2.2.3 Bioprocess engineering

For bioprocess engineering, 42 papers were carried out associate with DF modules due to their wider coverage (cell productions: prokaryote, eukaryote, microalgae, animal cells; biomolecule productions: recombinant proteins, antibody, exopolysaccharides, etc.). Most of tested fluids are biological suspensions （fermentation broth） containing microalgae [24, 108-123], yeast [19, 124-134], bacteria [135-137] and animal cell [138-140]. Other dispersions were produced by commercial or fermented biological products, including bovine serum albumin (BSA) [141-143], polygalacturonic acid 140, α-lactose monohydrate [144], ibuprofen [144], recombinant human growth hormone [145] and monoclonal antibody [146]. Within the research, 17 publications (40%) focused on the concentration and separation (biomass) of microalgae and constituted a new hotspot over the last decade. *Saccharomyces cerevisiae* (baker's yeast) was commonly used in DF for its widespread applications in the biotechnological industry. Model suspensions were formed by the mixture of yeast with ultrapure osmosed water [19, 127] and buffer [129, 130] or directly extracted from fermentation broth [124, 125].

In bioprocess engineering, flux decline induced by the fouling layer was discussed. Methods to improve critical flux are generally consistent with water treatment and food processing, but cell viability needs to be considered under high shear stress [97, 147]. Several publications dedicate to the formation of cell cake layers, which exhibit high specific filtration resistance due to their high compressibility. The empirical correlations between cake mass and operating conditions (TMP and wall shear stress) were reported and interpreted [112]. CFD has been combined with experimental data to investigate local operating conditions with biological fouling within DF devices [112, 114, 115, 140, 142-144].

3. SPECIFICATIONS OF LABORATORY AND INDUSTRIAL DYNAMIC FILTRATION MODULES

3.1 Classification of dynamic filtration modules

In recent decades, many efforts and a great number of studies have been achieved to develop novel DF modules at the lab or pilot-plant scales. From scientific and technical literature, 55 modules with 85 configurations were designed and produced by 29 industries and 21 laboratories. Reviewing the existing DF modules, they can be classified by the type of movement, including rotation, oscillation and vibration. These movements can occur to the membrane, the mechanical device (disk, impeller and cylinder) or the whole filtration module. Oscillating and Vibrating movements are easily confused, and there is no clear definition to distinguish them. In this paper, oscillation and vibration are defined as mechanical movement, which can be perpendicular and parallel to the direction of permeate flux, respectively. Based on the shapes of the moving part and the membrane, the 55 identified modules could be classified into 15 types considering the movement form and part (Table. 5). Table. 6 reports the technical specifications (trade name, filtration area, maximum rotating speed, oscillating or vibrating frequencies) of all modules.

Table. 5 Classification of DF modules according to the movement and shape

Movement form	Movement part	Shape of movement part	Shape of membrane	Type
Rotating	Membrane	Disk	Disk	1
		Rectangular	Rectangular	2
		Cylinder	Cylinder	3
		Hollow fibre	Hollow fibre	4
	Mechanical device	Disk	Disk	5
		Impeller	Disk	6
		Cylinder	Cylinder	7
	Mechanical device + Membrane	Disk + Membrane	Disk	8
Oscillating	Filtration module	Cylinder	Disk	9
		Rectangular	Rectangular	10
	Membrane	Rectangular	Rectangular	11
		Cylinder	Cylinder	12
		Hollow fibre	Hollow fibre	13
	Spacers	Rectangular	Rectangular	14
Oscillating + Vibrating	Membrane	Hollow fibre	Hollow fibre	15
Vibrating		/		

Table. 6 Classification and specification of DF modules (d: membrane diameter, S: membrane surface area, N/F: maximum rotating, vibrating and/or oscillating speed/ frequency, A: amplitude, displacement or vibrating angle, TMP: maximum operating transmembrane pressure)

Type	Manufacturer	Configuration	Status	Membrane size (mm)	S (m^2)	N/F (rpm, Hz), A (mm, °)	TMP (bar)	Fluid	Ref
1	Spintek, Huntington Beach, CA, USA	Spintek ST II	Industrial	d=340	0.05-2.3	1200 rpm	10	/	[148]
		Spintek ST IIL	Lab	d=203 (2)	0.05	1800 rpm	3.1	Cutting oil emulsion	[149]
	Spintek, Los Alamitos, CA, USA	High shear rotary membrane system, HSR-MS	Lab	d=74-267	0.0492	1750 rpm	5.17	Wastewater, O/W emulsion	[150-155]
	Novoflow GmbH, Rain/Lech, Germany	Single shaft disk filter, SSDF-312	Industrial	d=312 (75-100)	40	/	/	/	[156]
		SSDF-500+	Industrial	d=550 (75)	50	/	/	/	
		Compact rotating disk filters CRD	Lab	d=152 (3)	0.108	1800 rpm	1	Oily wastewater	[64]
	Diva Envitec Pvt. Ltd., India	Modular spin disk filtration, MSDF	Industrial	/	1-100	/	/	/	[157]
	Fraunhofer IGB, Germany, membrane supplier: KERAFOL	Rotating disk filter	Industrial	/	/	/	0.5-1.2	/	[158]
	Mio Vigneto Products, Automatic Filter System	Rocket M7	Industrial	(35)	7	/	/	/	[159]
	ANDRITZ KMPT GmbH, Vierkirchen, Germany	Rotational dynamic filtration, DCF 152/S	Lab	d=152	/	1150 rpm	/	Water/ ethanol	[53]
	HUBER (Berching, Germany), Vacuum Rotation Membrane VRM® Bioreactor	Vacuum rotation membrane bioreactor, VRM 20/36	Industrial	/	108	1.8 rpm	0.3	Wastewater	[160]
		VRM	Industrial	d=4500	540	/	/	/	[161]
	Hitachi, Japan	AQUA UFO	Industrial	/	/	/	/	/	[20]
	ANDRITZ KMPT (Vierkirchen, Germany), membrane supplier: KERAFOL	Dynamic cross-flow filter, DCF	Lab	d=152 (6)	0.138	1110 rpm	5.5	Microalgae	[109, 110]
	Westfalia Separator, Aalen, Germany	Multi shafts disks, MSD, two-shaft laboratory pilot	Lab	d=90 (12)	0.121	2000 rpm	2.5	$CaCO_3$	[77, 80, 162]
		MSD, eight-shaft pilot	Industrial	d=31.2	80	/	/	/	[28]
2	Gurpreet Engineering Works, Kanpur, UP, India	Spinning basket membrane, SBM	Lab	130×55 (4)	0.0286	600 rpm	9.7	PEG 6000, BSA, Polyving alcohol	[42, 50, 142, 163]
		Intermeshed spinning basket membrane, ISBM	Lab	105×55 (8)	0.046	480 rpm	9.7	BSA	[143]
	Key Laboratory of Industrial Ecology and Environmental Engineering, Dalian University of	/	Lab	300×30 (2)	0.018	160 rpm	0.065	Kaolin, yeast, $CaCO_3$	[164]
		/	Lab	230×20 (2)	0.0092	/	/	Halogenated compounds in water	[39]

Type	Manufacturer	Configuration	Status	Membrane size (mm)	S (m^2)	N/F (rpm, Hz), A (mm, °)	TMP (bar)	Fluid	Ref
	Technology, China								
3	Hemascience, Santa Ana, CA, USA	Plasmacell filter	Industrial	/	/	/	/	/	[165]
	Faculty of Engineering, University of Regina, Canada	/	Lab	/	/	10000 rpm	0.25	Oily-wastewater	[166]
	Membrex Inc. Fairfield, USA	Benchmark Biopurification system	Lab	/	0.02	2000 rpm	1.4	Yeast	[124]
	Department of Chemical Engineering, Nagoya University, Japan	/	Lab	2π×15×500	0.0471	1500 rpm	1.51	PMMA	[72]
		/	Lab	2π×15×320	0.03016	5000 rpm	1.51	PMMA, O/W	[68, 69, 74]
	Department of Mechanical Engineering, Northwestern University, USA	Rotating reverse osmosis	Lab	2π×241×127	0.0192	180 rpm	10	$CaSO_4$, model wastewater	[54, 63]
	Millipore Co.	/	Lab	2π×26×670	0.1094	600 rpm	/	SiO_2	[83, 85]
	Department of Chemical Engineering, Universitie de Technologie de Compiegne, France	/	Lab	2π×5×45	0.0014	7000 rpm	1	Al_2O_3	[86]
	Suker AG, Winterthur, Switzerland	Biodruck-filter, BDF-01	Lab	2π×33×200	0.04	3000 rpm	0.7	Yeast	[167]
4	Facultad de Ciencias-Seccion de Química, Universidad La Laguna, Spain	Rotating hollow fibre membrane, R-HFM	Lab	/	0.047	330 rpm	0.4	Anaerobic suspensions	[38]
5	University of Technology of Compiegne, France	Rotating disk module, RDM-1	Lab	d=154	0.019	3000 rpm	10	CaCO3, yeast, skim milk, juice, broth, dairy effluent, microalgae, PAA–Cd complex	[19, 23, 34, 57, 58, 61, 62, 65, 66, 78, 79, 90, 97, 99, 101, 105, 106, 127, 135, 168-179]
		RDM-2	Lab	d=260	0.046	1500 rpm	2	Skim milk	[178]
	School of Chemistry and Chemical Engineering, Central South University, China	Rotating disk module	Lab	d=176	0.0242	3000 rpm	2.5	Cd^{2+}, Zn^{2+}	[180, 181]
	Department of Chemical and Materials Engineering, Tamkang University, Taiwan, China	Rotating-disk dynamic filter-1	Lab	d=38	0.00112	3000 rpm	1	Microalgae, PMMA, artificial seawater	[48, 73, 84, 112]
		Rotating-disk dynamic filter-2	Lab	d=155	0.0377	3000rpm	1	Microalgae	[115]
	Pall Corp., Dreieich, Germany	Dynamic membrane filter, DMF LAB6 system	Lab	d=151	0.0137	3450 rpm	2	Yeast, coli	[125, 139, 147, 182]
	Grundfos BioBooster, Bjerringbro, Denmark	Rotating cross-flow, RCF MBR	Lab	d=312	0.12	350 rpm	15	/	[183]
	BKT Water & Energy, Korea	Anti-fouling	Industrial	/	94.9	270 rpm	15	/	[184]

Type	Manufacturer	Configuration	Status	Membrane size (mm)	S (m^2)	N/F (rpm, Hz), A (mm, °)	TMP (bar)	Fluid	Ref
		membrane filtration system FMX-S							
		FMX-E	Industrial	/	40	270 rpm	5	/	
		FMX-P	Industrial	/	0.0873-3.16	290-350 rpm	30	/	
		FMX-B	Lab	d=150	0.0146	1600 rpm	1	Microalgae	[114, 117, 119]
	Miltenyi Biotec, Germany	Life 18 disk separator	Industrial	/	/	/	/	/	[185]
	Michael Smith Laboratories, Canada	Controlled shear affinity filtration (CSAF)	Lab	d=30	0.0014	/	/	/	[186]
	Gesellschaft für Biotechnologische Forschung mbH, Biochemical Engineering Division, Germany	Controlled shear filtration, CSF	Lab	d=90	0.0515	/	/	BHK cell	[138]
6	Bokela GmbH, Karlsruhe, Germany	Dynotest	Lab	/	0.013	/	7	Alpha-lactose monohydrate suspension	[144]
		DYNO	Industrial	/	0.13-12	/	6	/	[187]
	Metso Paper Co, Raisio, Finland	Cross Rotational (CR)-Filter, CR 200/1	Lab	d=200 (1)	0.054	/	/	Paper mill waste	[188-190]
		CR 250/2	Lab	d=250 (2)	0.18		10		[191]
		CR 500/5	Industrial	d=500 (5)	1.75	470 rpm	2.7		[192]
		CR 550 / 15 to 30	Industrial	d=550 (15-30)	7.5-15	/	/		[29]
		CR 1000/ 26 to 60	Industrial	d=1000 (26-60)	35-84	/	/		[29]
		CR 1000/10	Industrial	d=1000 (10)	13.5	365 rpm	1		[189]
		CR 1010/70 to 100	Industrial	d=1010 (70-100)	98-140	/	/		[29]
	RVF Filtration, Paris, France	Rotating and vibrating filtration, RVF	Lab	d=142 (4)	0.024 per cell (1 to 5 cells)	50 Hz	3	Beer, wine, viscous, solution	[102, 103, 193-196]
		RVF 5	Industrial	d=800 (10)	1 per cell (1 to 5 cells)	30 Hz	20	Waste water, chemical sludge	[197, 198]
7	Fann Instrument Company, Houston, Texas, USA	Fann 90 Dynamic HPHT® Filtration System	Lab	/	/	300 rpm	7	Drilling fluid	[199]
	Department of Nuclear Methods in Process Engineering, Dorodna, Warsaw, Poland	Helical Couette-Taylor flow (CTF) filtration module	Lab	/	0.04	2800 rpm	0.7	Radioactive wastes, wastewater	[43, 44]
8	Gurpreet Engineering Works, Kanpur, UP, India	Rotating disk-membrane, RD-M	Lab	/	0.00246	Membrane:600 rpm stirrer: 1000 rpm	10	BSA, PEG6000, kraft black liquor	[32, 33, 49, 51, 141]
	Krauss-Maffei DCF, Andritz	Dynamic cross-flow	Lab	d=152 (4)	0.14	1000 rpm	5	Skim milk	[96]

Type	Manufacturer	Configuration	Status	Membrane size (mm)	S (m^2)	N/F (rpm, Hz), A (mm, °)	TMP (bar)	Fluid	Ref
	KMPT GmbH, Vierkirchen, Germany	filtration, DCF							
9	New Logic, CA, USA	Vibratory shear enhanced processing, VSEP series L 101	Lab	d=135	0.05	55-60.75 Hz	15	Skim milk, simulated tannery wastewater, microalgae, latex solution	[24, 35, 56, 75, 91, 92, 118, 122, 175, 200]
		VSEP series LP	Lab	/	1.53	/	40	Microalgae	[113]
		VSEP series L	Lab	/	0.446	/	40	/	[201]
		VSEP series P	Lab	/	1.57	/	40	/	
		VSEP series B	Lab	/	0.0111	/	10	/	
		VSEP series P-50	Lab	/	4.65	/	40	/	
		VSEP series i18	Lab	/	13.9-26.9	35-49 Hz	38	/	
		VSEP series i36	Lab	/	41.8-55.7	38-55 Hz	38	/	
		VSEP series i84	Lab	/	up to139	43-55 Hz	38	/	
	Pall Filtration, East Hills, NY, USA	Vibrating membrane filtration, VMF-PALLsep PS 10	Lab	/	0.2	55-55.75 Hz	2	BSA	[202]
		VMF-PALLsep Biotech Module	Industrial	/	0.2-5	/	3.5	/	[203]
10	Department of Mechanical Engineering, Texas A&M University, College Station, TX, USA	Vibration enhanced reverse osmosis (VERO) membrane	Lab	30×20	0.0006	60 Hz, 1.2 mm	55	Simulated seawater	[47, 55]
11	Chemical and Biochemical Engineering Department, Western University, London, Ontario, Canada	Oscillatory flat surface membranes, OFSM	Lab	89×68	0.006	25 Hz, 30 mm	0.6	Yeast	[131, 133, 204-207]
	State Key Laboratory of Pollution Control and Resource Reuse, Tongji University, China	Uniform shearing vibration membrane, USVM	Lab	/	0.02	5 Hz, 20 mm	0.7	Microalgae	[208]
	Faculty of Bioscience Engineering, Katholieke Universiteit Leuven, Belgium	Magnetically induced membrane vibration, MMV	Lab	/	0.016-0.0215	60 Hz, 20 mm	0.3	Wastewater, microalgae, anaerobic sludge, lignocelluloses hydrolysate	[37, 209-213]
	State Key Laboratory of Pollution Control and Resource Reuse, Tongji University, China	Axial vibration membrane, AVM	Lab	/	0.02	15 Hz, 40 mm	0.7	Microalgae	[214-216]
12	Department of Chemical Engineering, University of Engineering & Technology Peshawar, Pakistanb	Oscillating membrane module	Lab	/	/	0-100 Hz, 0-10 mm	0.4	Oil in water emulsion	[70]
	Chemical Engineering Department, Loughborough University, Leics, UK	Azimuthal and axial oscillation filtration	Lab	/	/	100 Hz, 3 °	0.3	Suspension of calcite	[217]

Type	Manufacturer	Configuration	Status	Membrane size (mm)	S (m^2)	N/F (rpm, Hz), A (mm, °)	TMP (bar)	Fluid	Ref
13	IMI Institute for R&D, Israel Chemicals Group, Israel	Vibrating hollow fibre microfiltration, VHM	Lab	/	0.0057	10 Hz, 40mm	/	Yeast	[218]
	School of Civil and Environmental Engineering, Nanyang Technological University, Singapore	Vibrating submerged hollow fibre membranes	Lab	/	/	0-15Hz, 0-12mm	0.4	Bentonite	[71]
	CAPEC, Department of Chemical Engineering, Technical University of Denmark, Denmark	HF membrane filter	Lab	/	0.0256	30 Hz, 1.175mm	0.25	Enzyme, yeast	[129, 130, 219, 220]
14	Nanyang Environment and Water Research Institute, Nanyang Technological University, Singapore	Spacer vibration of submerged flat sheet membranes	Lab	50×70×2	0.007	2 Hz, 12 mm	0.4	Bentonite and alginate solution	[221]
15	School of Chemical Engineering, The University of New South Wales, Australia	Transverse vibrating hollow fibre membrane	Lab	/	/	58 Hz, 5 mm	0.2	Yeast, milk	[132, 222]
	Department of Nephrology, San Bortolo Hospital, Italy	Shaking HF membrane module	Lab	/	/	20 Hz, 20 mm (20 °)	/	/	[223, 224]
	School of Chemical Engineering, The University of New South Wales, Australia	Rotational vibrating hollow fibre membrane	Lab	/	0.0131	10.3 Hz, 18.3-55°	0.8	Yeast	[22]
	School of Water Resource and Civil Engineering, Northeast Agricultural University, China	Vibration hollow fibre membrane	Lab	/	0.0045	2 Hz, 180 °	0.6	Microalgal	[123]
	Institute of Oceanic and Environmental Chemical Engineering, Zhejiang University of Technology, China	Pendulum type oscillation, PTO	Lab	/	0.2	70 rpm, 50 mm	/	Oily wastewater	[225]

537

538

3.2 Rotating systems

Rotating systems can be split into three categories: rotating membrane modules (21 modules), rotating mechanical devices (14 modules) and the association of rotating membrane and mechanical devices (2 modules).

3.2.1 Rotating membrane modules

3.2.1.1 Rotating disk membrane

The disk membranes are one of the most commonly used in rotating membrane filter. From the literature, 10 modules (corresponding to 16 configurations, Table. 6) were designed and produced by local companies. These modules consist of membranes mounted onto the porous support driven by one or more central shaft. Such supports can be one or more rotary disk, allow a flexible configuration, and lead to easy scale-up with larger filtration area capacity. Cell design, geometrical configurations and operating conditions are the most critical parameters to optimize module efficiency.

In high shear rotary membrane system (HSR-MS) [151-155], flat round membrane disk packs are attached to the highly porous nylon meshes. A solid disk pack is placed between two meshes and sets on a hollow rotating shaft for permeation channels. By the central shaft rotation, the maximum liquid velocities close to the membrane can reach up to 18 m/s, compared to 4.5 m/s for conventional cross-flow UF systems [155]. Henrik et al. [53] tried to add a metal insert in the rotary membrane chamber. It generates disturbances in the bulk flow, which increase the filtration pressure.

Industrial applications of DF modules require technical improvements in order to increase the filtration area. Compact rotating disc filter (CRD) is a lab-scale module with 3 disk membranes compressed on the same hollow rotating shaft. In wastewater treatment, it has an available effective filtration area of 0.1 m^2 [64]. Signal shaft disk filter (SSDF-312) can equip with 75-100 filter disks mounted on a single shaft with a 10-15 m^2 filter area [156].

With the same concept, modular span disk filtration (MSDF) is manufactured by Novoflow GmbH (Germany), with a lot of disk membranes mounted on the single shaft, and the filtration area ranging from 1 m^2 up to 100 m^2 [157]. Vacuum rotation membrane (VRM, HUBER, Berching, Germany) filtration unit also designed with an available large-scale membrane area (diameter approx. 2.3 and 3.2 m, and membrane surface approx. 900 m^2 and 3840 m^2) and coupled with a powerful aerator to clean the contaminated membrane [160, 161, 226]. Rocket M7 was designed for the purification of grape juice in winemaking; 35 disk membranes (total filtration area of 7 m^2) were installed in the rotating shaft and driven by a 3 kW power motor [159].

Besides, some systems equipped with multi-shaft (rotate in the same direction), overlapping membranes were developed and well-studied. A two-shaft system, Dynamic cross-flow filter (DCF) commercialized and made by KMPT, was tested with microalgae for biofuel production [109, 110]. In the optimized condition, pilot experiments achieved a concentration factor up to 200 and permeability up to 600 L/h/m^2/bar (with pre-concentration) [109]. Another two shafts filter, a lab-scale Multi-shaft disk (MSD, Westfalia Separator, Aalen, Germany) module, was studied by Ding et al. [77, 80, 162]. They found that the permeate with two shafts module is about twice higher than the stationary membrane module with the same azimuthal rim velocity. The overlapping of

583 disks generates the maximum shear rate [77]. With this knowledge, a larger MSD system
584 was commercialized by Westfalia Separator. It is equipped with 8 shafts and fixed a pile
585 of membrane-disks; all shafts and membrane-disks rotate at the same speed [28].
586 Bendick et al. [150, 151] used the zirconium dioxide ceramic MF membrane in
587 HSR-MS to treat shipboard wastewaters (bilge water, blackwater and thermal destruction
588 quench water). They changed different hub sizes resulted in various membrane diameters
589 and different angular speeds of the membrane. For every 100 rpm increase in angular
590 velocity, steady-state flux increased on average by 26 L/(h·m^2). While expanding the
591 filter disk diameter, it also provides excellent performance per disk in lower rotation
592 speed and reduces the number of discs required.
593 He et al. [80] modified the configuration of MSD (2 shafts). Previously, each shaft
594 equipped with 6 ceramic membranes (0.2 μm). The permeate flux for 12 membranes was
595 520 L/(h·m^2) when filtering 200 g/L of $CaCO_3$, while it was reduced to 503 L/(h·m^2)
596 when working with 6 membranes. However, after replacing one of the ceramic
597 membranes on each shaft by a smooth disk or a disk with 8 vans, the permeate flux was
598 further improved to 740 or 816 L/(h·m^2), respectively. With the same module, Tu and
599 Ding [78] replaced the ceramic membrane with nylon membranes of the same size and
600 pore diameter to concentrate $CaCO_3$. Maximum permeate flux was observed for the nylon
601 membrane to reach 850 L/(h·m^2) compared to 760 L/(h·m^2) for the ceramic membrane. In
602 the fractionation of milk protein, Espina et al. [97] found that the PVDF membrane
603 performed better than the ceramic one regarding permeate flux and casein rejection. In
604 another paper [99], the concentrated fluid from the MF for ceramic membrane achieved
605 the transmissions of α-lactalbumin and β-lactoglobulin between 0.8 and 0.98, further
606 filtration with UF was applied to separate them.
607 In UF, the West Virginia University team compared the performances of polymeric
608 (100 kDa) and ceramic (0.11 μm) membranes for treating oily wastes from metal-
609 working. The latter was superior to the polymeric membrane in terms of permeate flux
610 and quality, as well as for cleaning and durability [152]. With CRD, oily wastewater with
611 different concentrations was treated in MF and UF (ceramic membrane). High oil (>99%)
612 and TOC (>98%) rejection rates were achieved with both membranes; their performances
613 were independent of the rotational speed and the feed concentration [64]. With VRM, the
614 wastewater treatment was performed at a very low rotational speed (1.8 rpm), and UF
615 polyether sulfone flat membranes (NADIR P-150F) were compacted with a total filtration
616 area equal to108 m^2. The COD in final permeate flux was reduced to 3 mg/L without
617 suspended solids for an initial retentate concentration equal to 601 mg/L. Moreover, the
618 membrane immersed in wastewater could be used longer due to the air sourcing [160].

619 ***3.2.1.2 Rotating rectangular membrane***

620 Only two modules (lab scale) were identified with rotating rectangular membranes,
621 but their designs are entirely different.
622 Gurpreet Engineering Works in India [42, 50, 142, 163] developed the first module
623 named Spinning basket membrane (SBM). Four flat rectangular membranes (each of
624 dimension 65×145 mm^2 with an effective area of 55×130 mm^2) fitted on alternate sides of
625 adjacent radial arms, and the other side remains impermeable. These arms are driven by a
626 hollow shaft and allowed permeate to pass. In continuous running, the membrane
627 filtration cycle rotated as a normal run, followed by a short time cleaning cycle rotated in

the reverse direction. With the same theory, the intermeshed spinning basket membrane (ISBM) consists of two identical spinning baskets, which are intermeshed with a phase difference of 45° and able to operate at the same speed but in reverse direction [143]. Sarkar et al. [50]investigated the separation of PEG 6000 with the SBM module and PES (5kDa) UF membrane. It indicated superior performance in terms of shear enhancement and flux recovery compared with other shear enhanced systems, namely the single stirred (SS) and the rotating disk-membrane (RD-M) modules. The steady flux of the SBM module was 45-95% higher than its RD-M counterpart; in comparison with SS, it was 300-450% enhanced when rotating at 62.5 rad/s. With its inbuilt cleaning facility, the module restricts the flux decline within 15% of its start-up value, even after 21 h of continuous running. In the UF of Bovine Serum Albumin, the average permeate flux of ISBM was observed to be approximately 1.8 times higher than that of the SBM module due to comparatively higher membrane shear stress. Maximum permeate flux was evaluated to be as high as 2.4×10^{-4} $m^3/(m^2\ s)$ at moderate transmembrane pressure and rotational speed (588 kPa and 52.36 rad/s). It also showed better performance in treating extremely fouling feed solutions than other standard membrane units [142, 143].

The second module is named helical lab-scale filter [39, 40, 164]. Two pieces of the flat membranes are supported on an aluminium spacer to maintain the helical angles (0°, 180°, 270°, 360° and 450°). A tubing outlet is assembled in the central of the aluminium spacer, for one side is sealed out and allowed the collection of permeate water. The filter sheet is immersed in the tube container and driven by a DC motor, which is able to rotate at the speed of 75 and 160 rpm. Different particle suspensions (yeast, kaolin and $CaCO_3$) were tested in MF with dynamic membranes (PES, 0.22 μm) with a total filtration area of 0.018 m^2. 360° stood as an optimal helical angle considering the permeate flux, and the energy consumption for this condition was smaller (0.069 kWh/m^3) than the rotating flat membrane (0.081 kWh/m^3). The order of membrane fouling was yeast> kaolin> nano-$CaCO_3$ at the same concentration of 5.0g/L, even the mean diameter of yeast is smaller than others [164]. To remove halogenated compounds (Cl^-, Br^-) in water, pre-coated nano-$CaCO_3$ dynamic membranes with an effective area of 0.0092 m^2 were applied in the batch and the continuous photocatalytic experiments. This coated (fouling) layer enhanced the filtration performances and the retention of photocatalysts [39, 40].

3.2.1.3 Rotating cylinder membrane

In 1967, Sherwood et al. [227] suggested a rotating cylinder filter in reverse osmosis for salt and water transport, including an inner cylinder membrane rotating in a cylindrical stationary housing. 8 other modules with similar configurations have been reported in the literature. The reduction of membrane polarization is improved by taking advantage of Taylor vortices in the annular gap of the filter apparatus [167].

Early-commercialized filters, Biodruck-filter (BDF-01, Sulzer AG, Winterthur, Switzerland) was dedicated to cell harvesting and cell debris removal [167], with 66 mm diameter and 200 mm length inner cylinder membrane (0.04 m^2 filtration area) at rotation speed up to 3000 rpm. With the Teflon membrane (0.2 μm), 3.3 and 10 concentration ratios were tested. Flux increments have been observed during the increase of rotation speed and TMP. In *E. coli* broth concentration, the Biodruck-filter showed a significantly higher flux (about three-fold) than cross-flow filtration techniques over a broad concentration range.

673 Murase et al. [72] described the same dynamic microfiltration system with a rotating
674 ceramic membrane (0.2 μm alumina ceramic membrane). Polymethyl methacrylate as
675 slurry material was circulated in the annual gap of 3.3 mm. The same fluid was treated
676 with the increase of outer cylinder diameter to achieve a larger gap (12.5 mm) in the
677 filtration cell. PMMA solutions were diluted with glycerine at concentrations of 72, 53
678 and 0% to obtain different viscosities. Results showed that high-speed rotating dynamic
679 filtration was considered to be more useful when the slurry has a higher viscosity [74]. In
680 the separation of oil in water emulsion, high rotation speed helped to limit the oil layer at
681 the membrane surface. With additional suspended particle in the emulsion, a further
682 increase in steady-state flux was observed from 5.41×10^{-4} to 1.14×10^{-3} cm/s in 49 kPa,
683 from 5.1×10^{-4} to 4.65×10^{-3} cm/s in 147 kPa [69].
684 Park et al. (1994) [83] and Choi et al. (1999) [85] investigated another module from
685 Millipore Co. Different gap ratios 0.17, 0.54 and 0.65 (inner cylinder radius: 5.2 cm)
686 were achieved by changing the diameter of the outer cylinder. Fine silica particles filtered
687 with MF-cellulose ester membrane (with total filtration area of 0.1094 m^2) rotating varied
688 from 0 to 62.8 rad/s. In a higher rotating speed like 41.8 rad/s, filter flux decreased for the
689 cake layer formation during the initial transient period. The fouling accumulation and
690 sweeping effect came to equilibrium after 2 hours of work resulted in the pseudo steady-
691 state filtrate flux. This value would decrease for higher concentration fluids, but
692 normalized filtrate flux seemed to be constant. In the range of tests, normalized filtrate
693 flux increased by reducing the gap radio or working at a higher rotation speed; a linear
694 relationship was observed with Taylor number (*Ta*) when $\omega > 34.1$ rad/s [83].
695 A company 'Mebrex' [124], developed a Benchmark Biopurification System for the
696 steroid recovery from yeast suspensions. It equips with a 100000 molecular weight cut-
697 off hydrophilized polyacrylonitrile membrane (0.02 m^2 surface area). Steroid recovery in
698 the permeate showed a significant increase with the Taylor number and obtained the best
699 recovery conditions at *Ta=2346* (2000 r/min).
700 Lee and Lueptow [54, 63] took advantage of Taylor-Couette flow instabilities to
701 reduce the flux decline related to concentration polarization and membrane fouling in
702 reverse osmosis. Commercial polymeric RO membranes with an outer radius of 2.41 cm
703 and length of 12.7 cm (corresponded to the total area of 0.0192 m^2) were applied in the
704 filtration of space mission wastewater (wash water, condensate, and urine). Rotational
705 speed and TMP showed to enhance the flux and rejection in rotating RO [63]. In the
706 concentration test of $CaSO_4$, the permeate flux for rotating RO at $\omega=180$ rpm remained
707 constant up to a volume concentration factor (VCF) of 4.2. Further treatment would lead
708 to a sharp decrease in permeate flux due to the scale formation of soluble salts [54].
709 With the same concept, a plasmapheresis filter was commercialized for plasma
710 collection. An inner cylinder (capacity, 7 ml) was assembled in the filter, driven by a
711 magnet, and rotated inside the cell. Blood was separated for the centrifugal force and
712 reached into the collection system, which permits the collection of 500 mL of plasma
713 within 30 min [165].
714 The last one was described by Amgar [166] in oily-water systems. Three parameters
715 (membrane rotation speed, membrane radius and azimuthal velocity profile) were
716 investigated, the rejection capacity of the membrane and fouling problem were reported.
717 With the rotation of the membrane, due to the centrifugal force, the oil droplets will

gather in the middle and reduce the membrane fouling. The rejection rate of the oil phase increase with the rotation speed and diameter of the membranes.

3.2.1.4 Rotating hollow fibre

One module equipped with hollow fibre (HF) membranes has been investigated in a rotating system, named rotating hollow fibre membrane (R-HFM) [38]. In a 3 L tank (inner diameter of 0.15 m), 97 fibres package assembled vertically, and each fibre shows a length of 0.08 m with an outer diameter of 1.9 mm. The membrane modules have an average pore size of 0.04 μm and a nominal membrane surface area of 0.047 m^2. Compared with conventional strategy, HF membranes were immersed in the filtrate, but one top header of membranes rotated to restrict the cake layer formation. In the UF of anaerobic suspensions, the fouling rate increased with permeate flux. The turbulence promoters were introduced to evaluate the effectiveness of fouling limitations. With the increase of permeate flux from 8 to 14 L/(m^2·h), this value decreased from 44.4% to 40.7% within the conventional gas-sparging membrane module, while sharply improved to 96% and 93% at the rotation speed of 260 rpm [38].

3.2.2 Rotating mechanical device module

3.2.2.1 Rotating disk

Unlike the rotating membrane system, the filter cake layer formation was limited by the rotation of external mechanical devices (such as disks, impellers or cylinders). 9 rotating disk modules (14 configurations) have been well documented in the literature. They solved the problem of flux decline by the design of inlet/outlet, disk structure, and the distance between rotating disk and membrane, mixing rate and TMP.

Dynamic Membrane Filter (DMF, Pall Corp., Cortland, NY) appeared as the first commercial system [125, 147, 182]. This filtration unit houses a 6-in.-diameter stainless-steel solid disk with a maximum rotating speed of 3450 rpm rotating in the clockwise direction only. The gap between the membrane (7.5 cm radius and a total area of 0.0137 m^2) and the rotating disk is 4 mm. The feed entered the system from the centre at the bottom side of the rotating disk, flowing into the gap between the stationary membrane and disk toward the centre where the concentrate or retentate was collected. Lee et al. [125] used this system installed with the MF membrane to filtrate yeast suspension. Results showed no significant difference in flux with three different membranes (PVDF, 0.45 and 1.2 μm pore size for Nylon). Both Nylon membranes reached steady flux earlier than the PVDF membrane, at about 40 min. But 1.2 μm Nylon membrane performed better by 1.4 times higher than the 0.45 μm one according to their concentration factor profile. Moreover, compared with the conventional cross-flow system, steady flux and average shear rate of DMF were 100 L/(h·m^2) and 12000 s^{-1}, which were 5 and 7.5-fold higher than cross-flow systems, respectively.

Rotating Disk Module (RDM) has been largely reported concerning the filtration performances [19, 23, 34, 57, 58, 61, 62, 65, 66, 78, 79, 90, 97, 99, 101, 105, 106, 127, 135, 168-179]. 2 modules similar to DMF with different sizes were built. Both include a disk rotates inside a cylindrical housing around a hollow shaft, through which the retentate is evacuated. But the larger module (RDM-2) receiving a 460 cm^2 annular

membrane area, compared with a 190 cm^2 flat disk membrane in a smaller one (RDM-1). The module performances for 5 inlet/outlet configurations (lateral housing wall, back plate or axial) were compared at a 3 mm disk-membrane gap. The highest permeate flux was obtained at high speeds with the inlet at the backplate and axial retentate outlet. With the increase of the disk-membrane gap from 4 to 18 mm, almost no effect on the permeate flux was observed. In the gap of 10 mm, by equipping disk with nylon mesh in module 1, or eight pairs of 2-mm aluminium rods in module 2, permeate flux increased due to the increment of core velocity coefficient [168]. The gap ratio (disk-membrane gap divided by disk radius) seems relevant to this coefficient [19, 127, 178]. Bouzerar et al. [79] applied RDM in MF of $CaCO_3$ suspension. First, the disk speed was decreased in steps from 1500 rpm to rest in order to evaluate steady-state flux. Then speed was raised again to 1500 rpm to investigate the irreversibility of fouling. Initial peripheral pressure was fixed at 15 kPa, and experiments were performed with 0.1 μm PVDF membranes. Final permeate flux almost kept the same value but represented only 64% of the initial one when conducted at 50 kPa. When the rotation speeds up to 1100 rpm, permeate flux increased with radius and fouling almost disappeared at $r>4$ cm. But in the central part, relatively lower local velocity was not able to eliminate the cake layer. In dairy wastewater treatment [57], RDM configuration was a disk equipped with 4 pairs of 6 mm-high vanes (disk membrane-gap not specified), which can rotate at up to 2500 rpm. Performances were scrutinized versus shear rate (0.169×10^5 to 2.05×10^5 s^{-1}), TMP (3 to7 bar), temperature (35 to 55°C) and membrane cut-off (30 to 10 kDa). Flux decline was observed due to membrane blocking by lactose and milk protein. Shear rate and TMP showed a great effect on membrane fouling control and contributed to the cleaning process. Evaluating the membrane permeability recovery rate, it concluded that high shear rate combined with a cleaning agent is more conducive to fouling elimination. Low TMP presented that the concentration polarization of casein micelles and the cake layer was reduced on membrane surface [62]. In the concentration tests of leaf protein (MF, UF), Zhang et al. [105] modified the loop operation of RDM module into the retentate recycling process (CRDM) and retentate non-recycling process (DRDM). At rotation speed of 1000 rpm, TMP of 3 bar for MF and 4 bar for UF, results indicated the least flux decline, smallest irreversible fouling and highest permeability recovery after membrane cleaning in CRDM, while DRDM obtained the best leaf protein rejection due to the secondary filtration effect. In the treatment of detergent wastewater, NF was performed after the pre-treatment in UF. The permeate flux in NF increased linearly with TMP to reach 450 $L/(m^2\cdot h)$ at 40 bar at the rotation speed of 2000 rpm, while it reached a plateau at 350 $L/(m^2\cdot h)$ above 35 bar without pre-treatment in UF. The rejection of conductivity and COD could be more than 90% when the TMP is up to 20 bar. Increasing feed pH (4.5 to 9.9) and temperature (25 to 45°C) seemed to enhance electrostatic repulsion and led to the increase of permeate flux, but conductivity rejection showed the opposite trend [34]. In this rotating system, the net power consumed by the rotating disk was proportional to the square of rotation speed. Disk with vans presented much higher net power than smooth disk in the same condition. However, it was opposite with specific energy consumption [65, 135]. There were other studies focused on various test fluids [34, 45, 46, 58, 87, 90, 101, 108, 127, 136, 137, 186, 228], and were often compared to the other DF systems [19, 60, 66, 78, 88, 93, 94, 97-99, 104, 229].

The anti-fouling membrane filtration system (FMX) was produced by BKT Water & Energy (Korea), equipped with high-speed rotating vortex generators. They were veined discs and had two uneven and asymmetric surfaces. Standard class FMX-S and economic class FMX-E were proposed with a filtration area of 95 m^2 and 40 m^2. In the pilot-scale, FMX-P compacted several membranes on the rotating shaft in series and reached the space between 0.0873 m^2 to 3.16 m^2 [184]. FMX-B only equipped one rotating disk of 145mm diameter and 10mm thickness in the filtration cell (20 mm height). Membrane (surface area of 0.0146 m^2) was installed at the bottom of the module, while the feed inlet and concentrate outlet were connected to the upper surface. With this module, a CFD simulation was performed by Kim et al. [114]. Fluid velocity and average shear stress of perforated disk on the membrane surface were found to be 2 and 7-fold higher than an unperforated disk, respectively. As the average shear stress increased from 0.23 (0 rpm) to 28.99 Pa (800 rpm), the microalgal fouling resistance reduced by 87%, and the plateau permeate flux was increased 6.7-fold to 381 L/(h·m^2). Effect of rotation speed, TMP, membrane cut-off or biomass concentration on filtration performances had been illustrated associated with permeate flux and fouling resistance [117, 119].

Another rotating disk module derived from Central South University (China) was assembled to separate heavy metal from wastewaters [180, 181, 230]. It shared the same configuration of inlet and outlet with the RDM module. A disk with a radius of 83 mm was driving by a rotating shaft in an 88 mm inner radius circular housing, enable to speed up to 3000 rpm. The model waste of lead nitrate was fully complexed with poly acrylic acid sodium (PAAS) or copolymer of maleic acid and acrylic acid (PMA), then removed by UF. These metal complexes were sensitive to the high shear rate. The results indicated that the critical shear rate of the PMA-Pb complex was less than that of the PAA-Pb complex. But the former case was preferred for the treatment of lead contained wastewater due to its higher load capacity of Pb (II) and easier regeneration [230]. For the separation of Zn (II) from aqueous solutions, the critical shear rate for PAA-Zn complexes was 1.58×10^5 s^{-1} at pH 7.0 [181]. Another publication investigated the critical speed of two disks (smooth disk and disk with 6 vans) to remove the PAA-Cd complex. The critical shear rate for both disks calculated to be 1.31×10^5 s^{-1} at pH 6.0, and the rejection of Cd reached 99.7% [180].

A rotating-disk dynamic filter was designed by Tamkang University (China) [48, 73, 84, 112]. The diameter and height of the chamber are both 38 mm. Two vanes (10 mm×10 mm×1mm) are placed beneath a rotating disk with a diameter of 30 mm. A low circular inlet and a high circular outlet are connected to the chamber for feed inflow and concentrate outflow. A circular membrane is installed on the porous bottom plate with a filtration area of 1.12×10^{-3} m^2 [112]. In MF, SiO_2 was separated from artificial seawater. The pseudo-steady filtration flux was only 1.65 $m^3/(m^2\cdot s)$ for a static disk, but it increased by 170% as ω increased to 500 rpm at a distance of 1.5 mm between vans and membrane. This increase in the flux was more considerable for a smaller gap of 0.8 mm, and the filtration flux increases 2.4-fold as ω increases from 0 to 500 rpm [48]. From another article, 2 vans disk (Type 1), 4 vans disk (Type 2) or 2 vans disk with circular orifices (Type 3) was able to rotate 15 mm above the membrane. It indicated that increasing the disk rotation speed or the number of vanes improves the mean filtration flux, and the holes in the disk have no effect on flux enhancement. The specific filtration flux (flux divided by energy) could be ordered as Type 3＞Type 1＞Type 2, and it also

decreased with the increase of rotation speed [84]. For the same purpose, a larger module with a filtration area of 0.0377 m^2 was established by Hwang et al. [115]. By modifying the disk, 6 types of disks were constructed with different concepts (distance between disk and membrane, number of vans and vans' structure). Considering the filtration flux and power consumption, disk and disk with 2 vans (has an uneven rectangular cross-section) showed to be the optimal designs, and even 4 uniform vans could generate the highest shear stress and result in the highest permeate flux.

A particular configuration of the rotor could be observed in the controlled shear filtration (CSF) module [138]. It has a conical rotor (inclination angle of 4°) of 70 mm diameter rotating at 0.2 mm above a PVDF membrane (51.5 cm^2 effective filtration area) for MF of recombinant BHK cell suspension. The threshold level of shear stability was determined during the sharp decrease of cell viability for the step improvement of rotating speed. An optimal growing cell showed better resistance with shear stress up to 17.2 N/m^2 instead of 7.12 N/m^2 for a lower growing cell. Compared with traditional cross-flow filtration, constant flux 30 $L/(h \cdot m^2)$ and cell viability percentage 83% greatly improved to 97%-91%, 290 $L/(h \cdot m^2)$ with CSF, respectively. Almost with the same configuration, the controlled shear affinity filtration (CSAF) module was investigated with CFD simulation. A new rotor (0.2 mm gap to the membrane) was designed with a variable inclination angle, which permitted the constant shear stress at all radial positions except the centre-point. Meanwhile, the threshold shear stress of 0.17 Pa was achieved across virtually the entire membrane surface at a rotor speed of 250 rpm. It was 60% less than the rotor speed required in the original CSAF device [186].

In rotating cross-flow (RCF) MBR [183], a 156 mm radius of the membrane is placed in the support. With a gap of 5 mm, a disk of 140 mm radius can rotate between 50 and 350 rpm. A single-use medical product LIFE 18-Disk Separator, which was designed to separate plasma from whole blood, two membranes are configured with a spinning disk rotating between them within a plastic housing, and only reaches 50 ml for the volume [185].

3.2.2.2 Rotating impeller

Similar to the rotating disk module, the shape of the impeller also draws much attention. 3 modules were developed into 10 configurations by compacting even up to hundreds of membranes in the filtration cell and increasing the diameter of membranes for large scale applications.

Cross Rotational Filters (CR-filters) was designed by Metso-Paper corp., equipped with two-blade impellers between two membranes. The company proposed several scales for users; diameter could range from 200 to 1010 mm, e.g., the Opti Filter CR-1010/100, with 100 cassettes of 1010 mm diameter, achieve filtration area up to 140 m^2 [188-190, 231]. The DYNO (Bokela GmbH, Karlsruhe, Germany) filter was installed with a blade-like rotor for each filtration cell, reached 12 m^2 of total membrane area [187]. The same concept also has been applied to the Rotating and Vibrating Filtration (RVF) module. A lab-scale RVF module has two identical filtration cells. Each consisted of a three-blade impeller with 135 mm diameter and 8 mm thickness, rotating in a 14 mm gap between two porous substrates, which can operate up to 50 Hz [102, 193].

Gursch et al. [144] reported the continuous manufacturing of active pharmaceutical ingredients with a lab-scale Dynotest system, aluminium oxide disk membranes (0.5 μm)

were equipped with a total filtration area of 0.013 m^2. A material-dependent linear relationship of the permeate flow as a function of cumulated feed flow was found with different fluids; slope *k* made it possible to established a constant concentration factor to predict filtration performance for any given product.

In the paper industry, Jutta et al. [192] described the UF process with CR module, polymeric and ceramic membranes range from 8 to 200 kDa were tested. It was shown that the relatively low cut-off (30 kDa) hydrophilic C30G membrane made from regenerated cellulose had higher fluxes both at neutral and acidic pH. It could last six days of filtration with good permeation. The same reports also have been investigated in NF and RO [190, 231].

Rayess et al. [103] employed MF (PES and PTFE, 0.2 μm) with the RVF module in wine clarification. In the filtration of crude simulated wine, the permeability of PTFE membranes was slightly higher than PES membrane with *N=0* Hz, but it is opposite during filter wine filtration respectively for 1676 L/(h·m^2·bar) (PES) and 170 L/(h·m^2·bar) (PTFE). When N was increasing, PES seemed to be sensitive to the mixing effect, while PTFE showed to be unaffected by the frequency increase. Fillaudeau et al. [102] also tested two ceramic membranes (0.6 to 4 μm) with rough beer. In this research, the driving force at the membrane surface and the core velocity coefficient associated with fluid dynamics were determined with water. Afterwards, the performance of RVF was evaluated for two different rough beers and model beers, which resulted in the ceramic membrane achieving more satisfying quality and flux value than traditional filtrations.

3.2.2.3 Rotating cylinder

As discussed in the rotating cylinder membrane, studies on fixed membrane cylinders have also been reported. 2 modules have been designed in the lab-scale application.

The application of helical Couette-Taylor flow (CTF) [43] could help to reduce fouling in the process of filtration. A tubular membrane module is configured with a tubular metallic membrane (diameter of 30/34 mm, filtration area of 0.04 m^2) as a housing and a coaxial inner cylinder as a rotor (diameter of 20 mm). In order to be applied in radioactive wastes, cobalt ions solution was fed in UF with the metallic membrane. After 720 min circulation, the permeate flux decreased to 8 L/(m^2 s) without mixing. Due to the instability of the flow, it almost 3-fold when the inner cylinder was rotating up to 1500 rpm. Further improvement in the rotation speed seemed to have little effect on the permeation [43]. The optimal hydrodynamic conditions were established by response surface methodology, maximal permeate flux and the minimal flux decline were observed at TMP 70kPa, retentate flowrate 108 L/h and rotating speed 2800 rpm [44].

DYNAMIC HPHT Filtration system [199] equipped with a rotating cylinder, which could simulate the build-up of filter cake on the formation. A 6.3 mm thick porous walled cylinder (inner diameter of 25.8 mm) as the filter medium and rotating shaft of 19 mm diameter is placed within 250 ml high-pressure and high-temperature cell. The mud sample sheared in the annulus formed between the inside diameter of the filter core and the rotating shear shaft. A ceramic filter (5-90 μm) was used in the MF of the drilling fluid. The experimental results fitted with the Boluk-Balavi equation, which could help evaluate the spurt loss volume, the initial rate of fluid volume loss (flux), blocking and cake erosion in DF [199].

3.2.3 Rotating disk and membrane module

The request for DF of large shear stress led to the introduction of a rotating disk and membrane system (2 modules). Disk and membrane are mounted on different shafts, could rotate in the reverse direction.

A shear-enhanced system, namely rotating disk-membrane (RD-M) modules, were investigated on microfiltration of black liquor [32, 33], Ultrafiltration of PEG 6000 and Bovine serum albumin [49, 51, 141]. The membrane was placed on disk-shaped porous support with an effective filtration area of 24.6 cm^2. A stirrer is provided inside the cell, having the same diameter as that of the membrane. They rotate in the opposite direction and give a maximum shear rate of 2×10^5 s^{-1} at the membrane surface. In the UF of BSA, the increment of membrane rotation speed, stirring speed, and TMP are likely to improve the permeate flux. It has been demonstrated that 79.7% of steady-state permeate flux decreased on increasing bulk concentration from 1 g/L to 30 g/L, resulted in the mean residence time increasing from 0.17s to 0.28s. However, TMP did no effect on residence time by increasing 294 kPa to 882 kPa [141]. The influence of membrane disc rotation was found to increase the flux substantially, more than so obtained by stirrer rotation. Nevertheless, the pre-treatment steps proved to be highly efficient in minimizing flux decline [32, 33].

By modifying dynamic cross-flow filtration (DCF), Johannes et al. [96] described a new module. Two rotating shafts equipped with two ceramic membrane disks and one smooth metal blind disk individually, resulting in a membrane filtration area of 0.14 m^2. The disks from each shaft overlapped each other by 26.4% of their surfaces. As a result, MF (0.06 μm pore size) of pasteurized skim milk (3.4%, w/w, protein) could preferably be applied in small scale manufacture of milk retentate for protein contents of ≥14.8% (w/w).

3.3 Oscillating system

Considering the movement part, oscillating could happen in the whole filtration cell (3 modules with 12 configurations) or just occur in the membrane (9 modules with 9 configurations). These motions could be azimuthal, horizontal or axial oscillation. In addition, the spacer oscillation (1 module) also promoter turbulence in the flow.

3.3.1 Oscillating filtration cell modules

3.3.1.1 Oscillating disk cell

Disk membranes are placed on the support to permit the collection of permeate and filtration cell oscillated in the azimuthal direction to generate high shear stress. With this knowledge, 2 companies have designed 11 configurations in lab and industrial applications.

Commercialized by New Logic (USA), vibratory shear enhanced processing (VSEP) [24, 35, 75, 91, 92, 118, 122, 126, 200] represented as the first vibrating filtration device. These filtration bodies, which consist of alternative overlapping membranes or membrane-coated disks in series, are mounted on a torsion bar driven by a motor. It can reach 130 m^2 filtration area per module and scale up by installing more membrane

modules. A similar principle was introduced in the vibrating membrane filtration module (PallSep-VMF) [202]. Industrial VMF biotech modules were available in 0.2, 1 and 5 m² surface areas for more flexibility and easy scale up or scale down [203].

The VSEP L101 was a relatively small pilot-scale module. An annular membrane with an area of 503 cm^2 in a circular housing (with a gap of 3.5 mm) is placed at the top of a vertical shaft, and driven by a torsion spring. This shaft amplified the vibrations to reach the amplitude from 6.35 to 31.75 mm, corresponding to the frequency between 55 and 60.75 Hz. The feed and retentate channels are distributed on both sides of the rotating shaft at the bottom plate. The permeates through the membrane was collected through the holes in the membrane plate support [200]. Akoum et al. [126] investigated the MF of yeast suspensions and the UF of BSA solutions with this module. In the case of yeast MF, the permeate flux was found to be proportional to $\gamma^{0.19}$ at a frequency below 59.7 Hz and to $\gamma^{0.50}$ at a higher frequency. In UF of BSA, the permeate flux was proportional to $\gamma^{0.426}$ at all frequencies. As for the treatment of dairy process water, the membrane oscillated at 60.75 Hz and 40 bar, the highest permeate flux in NF was 270 L/(m^2·h) and the initial COD reduced from 36000 to 94 mg/L. While in RO, final permeate flux was 240 L/(m^2·h) and 36 mg/L COD [59]. Frappart et al. [60] compared the filtration performance of VSEP and RDM with dilute skim milk in RO. The permeate flux for the VSEP working at resonant frequency (60.75 Hz) was very close to the result for RDM rotating at 2000 rpm. The same device has also been applied in other suspensions, such as tannery wastewater [200], latex solution [75], metal working emulsions [67] and microalgae [24, 116, 118].

PallSep PS10 VMF unit consists of two membrane discs, both covered with a hydrophobic PTFE membrane on both sides, giving a total membrane surface area of 0.2 m^2. The feed is delivered to the first membrane disc through a feed channel at the bottom endplate of the VMF membrane assembly. Each membrane disk has 18 circular holes (8.5 mm diameter), whose 12 holes are located at 270 mm on the outer edge and 6 holes at 26 mm in the inner diameter of the disc. The fluid then flows outward in the retentate channel and inwards tangential to the membrane surface towards 6 equally spaced, which is collected in a series of grooves and exits the VMF system through the top end plate permeate port. In the recycle mode of 200 g/L yeast suspension, a decline in permeate flux was observed until a steady-state was achieved after about 20 min with the vibration at 19.5 mm amplitude. Without any vibration, permeate flux was seen to fall to zero in 10 min at the same cross-flow rate of 1 L/min. In the concentration tests of yeast suspension, increased the gap width from 1.4 to 4.2 mm, the maximum solids loading capacity was improved from 561 to 633 g/L. It also indicated that the volume concentration factor would increase with a larger gap width [202].

3.3.1.2 Oscillating rectangular cell

Another lab-scale oscillating filtration cell is vibration enhanced reverse osmosis (VERO) [47, 55, 232], derived from Texas A&M University (USA). A linear actuator was used to vibrate the RO membrane desalination cell at the given vibration curve shape, frequency, and amplitude. Feed solution enters from the left feed port at the top plate, flow into the membrane channel, and left the desalination cell through the retentate port at the other side of the top plate. The permeate flow is collected by the permeate carrier and flows out through the permeate ports at the bottom plate. The height of the feed channel is 0.78 mm and placed with a feed spacer, which just above the flat rectangular

membrane of 60 cm^2 (20 cm×3 cm) filtration area. With this module, Su et al. [47] investigated the desalination of artificial seawater in 3 feeding flowrates related to Reynolds number 344, 516 and 688, respectively. Increasing in flowrates led to the decrease of NaCl and $CaSO_4$ concentration polarization (CP) module without vibration, owing to the sweeping effect of flow. In the vibration cases, shear stress was further increased by the vibration; CP modules decreased when the frequency changed from 20 to 50 Hz. Periodic oscillations caused the fluctuation in normalized permeate flux; the higher the vibration frequency is, the higher the permeate flux. CFD simulation also showed excellent agreement with the results over different Reynolds number.

3.3.2 Oscillating membrane module

3.3.2.1 Oscillating rectangular membrane

Compared with the oscillation filtration cell modules, another kind of device is realized by immersing the oscillating membrane in the filtered liquid. The principle of shear enhancement by the oscillating membrane is generally applied in a rectangular membrane. Different technics aimed to create the horizontal motion of membranes, and 4 modules are reported in recent publications.

Oscillatory flat surface membrane (OFSM) module was proposed by Gomaa et al. [131, 133, 204-207]. A flat membrane (filtration area of 0.06 m^2) is mounted on a membrane frame, fixed with a metal mesh, and immersed in a yeast solution. A vacuum pump is used to collect permeate and control transmembrane pressure. Hydrophilic nylon membranes (0.22 μm) were used in the re-hydrated baker's yeast on the condition of 0-25 Hz (frequency), 3-30 mm (amplitude) and 0.2-0.6 bar (TMP). Increasing oscillation frequency or amplitude resulted in higher permeate flux; the effect of oscillation frequency was found to be stronger than the amplitude [131]. Using higher oscillation frequency and lower amplitude were found to be more effective for flux enhancement and energy utilization [133]. Furthermore, membrane surface equipped with both flat turbulence promoters and grooved turbulence promoters has been proved to improve microfiltration flux further. The combined effect of oscillatory motion and turbulence promoters can result in substantial flux augmentation. Such an effect increased with increasing the oscillation frequency but decreased with its amplitude [133, 206, 207].

With the same concept, a magnetically induced membrane vibration (MMV) system [37, 209-213] consists of one or more flat sheet membranes and is mounted on a metal frame. The oscillation is created by the magnetic attraction/repulsion forces to alternate membrane modules that move up and down with a specific frequency and amplitude. For UF of bio-ethanol from the hydrolysate, 4 membranes were placed in series with a gap of 1 cm with a filtration area of 0.04 m^2. With undiluted feeds (extremely viscous), permeate and TMP showed the same trends with oscillation (frequency:10 Hz, amplitude: 6 mm) and without oscillation. However, these differences were enlarged with diluted feeds (dilution rate: 4 or 6 times). It also indicated that fouling control could be improved by suitable membranes (nature) and higher oscillating amplitude [212]. In other fields such as wastewater treatment, [37, 209, 210] microalgae harvesting [211, 213] have also been investigated.

Tongji University (China) has designed a constant-shear vibration device named the uniform shearing vibration membrane (USVM) [208] system. By the rotating shaft, the

flat rectangular membrane (effective membrane area of 0.02 m^2) installed on a cassette can be operated with a uniform circular motion (not rotating), which induces a constant shear rate at the membrane surface. On the membrane frame, there is an outlet connecting a tube and the permeate can be taken away through the tube using a peristaltic pump. Another axial vibration membrane (AVM) [84, 215, 216] device that reduces membrane fouling by vibrating the shaft along the vertical axis was developed by the same lab. By controlling the servo motor and changing the structure of the rotating shaft, different vibration frequency and amplitude for both devices can be achieved. On a cassette, 1 to 100 flat membranes can be installed in the square frame (11 cm) with the distance between membrane from 1 to 50 mm. Zhao et al. [215] investigated AVM in microalgae harvesting; 0.1 μm PVDF membrane was used to work at any frequency up to 15 Hz and amplitude from 5 to 40 mm. The critical flux is proportional to $\gamma_{max}^{0.2284}$; the motion does not only prevent the deposition of algae cells on the membrane but also reduces the adsorption of extracellular organic matter on the membrane. Horizontal system (USVM) worked at a lower frequency (5 Hz) and amplitude of 20 mm, the same membrane was used. The TMP visibly reduced when the frequency increased from 1 to 5 Hz. Even at a relatively low frequency of 5 Hz, reversible and irreversible membrane fouling could also be limited [208].

3.3.2.2 Oscillating cylinder membrane

With the same concept, azimuthal or axial oscillation can be achieved with cylinder membrane. 2 lab-scale modules were described, the effect of oscillating frequency, amplitude or angle were investigated.

A cylinder membrane (14 mm outside diameter, 64 mm membrane working length) was immersed in calcite suspension, and two modes of oscillations were performed [217]. The axial oscillations can be operated with an adjustable displacement and frequency up to 100 Hz. The azimuthal movement oscillates at 3 degrees with 20 to 100 Hz, the highest shear stress of 240 Pa is reached. The vibration mode did not influence the filtration performance, while it corresponded to the shear stress peak delivered by the oscillating system [217].

With a vibrating head, an axial oscillation of the slotted-pore nickel membrane is controlled up to 100 Hz (frequency) and 10 mm (amplitude) [70]. The fouling of membrane pore area is reduced in the presence of the shear. Compared with crude oil, Tween 20-stabilized oil with decreasing interfacial tension and smaller droplet size, and led to a lower blocking area. The blocking constant at 1000 $L/(m^2 \cdot h)$ (permeate flux) were approximately five times smaller than 200 $L/(m^2 \cdot h)$, caused by the increased permeation of the deformable oil droplets [70].

3.3.2.3 Oscillating hollow fibre membrane

The principle of shear enhancement by oscillation has also been applied to hollow fibre membranes by attaching them to a sliding rod connected to a rotating head. 3 modules have investigated the oscillation of the HF membrane in the axial direction.

A Vibrating hollow fibre microfiltration (VHM) system [218] has 7 MF hollow fibre membranes (40 cm length) with a surface area of 0.0057 m^2. They were potted in a cassette using Araldite glue and then submerged in a yeast suspension tank. This cassette vibrated using a 250 W electric motor at any frequency up to 10 Hz with an amplitude of 4 cm. A relatively monotonic increase in critical flux was observed during the frequency

increased from 0 to 10 Hz. Two-step correlation between critical permeate flux and rotating frequency was established and separated in the frequency of 5 Hz [218]. A similar observation has been investigated by Jaffrin et al. [19] with RDM and VSEP. Specific critical flux was defined as the ratio between critical flux and specific power consumption. The peak value was observed at a low oscillating frequency below 2 Hz and followed with a subsequent drop to low values as the specific power consumption increased [218].

The second module was described by the Technical University of Denmark [129, 130, 219]. The vibrating membrane bioreactor (VMBR) system consists of a module with hollow fibres fixed in parallel between a steel plate at the bottom of the module and a permeate gap at the top. Despite different versions of modules equipped with diverse membranes (filtration area range between 84 and 488 cm^2) and liquid level, these systems were almost identical. A total membrane area of 488 cm^2 is composed of 54 hollow fibres with a length of 12.5 cm; it oscillates with the displacement of 1.175 mm (the peak-to-peak amplitude is twice as big) and frequency up to 30 Hz. In yeast suspension, the PES membrane with a nominal pore size of 0.45 μm was tested, the critical flux was improved up to the maximum oscillating degree. The correlation between shear rate and critical flux was similar to the oscillating rectangular membrane module [215, 219].

The last module was described by Li et al. [71]. Membrane modules (13 HFs with a length of 40 cm, inner/outer diameters of 1/1.7 mm and 1/2 mm) were aligned vertically in parallel, with the distance between two adjacent fibres of 15 mm, and driven by a rotating head. The vibration amplitude varied from 0 to 12 mm accurately, while the vibration frequency from 0 to 15 Hz. In a 4 g/L bentonite solution, experiments were conducted at both constant permeate flux and constant suction pressure conditions. In the constant permeate flux of 30 $L/(m^2 \cdot h)$, the fouling rate of 1.7 mm HFs was almost twice as in 2 mm HFs without oscillation. The fouling rate typically decreased when vibration was applied. There was an 85% reduction in the fouling rate when the 2 mm HFs vibrated with 5 mm amplitude and 5 Hz frequency, comparing to no vibration. At constant suction pressure of -24 kPa, cake resistance implied that the larger fibre size could perform better in an oscillating system. As for the power consumption, 95% fouling reduction was observed with 8 mm amplitude and 10 Hz frequency, and consumed 16.6 W power. With the same setup, 21 W power was needed to achieve a 10% fouling reduction by 5 L/min bubbling rate [71].

3.3.3 Oscillating spacers module

3.3.3.1 Oscillating rectangular spacers

Rotating or oscillating membrane/filtration cell involves the movement of membrane cassette and permeates inside of the membrane module. It requires a relatively high mechanical energy and a complicated membrane module. The alternative of a lightweight spacer in turbulence promoter permits to minimize energy consumption regarding oscillation.

A submerged flat sheet membrane filtration system with vibrating spacers was introduced by Nanyang Technological University (Singapore) [221]. Two pieces of flat sheet membranes (8 cm×12 cm) with a total area of 70 cm^2 were mounted into a membrane module and then submerged into a tank. With a distance of 0.1 or 1 mm, both

spacers were placed at each side of the membrane module and enabled to oscillate at 1-2.5 Hz (frequency) and 0.8-2 cm (amplitude). At a distance of 0.1 mm between the spacers and membrane, the hill-like spacers more efficiently alleviated membrane fouling than smooth and grooves spacers. The increase in vibration frequency and amplitude led to the reduction of fouling, but the threshold operation presented to be 2 Hz and 1.2 cm with a hill-like spacer. As expected, spacer vibration consumed significantly less power (<0.008 W/m^2) than gas sparging (5.7 W/m^2) under the comparable fouling control effectiveness [221].

3.4 Oscillating and vibrating system

Vibrating system is not helpful for the permeate flux due to the compacting/cleaning effect during the back-and-forth movement of the membrane, a pure vibrating system does not exist yet. By the oscillation or vibration of HF membranes, transverse or axial movements may lead to a variety of flux directions, which corresponded to the combination of oscillating and vibrating modes. Five devices at a lab-scale were investigated.

The transverse vibrating hollow fibre membrane system was reported and compared with the case of oscillating liquid [132]. The former one was driven by the rotor to vibrate the hollow fibre membrane, with the displacement varying from 0.5 to 5 mm. Another one performed the circular movement of container (liquid) with an eccentric axis (fixed radius: 2.5 mm), and frequency up to 2200 oscillations per minute (36.6 Hz). MF of 100mg/L alginate solution with 0.2 μm HF membrane resulted in the permeate flux of 70 $L/(m^2 \cdot h)$, increased to 105 $L/(m^2 \cdot h)$ with the aid of liquid oscillation frequency of 6.7 Hz. However, this method was limited to small scale applications. Oscillating transverse motion via vibrating membranes was expected to be more practical for large-scale applications. The critical flux of 4 g/L yeast solution with the transverse membrane vibrations (10.3 Hz, displacement 2.5 mm) was found to be 40 $L/(m^2\ h)$, while it was 35 $L/(m^2\ h)$ under the oscillating liquid (at 10 Hz, displacement 2.5 mm) [132]. In the separation and concentration of milk proteins with 0.04 μm PVDF HF membrane, Chai et al. [222] summarized that the frequency of 10.3 Hz applied could fully reject the casein micelle and maintain very high transmission rates of whey proteins (α-LA and β-LG) and lactose.

Derived from the same institution (University of New South Wales, Australia), the axial vibration module was introduced [22]. 32 hollow fibre membranes (total membrane area: 0.0131 m^2) were arranged in a tube-like shaft, immersed in a 6 L filtration column and held in place through a rod connected to an oscillation converter. This configuration allows the angular displacement to vary from 18.3° to 55°. Different yeast concentrations of 10, 100 and 200 g/L in MF had little effect on the permeate flux with the aid of oscillating or vibrating at 10.3 Hz. The critical flux was not sensitive to the packing density of HFs in the module but highly dependent on frequency [22].

The same idea was also applied in another module. Two ends of the hollow fibre membrane were potted together to access the permeable channel, 7 fibres with a length of 10 cm, resulting in a total membrane area of approximately 45 cm^2. Angular vibrations generated by the motor convertor worked with fixed angular displacement of 180°, and frequency controlled between 0 and 2 Hz. The results indicated the effects of angular vibrations on the fouling rate at the frequency of 2 Hz in the following order: algal cells

(~97.4%) > debris (~93.6%) > intracellular organic matter (~81.8%) > extracellular organic matter (~52.3%). A poor effect was found on pore blocking due to a large portion of extracellular organic matter fouling [123].

Zhejiang University (China) introduced a vibrated submerged HF membrane module that achieved two motion modes by adjusting the vibrating shaft. The membrane was moved from forth and back in axial (mode-1) or left to right (mode-2) displacement through a sine wave pattern. Membrane oscillation could be vertical or parallel to the module, respectively. In the standard module (without oscillation), the steady-state membrane permeability was 3.27 L/(m^2·h·bar), whereas, mode-1 and mode-2 (optimal) were stabilized over 21 L/(m^2·h·bar) at 20 rpm. Increasing the vibrating speed also helped to reduce the permeability decline [225].

The San Bortolo Hospital (Italy) introduced the concept of mechanical vibration to the hollow fibre dialysis membrane system [223, 224]. Four types of shaking models were established to increase the shear rate at the membrane surface: i) longitudinal shaking produced the reverse flow in the central and peripheral region of single hollow fibre; ii) transverse shaking developed a symmetric swirling to shaking direction and spiral flow pathlines; iii) rotational shaking to longitudinal axis also developed symmetric swirling flow regimes inside the HF, but the local shear rate presented non-uniform distribution in the radial position of HF bundle; and iv) rotational shaking to the centroid resulted in lengthwise non-uniform hemodynamic enhancement and reached the maximum at the inlet and outlet [223].

4. CHARACTERIZATION OF FLUID FLOW IN DYNAMIC FILTRATION

It is well known that the principle of dynamic filtration consists of creating relative motion between the membrane and its housing to generate a high shear rate at the membrane surface and/or oscillating flows. Among the advantages of DF devices, the ability to generate a high shear rate independently of the feed flow, the preservation of a high membrane permeability associated with the filtration at low TMP, and the reduction of the filtration loop volume, can be highlighted. Combining all these factors limits the fouling propensity and compressibility at the membrane surface [57, 79, 88, 97, 127, 168], which appears as major advantages for UF and MF, especially for the filtration of biological matrices. Film theory stands as the most common theoretical approach to describe permeation flux independently of pressure for mass transfer limited system.

4.1 Global approaches

4.1.1 Dimensionless analysis

4.1.1.1 Reynolds number

The well-known Reynolds number, *Re*, is the most common number used in fluid mechanics to characterize the flow regime (laminar, transient or turbulent). It is defined as the ratio between the inertia forces and the viscous forces. For convenience, it is generally written in the form of a length scale, the so-called hydraulic diameter d_h, a velocity scale *u* and the kinematic viscosity *v* of the fluid, as follows: $Re = \frac{u d_h}{v}$.

Due to the complex geometry and operating conditions encountered in dynamic filtration devices (enclosed rotating disc/ impeller, static or rotating membrane, oscillating and vibrating module), different expressions of the Reynolds were proposed (see Table. 7). Based on $v = \frac{\mu}{\rho}$, all equations are given with dynamic viscosity μ, where ρ is the fluid density.

Table. 7 Dimensionless numbers used to describe hydrodynamic within Dynamic Filtration device (d: diameter, u: velocity, Q: flowrate, r: radius, d_h: hydraulic diameter, r_h: hydraulic radius, d_o: outer diameter; d_i: inner diameter, u_z, axial flow velocity, N: mixing rate, d_m: rotor diameter, k: core velocity coefficient, ω: angular velocity, h: rotor height, α : inclination angle of conical rotor, s: characteristic length scale, F: oscillating/ vibrating frequency, H: vertical distance)

Mode	Formula	Equation
Tube	$\mathrm{Re} = \frac{\rho \mathrm{d} \mathrm{u}}{\mu}$ or $\mathrm{Re}_Q = \frac{\rho \mathrm{Q}}{\mu \pi r}$	*Eq. 1*
Equivalent tube	$\mathrm{Re} = \frac{\rho \mathrm{d}_h \mathrm{u}}{\mu}$ or $\mathrm{Re}_Q = \frac{\rho \mathrm{Q}}{\mu \pi r_h}$	*Eq. 2*
Annulus tube	$\mathrm{Re} = \frac{\rho (d_o - d_i) \mathrm{u}}{\mu}$	*Eq. 3*
Axial flow in annulus	$\mathrm{Re}_a = \frac{2 \rho \mathrm{d} \mathrm{u}_z}{\mu}$	*Eq. 4*
Rotating system (mixing)	$\mathrm{Re}_m = \frac{\rho \mathrm{N} \mathrm{d}_m^2}{\mu}$	*Eq. 5*

Rotating system*	$\mathrm{Re}_r = \frac{\mathrm{k}\rho\omega r^2}{\mu}$	*Eq. 6*
Rotating cone	$\mathrm{Re}_s = \frac{\rho\omega(\mathrm{h} + \mathrm{r}\tan\alpha)^2}{\mu}$	*Eq. 7*
Gap based Ekman number	$\mathrm{Ek} = \frac{1}{Re_s} = \frac{\mu}{\rho\omega s^2}$	*Eq. 8*
Oscillating/Vibrating system	$\mathrm{Re}_v = \frac{2\pi \mathrm{F} H^2}{\rho}$	*Eq. 9*

As can be seen, the hydraulic diameter d_h is equal to the outer diameter of the tube minus inner diameter (d_o: outer diameter; d_i: inner diameter) for an annulus tube in Eq. 3. According to the different operating conditions, the velocity scale can be defined using flowrate Q, see Eq. 1 and Eq. 2. However, when this annulus coaxial cylinder was fed by axial flow, it can be defined as the axial velocity [83, 233].

In the rotating system, the Reynolds number is calculated from the angular velocity ω as $Re = (\rho\omega r^2)/\mu$ or by mixing rate N as shown in Eq. 5. But in practical applications, angular velocity should be replaced by $k\omega$ considering the transmission of impeller velocity to the fluid. Reynolds number induced by rotating disk/impeller is described by Eq. 6. An axial Reynolds number of a rotating conical rotor system was given as Eq. 7, where the rotor height h and the inclination angle α were taken into account [138, 186]. And Reynolds number can be expressed as a reverse of the Ekman number Ek as Eq. 8 shows. Ekman number characterizes the ratio of viscous drag forces in a fluid to the Coriolis forces [234].

Four different flow patterns of rotating disk in a housing system were proposed by researchers[125, 183]: Re_r is radial Reynolds number, z/R_m refers to the gap ratio (z is the distance between rotor and membrane, R_m is the radius of the rotor). With a flowrate equal to zero, four flow regimes (Table. 8) may appear in the filtration cell, and they have been described by Murkes & Carlsson (1988) [235]:

Table. 8 Four flow pattern in rotating system

$\mathrm{Re_r}$	$\mathrm{z/R_m}$	Flow regime	Pattern
$<2\text{-}3\times10^5$	<0.05	Laminar	I
$<2\text{-}3\times10^5$	>0.05	Laminar	II
$>2\text{-}3\times10^5$	<0.05	Turbulent	III
$>2\text{-}3\times10^5$	>0.05	Turbulent	IV

Laminar regime I correspond to a small gap, with Couette flow and pressure gradient. When it comes to laminar regime II, the gap is more critical, and limiting layers are developing at stator and rotor surfaces. Close to the rotor, centrifugal forces eject the fluid outwardly compared to the shaft, whereas, at the membrane surface (stator), radial velocity induced centripetal forces concerning the continuity equation. The thickness of the limiting layer on the stator surface is theoretically four times higher than on the stator for an infinite disk. With this theory, limiting layers are separated in turbulent regime IV.

In the oscillating system, the flow is governed by various parameters (oscillation frequency, amplitude, gap). This system was early studied by Rosenblat [236], who used two parallel infinite plane disks, oscillate torsional driven by a common axis for a Newtonian fluid. The Reynolds number is defined as a function of oscillation frequency

F and the distance between disks, shown as Eq. 9. It has been applied to a commercial VSEP system, Reynolds number could reach 3×10^5 [116, 126].

4.1.1.2 Taylor number

The flow between two concentric cylinders with the inner one is rotating and an axial flow in the annulus cylinder. Due to the shear generated by the rotation, inertial forces tend to destabilize a system, whereas viscous forces tend to stabilize the turbulence. Taylor number (*Ta*) is defined as the centrifugal force due to rotation of a fluid relative to viscous forces, which is well discussed in Taylor–Couette flow [83, 167]. Taylor vortices would appear when the *Ta* reaches specific values. As shown in equation $Ta = \frac{\omega r_i z}{v}(\frac{2z}{r_i+r_o})^{0.5}$, r_i and r_o indicate the radius of the inner cylinder and housing cylinder, respectively, z is the distance between them. When $z/r_i \ll 1$, it could be simplified with $Ta = \frac{\omega {r_i}^{0.5} z^{1.5}}{v}$. *Ta* <*42*, the flow is in laminar regime. Further increase the rotation speed, Taylor vortices start to form, and these vortices increase until 400 (as described in the transition zone) [237]. When the Taylor number is above 400, these vortices degenerate into fully developed turbulent flow.

4.1.1.3 Mass transfer

Dimension analysis of mass transfer (by analogy with heat transfer) lead to establishing the semi-empirical correlation between dimensionless numbers,

Sherwood *(Sh)*, $Sh = \frac{k_m d_h}{D} = \frac{d_h}{\delta}$, Schmidt *(Sc)*, $Sc = \frac{\nu}{D} = \frac{\mu}{\rho D}$ and Reynolds *(Re)*, $Re = \frac{\rho d_h u}{\mu}$ such as *f(Sh, Re, Sc)=0,* in laminar regime $Sh = A'Re^{\alpha}Sc^{\beta}\left(\frac{d_h}{L}\right)^{\varepsilon}$ and in turbulent regime $Sh = A''Re^{\alpha}Sc^{\beta}$ [6] (*D*: diffusion coefficient, k_m: transfer coefficient, d_h: hydraulic diameter, *L*: channel length, δ: thickness of limiting layer, μ: viscosity, *u*: velocity, ρ: density).

For laminar flow in a thin rectangular channel [238-240], Sherwood was presented with Graezt-Lévêque's correlation): $Sh = 1.62\left(ReSc\left(\frac{d_h}{L}\right)\right)^{1/3}$ with $100 < ReSc\left(\frac{d_h}{L}\right) < 5000$. By rearranging, it becomes $k_m = 1.62\left(\frac{uD^2}{d_h L}\right)^{1/3}$ and $k_m = 0.816\left(\frac{\gamma}{L}D\right)^{1/3}$ with $\gamma = 8u/d_h$. In turbulent regime (Dittus-Boelter's equation): $Sh = 0.023Re^{0.80}Sc^{1/3}$ with *Re*>*10000*.

In an agitated cylindrical vessel, Colton [241] has proposed the following correlation: In laminar boundary layer, $8000 < \frac{\omega r^2}{v} < 32000$, $Sh = 0.285\left(\frac{\omega r^2}{v}\right)^{0.55}(\frac{v}{D})^{0.33}$. In turbulent boundary layer, $32000 < \frac{\omega r^2}{v} < 82000$, $Sh = 0.0443\left(\frac{\omega r^2}{v}\right)^{0.75}(\frac{v}{D})^{0.33}$. Both cases share the same exponent of Schmidt and similar Reynolds, but the slop is higher at mixing condition.

These relations make it possible to evaluate the mass transfer coefficient, k_m. It leads to determine how membrane geometry and operating conditions may be selected to improve the filtration flux. These expressions require the identification of diffusion coefficient, *D* of solutes retained by the membrane in water (solvent). These relations highlight that flux may increase if flowrate increases or cross-section reduces. From a

general standpoint, all hydrodynamics techniques to increase flow velocity and the shear rate at the membrane surface enable to increase flux [238]. In microfiltration, various recent theories take into account the hydrodynamics: i) lateral migration of particles (tubular pinch effect), ii) axial migration of deposit (flowing cake) or hydrodynamic diffusion generated by shear rate (shear-induced diffusion). To enhance the understanding of the transfer mechanism in the membrane process, it seems essential to investigate and characterize hydrodynamics (velocity field, shear rate, flow regime) at local and global scales.

4.1.2 Friction and power consumption curves

In mixing device, the power consumption curve is the representation of Power number, N_p (Eq. 10) against mixing Reynolds number, Re_m (Eq. 5). The characteristic curve integrates the tank configurations, fluid rheological behaviours and operating conditions. The mixing Reynolds number informs about the flow regimes while the Power number N_p is associated with power consumption (P).

$$N_p = \frac{P}{\rho N^3 d_m^5} \qquad \textit{Eq. 10}$$

In a continuous process, the friction curve represents Darcy's number, Da (Eq. 12) against Reynolds number, Re_Q (Eq. 11). This curve predicts the frictional energy loss in a pipe or equivalent pipe based on the geometrical properties, fluid characteristic and operating conditions. The friction curve can be described using a unique expression (Eq. 13) based on Churchill's model [242]. This general expression can be used for laminar, transitory or turbulent flow regimes.

$$Re_Q = \frac{\rho u d_h}{\mu} = \frac{2\rho Q}{\mu \pi d_h} \qquad \textit{Eq. 11}$$

$$Da = \frac{8\tau_p}{\rho u^2} = \frac{\Delta p d_h}{4L\rho u^2} \qquad \textit{Eq. 12}$$

$$Da = \left(((Da)_{tur}^{n1} + (Da)_{tran}^{n1})^{\frac{n2}{n1}} + (Da)_{lam}^{n2} \right)^{\frac{1}{n2}} \qquad \textit{Eq. 13}$$

The friction (Fig. 7) and the power consumption (Fig. 8) curves of the RVF module were previously established [193] and aim to predict the pressure drop and energy demand for mixing. Considering Churchill's model, a unique correlation between $Da/Da_{N=0}$ and $Re_Q^{0.72}/Re_m^{1.08}$ was proposed. It indicated that this friction is related to the mixing rate and flowrate (laminar flow regime: $Re_Q<3$, $Re_m<2000$, transition flow regime: $3<Re_Q<50$, $2000<Re_m<300000$ and turbulent flow regime: $Re_Q>50$, $Re_m>300000$). On the opposite, power number seemed to be independent of the flowrate.

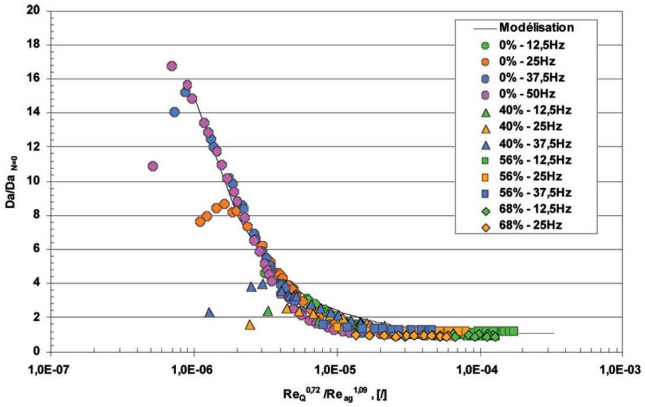

Fig. 7 Friction curve established with RVF lab-scale module [193]

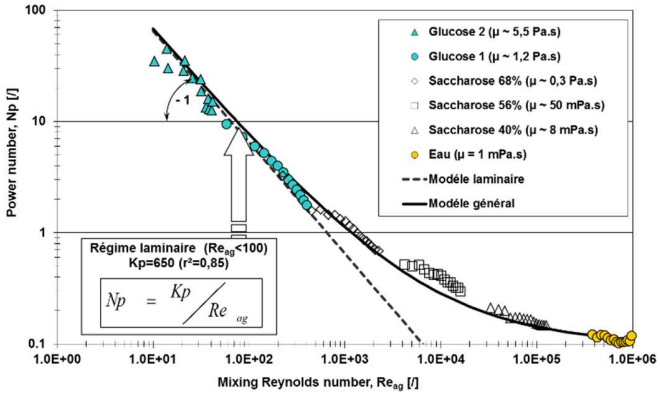

Fig. 8 Power consumption curve established with RVF lab-scale module [193]

4.2 Semi-local approaches

4.2.1 Radial pressure and core velocity coefficient

In the rotational DF device, the mechanical pieces in rotation and fluid flow generate additional radial pressure. The core velocity coefficient appears as a critical parameter to define the additional pressure, whose value is a complex function of the gap, radial position, mixing rate and geometry of rotating disk (smooth disk, modified surface disk, flat blade mixer).

4.2.1.1 Radial pressure

The impact of additional pressure due to mixing was studied previously [102, 103, 193], Permeate flux J is calculated according to Darcy's law,

$$J = \frac{Q_p}{S} = \frac{\Delta P}{\mu_p R_h} = Lp\Delta P \quad with \quad \Delta P = \frac{(P_{in}+P_{out})}{2} - P_p \qquad Eq.\ 14$$

where J: flux, Q_p: permeate flowrate, S: membrane surface area, ΔP: the transmembrane pressure, μ_p: the permeate viscosity, R_h: the total hydraulic resistance, L_p: the permeability, P_{in}, P_{out} and P_p are respectively inlet, outlet and permeate pressures.

Bouzerar et al. [19, 168, 239] indicated that in the core fluid layer, fluid velocity could be calculated by $\cdot 2\pi kN$, where k is the core velocity coefficient inferior to 1. The core velocity coefficient highly depends on system geometry, such as the configuration of the mixer, distance from the mixer to the membrane. Therefore, the radial pressure gradient in the core layer can be expressed by:

$$\frac{\partial p}{\partial r} = \rho r(2\pi kN)^2 \qquad \textit{Eq. 15}$$

$$p(r) = p_0 + \rho g z(r) + 2\rho(k\pi N)^2 r^2 \qquad \textit{Eq. 16}$$

where p is the pressure and R is the radius.

The pressure field is then obtained by the integration of Eq. 15, and achieved the mean additional pressure by Eq. 16 over membrane area from R_0 to R_{max}. Due to the specification of impeller design [102], the hydrodynamic perturbation generated by this three-blade impeller in the gap (membrane to impeller) is different from a full flat disk. This perturbation is including the contribution of rotation speed (N) and additional pressure fluctuation (ΔP_{ag}). Additional pressure ΔP_{ag} deduced by measuring the flux versus the radial position and the rotation speed (Fig. 9). The flux was measured versus the frequency and compared to the case rotation speed equal to zero (Eq. 17 and Eq. 18):

$$J(0, R\ to\ R + dR) = \frac{\Delta P}{\mu_p R_h} \qquad \textit{Eq. 17}$$

$$J(N, R\ to\ R + dR) = \frac{\left(\Delta P + \Delta P_{ag}(N, R)\right)}{\mu_p R_h} \qquad \textit{Eq. 18}$$

where R_h is the hydraulic resistance of the clean membrane. Transmembrane pressure can be expressed by $\Delta P = p(r) - \Delta P_{ag}(N,\ r)$.

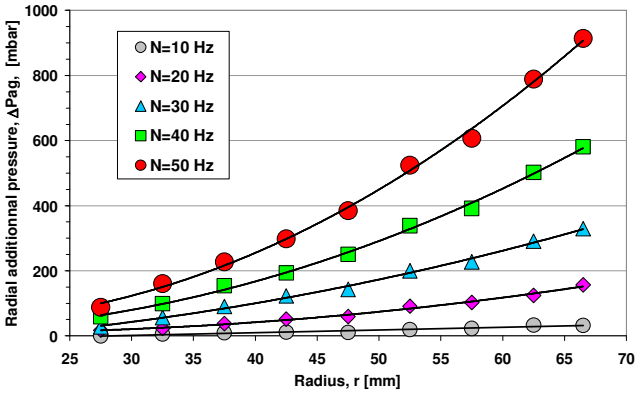

Fig. 9 Determination of hydrodynamic performances, evolution of the radial pressure distribution versus the radius and the rotational speed [193]

TMP is related to the permeate flowrate in dynamic filtration. Fig. 9 showed the linear relationship between the additional pressure induced by the rotating impeller with R^2. The rotating disk equipped with 8 vans increases peripheral pressure in the filtration cell [168]. Fillaudeau et al. [102] have investigated the local pressure by replacing the membrane with radial permeable crowns in a rotating system. A 5 mm gap permits measurement of the radial pressure at the membrane surface. The final results agree with

the empirical equation (Eq. 15) and almost share the same core velocity coefficient with the same configuration [102, 168], indicating that the k value could help to estimate the local pressure. It means that local pressure is highly dependent on the configurations of devices and operating conditions. Furthermore, many efforts (special-designed rotors [84, 115, 168], inserts [53, 95], turbulence promoters [133, 221], and aeration [213]) focused on the improvement of shear stress by generating the disturbance of flow, which resulted in the variation of local pressure over time. The fluctuation of local pressure should be further investigated to reveal the benefits of non-stationary effects on the improvement of filtration.

4.2.1.2 Core velocity coefficient

Core velocity coefficient, k, the ratio of mean fluid velocity to impeller velocity, is one of the critical factors that present the mechanical efficiency of the rotating system as an indicator to quantify the mechanical efficiency. The k for different configurations of DF modules were displayed in Table. 9.

The flow between a stationary and a rotating disk system was early studied by Wilson et al. [243]. They proved that the flow pattern between these two disks was different. Radial flow close to the rotor was centrifugally outwards, and it was directly inwards close to the stator. Two cases had different boundary layers, and suction effect will reduce the thickness. Then a concept of rotation rate was presented and equal to 0.3131 at $Re=10^4$; it characterized the fluid rotating at an angular velocity $0.3131\times2\pi N$ with the rotor rotating at $2\pi N$.

Most people are likely to be interested in improving k by increasing surface roughness or modifying device configurations. The flow field between a stationary membrane and a rotating disk was studied by Bouzerar et al. [168], resulting in the velocity coefficient was influenced by system geometry and configuration, to be 0.34 for a smooth flat disk, and rise to 0.62 for a flat disk equipped with vanes. Furthermore, this influence was further investigated by Brou et al. [127] by modifying the distance of disk to the membrane, and they found that coefficient rises from 0.45 with the smooth disk in 17 mm gap to 0.65 in 15 mm gap for disk equipped with 8 pairs of 2 mm thickness vanes. In addition, a disk equipped with more vans or vans with larger height but with the same gap between disk and membrane has been confirmed to be useful in increasing the core velocity coefficient. The disk has reached a larger k value (0.84) with 8 pairs of 6 mm thickness vanes [127, 178]. As for another rotor, a three-blade impeller in a 3 mm rotor-to-membrane gap has been performed in the RVF module with k equal to 0.71 [102].

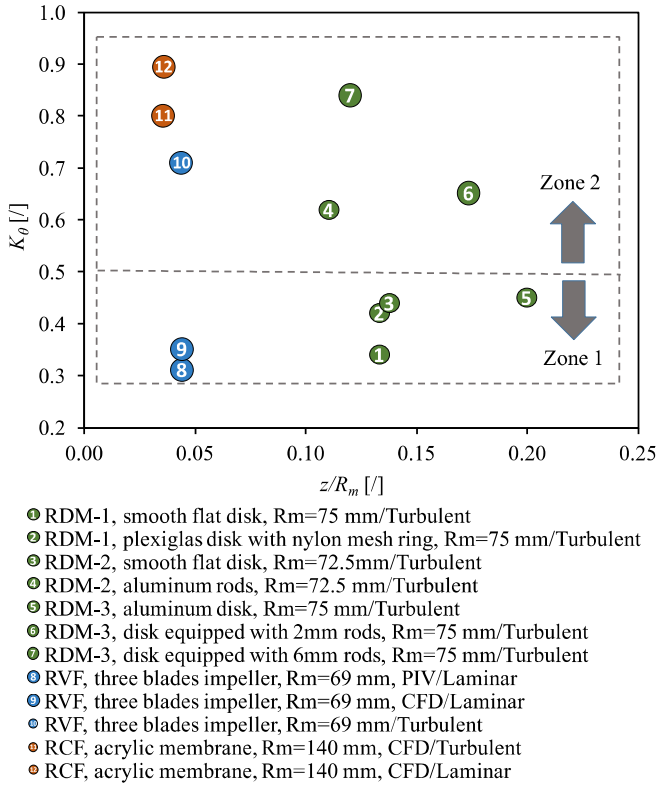

Fig. 10 Evolution of core velocity coefficient, K_θ as a function of gap-to-radius ratio, z/Rm. Values are reported from literature for DF modules using confined rotating impeller close to the membrane and established under laminar or turbulent regimes [195]

Among the different rotating systems, the ratio z/R_m was used to characterize the geometry of the DF module, where z is the minimal distance between impeller or disk (considering geometrical modification) and the membrane, R_m is the radius of the rotor. The lowest values in Zone 1 ($k=0.3–0.5$) and the enhanced mechanical efficiency in Zone 2 ($k>0.5$) were described by Xie et al. in Fig. 10 [195].

Little researches are focused on the investigation of the core velocity coefficient in the laminar regime. Bentzen et al. [183] have conducted CFD simulations in laminar and turbulent regimes. They report $k=0.8$ (turbulent) and 0.9 (laminar) for a rotating cross-flow MBR installed with a plastic disk rotor ($z/R_m=0.0357$). These values are very close, which is unexpected for the laminar regime. In RVF module (with a 3 blades impeller), the local flow was identified by PIV measurements and CFD simulation in laminar regime, which provides a similar value of 0.3 and 0.35, respectively [195].

Table. 9 Core velocity coefficient of different DF filters

Module	Rotor	z (mm)	z/R_m	Flow regime	Testing fluid	k	Ref.

Rotating infinite disks	One disk rotates	/	/	/	Reynolds numbers $Re=l0^4$	0.3131	[243]
RDM (154 mm housing)	Plexiglas flat disk (smooth)	10	0.13	Turbulent	CaCO3 suspension, 60 kg/m^3	0.32	[168]
	PVC flat disk			Turbulent		0.35	
	Disk with mesh		0.13	Turbulent		0.43	
	Smooth flat disk			Turbulent		0.44	
	Disk with 8 pairs of 2mm rods		0.14	Turbulent		0.62	
RDM (154 mm housing)	Smooth flat disk	8	0.11	Turbulent	Water	0.45	[19]
	Disk with 8 pairs of 6mm vans		0.11	Turbulent		0.84	
RDM (154 mm housing)	Smooth flat disk	15	0.21	Turbulent	Water	0.42	[178]
	Disk with 8 pairs of 2mm vans			Turbulent		0.65	
	Disk with 8 pairs of 4mm vans			Turbulent		0.71	
	Disk with 8 pairs of 6mm vans			Turbulent		0.79	
RDM (176 mm housing)	Flat disk	14	0.17	Turbulent	Water	0.44	[180]
	Disk with 6 of 2mm rectangular vanes	12	0.14	Turbulent		0.79	
	Smooth flat disk	17	0.23	Turbulent		0.45	
	Disk with 8 pairs of 2mm vans	15	0.21	Turbulent		0.65	
RDM (154 mm housing)	Disk with 4 pairs of 4mm vans	15	0.21	Turbulent	Baker yeast suspension, 3g/L	0.69	[127]
	Disk with 8 pairs of 4mm vans	15	0.21	Turbulent		0.71	
	Disk with 8 pairs of 6mm vans	15	0.21	Turbulent		0.84	
RVF (154 mm housing)	3 blades impeller	3	0.04	Turbulent	Water	0.71	[102]
				Laminar	PIV	0.3	[195]
				Laminar	CFD	0.35	
RCF (352.6 mm housing)	Plastic flat disk	5	0.04	Laminar	CFD	0.895	[183]
				Turbulent	CFD	0.795	

4.2.2 Shear rate and shear stress

In dynamic filtration, separation efficiency and productivity are highly dependent on the selection of membrane types and materials. However, as mentioned previously, the shear rate is one of the crucial factors, which can control membrane fouling and enhance permeate flux. Some theoretical and semi-empirical mathematical models for calculating the shear rate in different systems are presented in this section.

In general, the shear rate between two disks can be estimated according to viscosity law, with the flow velocity, u and the gap, y:

$$\gamma = \frac{du}{dy} \qquad \textit{Eq. 19}$$

Or by the shear stress, τ and the fluid viscosity, μ:

$$\gamma = \frac{\tau}{\mu} \qquad \textit{Eq. 20}$$

4.2.2.1 Rotating systems

In rotating systems, flow is governed by centrifugal forces generated by rotors, and induce different flow pattern near the rotor and the stator. Considering the boundary theory, four different flow regimes were presented, according to azimuthal Reynolds number and the gap to radius ratio z/R_m, and shear rates at rotor (γ_R) and membrane (γ_S) surfaces were defined in Table. 10:

Table. 10 Shear rate of four flow regimes in a rotation system

Regime	Rotor		Stator	
I	$\gamma_R = \frac{\omega r}{z}$	*Eq. 21*	$\gamma_S = \frac{\omega r}{z}$	*Eq. 22*
II	$\gamma_R = 1.81\frac{(k\omega)^{3/2} r}{v^{1/2}}$	*Eq. 23*	$\gamma_S = 0.77\frac{(k\omega)^{3/2} r}{v^{1/2}}$	*Eq. 24*
III	$\gamma_R = 0.008\frac{(\omega r)^{7/4}(v/z)^{1/4}}{v}$	*Eq. 25*	$\gamma_S = 0.0115\frac{(\omega r)^{7/4}(v/z)^{1/4}}{v}$	*Eq. 26*
IV	$\gamma_R = 0.057\frac{(k\omega)^{9/5} r^{8/5}}{v^{4/5}}$	*Eq. 27*	$\gamma_S = 0.0296\frac{(k\omega)^{9/5} r^{8/5}}{v^{4/5}}$	*Eq. 28*

Bouzerar et al. [168] obtained the same expression of Eq. 24 and Eq. 28 for laminar and turbulent flow for investigating the RDM system. By assuming a thinner gap between the rotor and membrane, boundary layers merged. The narrow gap, s represents the layer thickness, Eq. 25 and Eq. 26 give the shear rates for rotor and stator, respectively [87, 235, 244]. Bendick et al. [150] assumed that steady state flux J_{ss} evolves as a function of γ and Re in the rotating membrane system HSR-MS. They confirmed the Jss-Re and Jss-γ relationships and extended the model for further prediction with larger membranes. With this theory, shear rates on the rotating membrane surface with a membrane diameter of 267 mm were characterized using Eq. 23 in laminar flow and Eq. 27 in turbulent flow.

Vogel et al. [138] considered the average shear rate γ_{av} in the gap between the conical rotor and the membrane in CSF system. It could be estimated by the angular velocity ω, the radius of the rotating cone r, the distance between the cone and the membrane h, and the inclination angle of the cone α as Eq. 29 shown.

$$\gamma_{av} = \frac{\omega r}{h + r tan\alpha} \quad \textit{Eq. 29}$$

Lee et al. [54] calculated the shear rate in an annulus of coaxes cylindrical RO membrane system as Eq. 30 shown, where f was a velocity factor and depended on the flow regime. They considered the circumferential velocity was uniform in the centre of the annulus at about $r_i\omega/2$. The maximum shear rate was generated close to the rotating inner cylinder.

$$\gamma_{max} = f\left(\frac{\omega r_i}{r_0 - r_i}\right) \quad \textit{Eq. 30}$$

Atsumi et al. [245] described the shear rate in an annulus of a coaxes cylinder. The Couette-Taylor flow has been studied intensively and the wall shear stress, τ is given below (Eq. 31):

$$\tau = f\rho\omega^2 r_i^2/2 \quad \text{for} \quad 0.03 \leq d/r_i \leq 1.0 \quad \textit{Eq. 31}$$

where ω was angular velocity, r_i was the radius of the inner cylinder, d was the gap between two cylinders, f denoted the friction factor, was determined by the flow and could be described as the following equation Eq. 32 and Eq. 33. Reynolds number is given in Eq. 3, while Re_C stood as the critical Reynolds number, at which Taylor vortex begins.

$$f = \frac{4(1+\frac{d}{r_i})^2}{(2+\frac{d}{r_i})Re} \quad \text{for } 20 \leq Re \leq Re_C \quad \textit{Eq. 32}$$

$$f = 0.08(\frac{d}{r_i})^{0.35} Re^{-0.53} \quad \text{for } Re_C \leq Re \leq 10^4 \quad \textit{Eq. 33}$$

4.2.2.2 Oscillating systems

Azimuthal and axial oscillation are two strategies to reduce fouling by generating torsion or oscillating on the membrane. VSEP is a general module that has been largely reported.

Rosenblatt et al. early studied the flow between oscillating disks [236]. And Akoum et al. [126] calculated the local shear rate on the membrane in a lab-scale VSEP system by Eq. 34:

$$\gamma_w(r,t) = \left.\frac{\partial V}{\partial Z}\right|_{z=0} = \left.\frac{\partial V}{\partial Z}\right|_{z=h} = \frac{r\Omega}{h}\sqrt{\frac{Re}{2}}G(t) \quad \textit{Eq. 34}$$

$$\gamma_w(r,t) = \frac{r}{R_2} d_r (\pi F)^{1.5} v^{-0.5} (\cos(2\pi Ft) - \sin(2\pi Ft)) \quad \textit{Eq. 35}$$

With $G(t) = \cos(2\pi Ft) - \sin(2\pi Ft)$, wall shear stress represented as Eq. 35, where d_r was the membrane displacement at radius r, R_2 was the outer radius of the membrane, h was the gap between the disks, t was the operating times, F was oscillation

frequency. The maximum shear rate occurred at the periphery ($r=R_2$), which generated the maximum displacement d, and could be calculated by Eq. 36:

$$\gamma_{w\,max} = 2^{0.5} d (\pi F)^{1.5} v^{-0.5} \quad \textit{Eq. 36}$$

Moreover, the mean value of the shear rate can be defined by computing the absolute value over a specific area. For example, the annular limited by inner radius R_1 and outer radius R_2, in this case, showed as Eq. 37.

$$\bar{\gamma_w} = \frac{2^{3/2}(R_2^3 - R_1^3)}{3\pi R_2 (R_2^2 - R_1^2)} \gamma_{w\,max} \quad \textit{Eq. 37}$$

For the VSEP system [126], the result showed that the maximum and mean shear rates at the membrane was 112000 and 37000 s^{-1}, respectively, with water at 20°C. These expressions were also used to estimate the maximum shear rates with Eq. 36 [92] and calculate the mean shear rate with Eq. 37 [59, 91] in 45°C milk solution.

Gomaa et al. [131] investigated a flat vertical vibrating membrane unit with turbulence promoters. They gave a surface shear rate expression in Eq. 38 and the maximum shear rate in Eq. 39.

$$\gamma(t) = \frac{A w^{1.5}}{2 v^{0.5}} \left(\cos \omega t + \frac{\pi}{4} \right) \quad \textit{Eq. 38}$$

$$\gamma_{max} = \frac{A w^{1.5}}{2 v^{0.5}} \quad \textit{Eq. 39}$$

As described in the oscillating rectangular membrane, AVM [215] stands as a typical system; the membrane moves horizontally in a direction parallel to them. The local shear rate is evenly distributed on the membrane surface, could be expressed by Eq. 40:

$$\gamma_w(t) = d (\pi F)^{1.5} v^{-0.5} (\cos(2\pi F t) - \sin(2\pi F t)) \quad \textit{Eq. 40}$$

Zhao et al. [215] found the shear decrease with the increment of distance to the membrane. At 10 Hz frequency and 1 cm amplitude, shear rate induced by the oscillation membrane could be ignored and decreased from 4000 to 0 s^{-1} at the distance of about 1 mm.

Another similar device described by Su et al. [47] achieved the oscillation frequency up to 50 Hz, but with a lower amplitude (1.2 mm) in the desalination of simulated seawater. The membrane boundary shear rate was more than 6000 s^{-1} in this condition (*Re=344*).

Hollow fibre membranes are often applied in the oscillating system. The shear rate in this membrane module was calculated by Beier et al. [129]. They showed that the shear rates (Eq. 41) at the membrane surface should be:

$$\gamma_s = v_0 \sqrt{\frac{\omega}{2v}} [\sin(\omega t) - \cos(\omega t)] \quad \textit{Eq. 41}$$

where ω was angular velocity ($\omega=2\pi f$), v_0 was the amplitude of velocity ($v_0=A\omega$, A was the peak-to-peak amplitude), t was time.

Based on this expression, a time mean average of shear rate was computed as Eq. 42. At the frequency of 30 Hz and amplitude of 1.175 mm, it could reach up to approximately 2000 s^{-1} with the permeate flowrate of 68 L/(m^2 h).

$$\bar{\gamma_s} = \frac{\sum_{i=0}^{1000} |\gamma_s(t = i/1000)|}{1000} \quad \textit{Eq. 42}$$

$$\frac{\gamma_{max1}}{\gamma_{max2}} = \frac{d_1}{d_2}\left(\frac{\omega_1}{\omega_2}\right)^{1.5} \quad \textit{Eq. 43}$$

The maximum shear rate of these kinds of systems was compared as following Eq. 43. The shear rate for VSEP (frequency 60 Hz, amplitude 30 mm) is 28-fold higher than the hollow membrane system (30 Hz, 3 mm) [20]. It is 33-fold higher than VERO system (50 Hz, 1.2 mm). But what we also need to take into consideration is the distribution of shear rate at the membrane surface. The shear rate in VSEP increases with a higher radius of the disk membrane, while the other two modules are uniformly distributed at the membrane surface.

4.2.2.3 Oscillating and vibrating systems

Except for oscillating parallel to the HF membrane, other forms of movement applied with HF membrane would be classified into Oscillating and vibrating, where the motion is perpendicular to the fibre axis [132] or with a defined angle [225]. The shear force is cylindrically asymmetric around the fibre, and using a simple equation to describe it is not available.

4.3 Local approaches

4.3.1 Local velocity and shear stress

In DF system, the complexity of the flow field is of course expected to improve filtration performances. It is promoted by different phenomena related to the specific geometrical configuration and the associated moving walls. Indeed, the flow pattern is not only time dependant but also highly influenced by the different length scales that exist in the system. Moreover, the rheological behaviour of the fluid that can be Non-Newtonian in some applications may also affect the flow field. Global and semi-local approaches to get quantitative information on velocity, pressure and shear stress show their limitation to reveal what really happens in the system.

From an experimental point of view, recent optical measurement/visualization techniques are becoming more and more popular for accurate and reliable local measurements, resulting in the velocity field, concentration field, temperature field, etc.

4.3.1.1 Particle Image Velocimetry (PIV)/ Particle Tracking Velocimetry (PTV)

PIV allows the estimation of the velocity field by the average displacement of multiple small tracer particles in a given interval Δt. In comparison, PTV is developed in the case of low seeding densities to calculate the particle velocity by measuring the optical track length of the particle under a specific exposure time [246, 247]. Typically, the tested device needs to have a good light transmission to ensure a better acquisition of particle images by laser light scattering. Trace particles seeded in the flow are assumed to move with the fluid without any velocity lag, fluorescent, polystyrene, silver-coated particle, or other reflective particles are used [247]. Li et al. [71] seeded 0.1 g/L particles

with a diameter of 20 μm in the oscillating system to establish a velocity vector map; the data acquisition system was performed at 6Hz. In rotating system, Xie et al. [195, 196] investigated the velocity fields in radial and vertical profiles with BREOX solution. They found that velocity is highly organized and stable within the filtration cell and is mainly governed by the impeller shape.

4.3.1.2 Molecular Tagging Velocimetry (MTV)

MTV determine the velocity field in fluid flow by tagging specific molecular instead of macroscopic particles as in PIV, and tracking its displacement by imaging twice. There are three optical ways to visualize these tagged molecules: fluorescence, phosphorescence and laser-induced fluorescence [248]. This technology is achieved on a molecular basis to avoid the non-uniformed seeding and the impact of the suspended particle on the fluid itself. Simultaneously, the capital cost would increase sharply for the complex experimental system [249].

4.3.1.3 Laser Doppler Velocimetry (LDV)

LDV is also known as Laser Doppler Anemometry (LDA), is one of the techniques of using the Doppler shift in a laser beam to measure the velocity in transparent or semi-transparent fluid, or the linear or vibratory motion of opaque, reflecting, surfaces. The measurement with LDA is absolute, linear with speed, and requires no pre-calibration [250-252]. But the drawbacks are the high precise optical arrangement and bothersome signal processing [247]. Bentzen et al. [183] measured tangential velocity with LDA system at the rotating speed between 50 and 350 rpm. Wall shear stress in 15 locations was achieved and indicated a good agreement with CFD simulation.

4.3.1.4 Electrochemical method

Electrochemical method is based on the redox reaction of the electrolyte combination. The magnitude of the current was measured and derived from calculating the shear stress from the theoretical relationship. For most of these solutions, ferried and ferrocyanide is used as oxidizing and reducing ions, respectively [253]. A reaction is conducted at high enough voltages to reduce the concentration of the reacting species to zero at the surface of the working electrode. Therefore, the reaction rate is controlled by the speed of mass transfer, which is directly related to the local shear stress. What should be concerned are the non-uniform flow across the probe and the response of the instrument to fluctuations in the velocity field [254, 255].

4.4 Computational Fluid Dynamics (CFD)

As an alternative to the experimental studies, Computational fluid dynamics can be used to solve mass and momentum balances governing equations for fluid flow, the so-called Navier-Stokes equations, to determine the velocity and pressure fields in the geometrical domain. It is of great use to replenish our knowledge about increasing the filtration performances without further experimental verification. Although attractive, this theoretical approach is often complicated to implement in particular to take into account the mobile walls of the domain and the turbulent flow regime, especially in the complex-geometries modules. Moreover, a proper calculation mesh should adapt to the geometry

and the numerical method, according to the specific problem [256-258]. In laminar flow, a relatively lower mixing rate of 2 Hz in RVF module, CFD simulation was in good agreement with PIV regarding velocity fields and profile [195]. The simulated shear stress distributions indicated that the rotating speed and disk structure are the main factors affecting shear stress on the membrane surface [84, 115]. For the requirement of uniform surface shear stress, CFD simulation was used to optimize the design of rotor in rotating system, which permits the same mean shear stress with relatively low rotation speed [186].

5. DISCUSSION

Dynamic filtration permits to reduce fouling and concentration polarization thanks to high local shear stress generated by rotating, oscillating or vibrating movements. Various systems have been described and investigated, but no instruction or procedure helps engineers select a suitable DF module.

As for conventional filtration, engineers should previously define the specifications of the application, including objectives (separation, concentration), expected performances and operating limitations. Capital expenditure (CAPEX) and operational expenditure (OPEX) associated with DF modules should be evaluated in the business plan. For CAPEX (equipment, land, construction, etc.), production capacity and scaling should be known. For OPEX, the main cost will be associated with DF energy demand. In this last situation, several approaches can be proposed to estimate total power consumption.

5.1 Energy demand associated with DF module

Compared with cross-flow filtration, dynamic filtration shows great performances in fouling control with higher critical flux, which leads to longer filtration run between cleaning steps. However, the power consumption is much more delicate to estimate in DF modules than the conventional one (DEF, CFF).

The total power P_T in the basic filtration unit includes mechanical power P_M and pumping power P_P (Eq. 44). Energy consumption for the mixing, oscillating or vibrating movements is usually much higher than pumping energy. The driving force for filtration (TMP) is highly dependent on the filtration type: MF (0.2 to 3 bar), UF (1 to 10 bar), NF (10 to 40 bar) and RO (10 to 100 bar). Its magnitude for filtration will affect pumping powers in different ways for each filtration mode present in Fig. 11. Two conventional filtration modes [259] are considered: single-pass continuous filtration and continuous filtration with partial retentate recycle (Feed & Bleed), as illustrated in Fig. 11.

$$P_T = P_M + P_P \qquad \textit{Eq. 44}$$

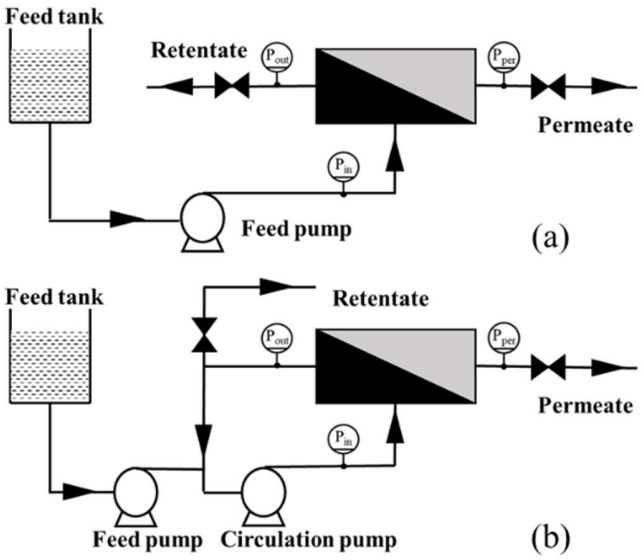

Fig. 11 Filtration modes, (a). Single-pass continuous filtration (b). Continuous filtration with partial retentate recycle (Feed & Bleed)

5.1.1 Mechanical power

Considering a DF module, the mechanical power consumption can be estimated by generated movement (mixing, oscillating, vibrating) and the flow through the module. Therefore, three strategies are described: i) the global approach (power consumption curves, friction curves), ii) semi-local empirical correlation estimating the mean shear stress and iii) local measurements (or simulation) of the velocity field.

For global approach, power consumption curves and friction curves (friction factor or Euler) can be determined for each module, as reported by Fillaudeau et al. [193] for RVF lab-scale module. With mixing Reynolds number ranging from 10 to 10^6, semi-empirical dimensionless correlations were established. The power number was calculated with the global electrical power of the motor, and the mechanical power was estimated by subtracting consumed power without charge. They demonstrated that the power consumption curve was independent of the flowrate. On the opposite, the friction curve was strongly affected by mixing conditions and a semi-empirical correlation was established to take it into account.

For semi-local approach, the mechanical power could be estimated by the local shear stress, which has been presented in §4.2. In RDM module (rotating system, type 5), the mechanical power P_M developed by friction force was given in Eq. 45 [127]. τ_d and τ_{db} are the shear stress on two sides of the disk (*b:* smooth backside); k_d and k_{db} are the core velocity coefficients. Mechanical power was found to vary linearly with electric power (efficiency close to 0.39 for disks with vanes and 0.63 for smooth disk). Using Murkes and Carlson's equation (Table. 10, Eq. 27), the turbulent shear stress was estimated. It implied that electrical power varied as $\omega^{14/5}$ [127], which was verified by Brou et al. [135]. In SBM module [50] (rotating system, type 2), with a different configuration, it was reported that electrical power was proportional to ω. In laboratory oscillating (type 11, [133]) and/or vibrating (type 15, [132]) systems, time average values should be taken

into account over a period for different frequencies, as seen in Eq. 46. The function *f(t)* represents the force balance with drag force, gravity, buoyancy and viscous force according to the motion; *v(t)* is the local velocity in the time domain. It gives the maximum value of $2\pi FA$.

$$P_M = 2\pi \int_0^R (\tau_d + \tau_{db})\, r^2 \omega d_r = 0.0779 \rho v^{1/5} \omega^{14/5} R^{23/5} (k_d^{9/5} + k_{db}^{9/5}) \qquad \textit{Eq. 45}$$

$$\overline{P_M} = \frac{1}{T} \int_0^T f(t) v(t)\, d_t \qquad \textit{Eq. 46}$$

For local approach, Xie [260] has investigated the local shear stress with PIV measurements at the static walls in RVF module (rotating system, type 6). Considering the angular momentum balance, the torque along the rotor is equal to the torque on the surrounded housing. The corresponding mechanical power was lower than those estimated with the power consumption curve, due to the non-uniform distribution of torque on the lateral/external walls. The contribution of periodic motions and turbulence needs to be considered.

5.1.2 Pumping power

In industrial applications, the pumping power is represented by the electric consumption (Eq. 47) by knowing current (*U*) and tension (*I*). Mechanical power can also be estimated from the pressure difference between inlet and outlet and the flow rate. In both filtration modes (Fig. 11), the contribution of pumping will significantly differ.

$$P_P = UI \qquad \textit{Eq. 47}$$

For single-pass continuous filtration, the power is calculated from feeding flowrate (Q_f) and pressure difference with Eq. 48. It is equivalent to the pressure differences associated with permeate and retentate flowrate. P_{in}, P_{out} and P_0 represent the inlet/outlet pressure of DF module and the atmospheric pressure; Q_r and Q_p are the retentate and permeate flowrate. By neglecting the pressure drop in the DF module, it could be assumed that $(P_{out} - P_0) \approx \Delta P$. In NF and RO where TMP is maintained at high pressure (>10 bar), pumping power cannot be neglected. But these powers are still greatly reduced for the relatively lower feeding flowrate applied compared with conventional CF, which needs a high shear rate produced by high feeding flowrate. In DF modules, the uncoupling of flowrate and local shear rate is ensured by mechanical power. Feeding flowrate should satisfy permeate and retentate concentration and volume reduction ratio. Consequently, pumping power can be drastically reduced up to a negligible contribution.

$$P_P = Q_f(P_{in} - P_0) \approx Q_r(P_{out} - P_0) + Q_p \Delta P \qquad \text{Eq. 48}$$

For Feed & Bleed mode, the pumping power is equal to the sum of feed and circulation powers associated with Q_f and Q_c, given in Eq. 49. In conventional filtration, this configuration enables to uncouple the feeding and circulation flowrate. Consequently, the pumping power can be significantly reduced for the high-pressure filtration process (NF, RO). With DF module, this configuration will be simplified by eliminating the circulation pump. Feed & Bleed mode will have a negligible interest except if a pre-concentration of the fluid is used. The knowledge of the friction curves is required to

estimate the pressure loss within the DF module [193]. However, the pumping power (feed) is expected to be lower than in a single-pass configuration.

$$P_P = Q_f(P_{out} - P_0) + Q_c(P_{in} - P_{out}) \qquad Eq.\ 49$$

Luo et al. [170] proposed a linear relationship between pumping power and TMP, within the range 0 to 40 bar, P_{in}–P_0 would approximate the transmembrane pressure in the open-loop when neglecting the pressure drop of DF. In the UF of PEG 6000 with SBM, the retentate flowrate was fixed at 10^{-4} m^3/s, but the maximum permeate flowrate was 8×10^{-7} m^3/s, which is negligible in comparison with the retentate flow [50]. These limited permeate flux would reduce the output of the feeding pump, especially in configuration (b) in Fig. 11.

5.1.3 Specific energy demand

Specific energy demand E (Eq. 50) is defined as the total energetic consumption per m^3 of permeate, equal to the ratio between total power and permeate flowrate. The total power is supposed to be the sum of pumping and mechanical power previously discussed. But in most publications, the pumping power is negligible or a very low concern in MF and UF. It could be ignored compared with mechanical power as demonstrated in RDM module for mixing rate up to 2000 rpm [170].

$$E = \frac{P_T}{Q_f} \approx \frac{P_M}{JS\eta} \qquad \text{Eq. 50}$$

For laboratory or industrial DF devices, energy demand is rarely reported and resumed in Table. 11. Specific energy varies to a large extend from 0.29 to more than 1000 kWh/m^3 due to the different configurations and scales. Other parameters such as disk design, fluid concentration and temperature also affect power consumption. Consequently, the comparison of DF modules is hardly reliable or feasible.

Table. 11 Specific energy demand in different modules

Module	Fluid	Membrane	N (Hz, rpm)/ A (mm)	S (m^2)	J (L/m^2h)	TMP (bar)	E (kWh/m^3)	Ref.
RDM	1:2 diluted skim milk	NF	2000 rpm	0.0176	350	40	170	[170]
RDM	1:2 diluted skim milk	NF	1000 rpm	0.0176	135	40	303	[170]
RDM	1:2 diluted skim milk	UF	2000 rpm	0.019	/	/	65	[178]
RDM	1:2 diluted skim milk	UF	2000 rpm	0.019	/	/	30	[178]
RDM	Baker yeast	MF	2000 rpm	0.019	200	/	15	[127]
MSD	$CaCO_3$	MF	1930 rpm	0.06	/	3	1.7	[78]
MSD	$CaCO_3$	MF	1930 rpm	0.033	/	3	2.9	[78]
VSEP	Skim milk	RO	60.2 Hz	100	55	40	1.63	[60]
VSEP	Skim milk	UF	60.4 Hz	151	56	/	1.05	[92]
OFSM	baker's yeast	MF	25 Hz/1.5 mm	0.006	500	0.6	0.3	[133]
SBM	PEG 6000	UF	400 rpm	0.0286	411	5.884	80	[50]
MMV	Activated sludge	MF	/	0.016	16	/	12.2	[210]
MMV	Activated sludge	MF	/	0.096	16	/	2.03	[210]
VHM	Yeast	MF	1.7 Hz	0.0057	46	/	0.29	[218]

VERO	Silica colloids and sodium chloride	RO	/	0.006	/	/	~10^3	[55]

For several rotating and oscillating DF modules (MSD, RDM, VSEP, VHFM), membrane type (NF, MF, UF with polymeric and ceramic membranes) and experimental fluids, Zsirai et al. [30] demonstrated that permeate steady-state flux increased as a power law of shear rate, $J = k\gamma^n$ with $0.186<n<1.560$ and $0.00003<k<6.7$. The empirical correlation of $n = (1.98 - logk)/5.04$ was fitting well except for the high viscosity liquid and non-uniform shear rate distributed in MSD. However, confusion remains between the mean and maximal shear rates being applied.

In rotating RDM modules, since the maximum shear rate was proportional to $\omega^{9/5}$ (Eq. 27 and Eq. 28), and permeate flux increased as a power law of maximum shear rate, γ_{max} with an exponent of 0.5-1 [19, 20, 90, 101, 127, 178, 261]. Then the specific energy demand can be easily estimated knowing the mechanical power and the steady-state flux, indicating that E is proportional to $\omega^{1\text{-}1.9}$. In the concentration of skim milk with NF membrane, operating conditions at 2000 rpm and extreme TMP (40 bar) resulted in the lowest mean specific energy demand around 170 kWh/m^3. In comparison, it increased up to 303 kWh/m^3 under 1000 rpm and 40 bar [170]. The same fluid was tested by Ding et al. [178] in UF, and specific energy demand increased from 30 kWh/m^3 with smooth disk up to 65 kWh/m^3 with disk equipped with vans. In MSD, a solution of 200 g/L $CaCO_3$ was filtered at 3 bar TMP. The maximum specific energy consumption was 2.9 kWh/m^3 for the nylon membranes and 1.7 kWh/m^3 for the ceramic ones [78].

In oscillating VSEP (type 9) system, Frappart et al. [60] estimated the power consumed by the oscillation of module at 60.2 Hz (amplitude: 2.5 cm). Specific energy demand was evaluated at 1.63 kWh/m^3 by assuming a permeate flux equal to 55 L/(m^2·h). With defined operating conditions (Q_p=*8.42* m^3/h, *S=151* m^2, *TMP=1500* kPa and *F=60.4* Hz), the power demand for the oscillation and pumping are 8.83 kW and 6.58 kW, respectively. The estimated specific energy demand was below 1 kWh/m^3 for oscillating [92]. Gomaa et al. [133] compared the specific energy consumption based on low and high-efficiency power recovery of 20% and 80% with the oscillating membrane (type 11), they were 0.3 kWh/m^3 and 0.1 kWh/m^3 at the highest frequency (25 Hz), respectively. In VERO module (type 10), equipped with a small membrane area of 0.006 m^2 for desalination, the estimated specific energy demand was in the order of 10^3 kWh/m^3.

In oscillating and vibrating systems, Kola et al. [132] investigated the energy consumption in terms of productivity in a linear transverse vibration HF system (type 15) with the vibration frequency at 3.7 Hz and displacement of 2.5 mm for 0.04 µm PVDF membrane. The specific energy consumption for oscillation and vibration was around 0.0009 kWh/m^3 at permeate flux of 30 L/(m^2·h). It increased to 0.20 kWh/m^3 at the same permeate flux for the highest frequency of 21.8 Hz and 2.5 mm displacement.

In conclusion, specific energy demand can be estimated if information about power consumption and permeate flux are known. However, the different configuration and scale do not allow to compare absolute values between different modules.

5.2 Specifications and decision tree for DF application

Dynamic filtration is a reliable alternative to dead-end and cross-flow filtrations as reported in the present documents. Their performances are associated with complex flow patterns generating high and fluctuating local shear rates and pressure at the membrane surface.

Considering the 15 types of DF devices (corresponding to 55 known modules), the overarching aims propose to elaborate the main criteria helping engineers to select a DF module or to identify the missing information about DF module or fluid to be treated. The best choice for a given application will be driven by several basic questions:

- What is the limitation associated with the fluids?
- How to determine the operating conditions?
- What should we know about dynamic filtration equipment?

A framework (Fig. 12) is proposed with criteria operating conditions and knowledge barriers in DF application, which would help to select a module with available information and identify the missing knowledge.

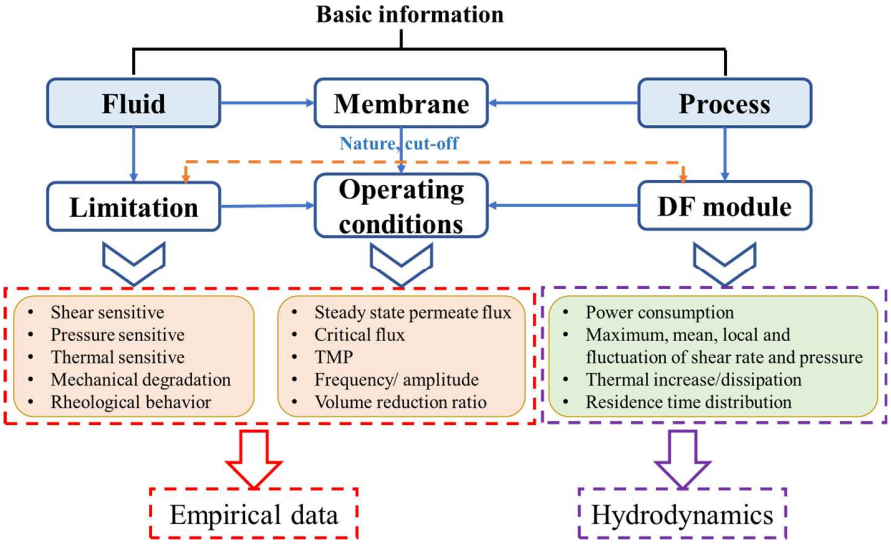

Fig. 12 Main criteria and knowledge gap in DF application

Firstly, basic information about nature, composition, physico-chemical properties of the fluid to be treated (ex. rheological behaviour, density, temperature, pH, particle size distribution, concentration) and the objectives of the process (concentration, purification or separation), as well as the production capacity and mode (volume, time, batch, continuous…), should be known. This information will help to select the filtration type (MF, UF, NF or RO) and the membrane (cut-off and nature). Coupled with the limitation of fluid and DF module, the operating conditions can be defined in terms of steady-state/ critical flux, TMP, frequency/ amplitude and volume reduction ratio.

In dynamic filtration module, the behaviour of experimental fluid under stringent hydrodynamics conditions should be investigated (ex. sensitivity to shear rate magnitude, to temperature increase, to mechanical degradation such as cell or particles…) before process design and scaling (filtration area, power consumption, acceptable operating conditions). Meanwhile, the knowledge of local hydrodynamics (velocity, shear or

pressure field), including maximum, average and time-dependent values may enable to estimate performances as well as critical local operating conditions.

Finally, Table. 12 summarizes the empirical applicative and hydrodynamics data available for the 15 types of DF modules as discussed in **Part 3 and 4**. It leads to highlight the knowledge gap for future scientific research and industrial applications.

Table. 12 Resume of available data about hydrodynamics and applications with the different type of DF module (n.a: not available)

	Empirical data					Hydrodynamics investigation							
	Application / Performances			Global approach				Semi-local approach (membrane or rotor surface)			Local approach (filtration cell volume)		
Type	Water treatment	Food processing	Bioprocess engineering	Dimensionless analysis	Dimensionless correlation	Pumping power	Mechanical power	Core velocity coefficient, k	$\bar{P}(x,y,z)$	γ(x,y,z)	U(x,y,z,t)/ γ(x,y,z,t)	P(x,y,z,t)	CFD
1	X	X	X	X	X	n.a.	n.a.	X	X	X	n.a.	n.a.	X
2	X	n.a.	X	X	n.a	X	X	n.a	n.a	n.a	n.a.	n.a.	X
3	X	n.a.	X	X	X	n.a	n.a	n.a	X	X	n.a.	n.a.	X
4	X	n.a.	n.a.	X	n.a	n.a	n.a	n.a	n.a	n.a.	n.a.	n.a.	n.a.
5	X	X	X	X	n.a	X	X	X	X	X	X	n.a	X
6	X	X	X	X	X	X	X	X	X	X	X	n.a	X
7	X	n.a.	n.a.	X	n.a	n.a	n.a	n.a	X	X	n.a.	n.a.	n.a.
8	X	X	X	X	X	n.a	n.a	n.a	X	X	n.a.	n.a.	n.a.
9	X	X	X	X	X	n.a	n.a	n.a	n.a.	X	n.a.	n.a.	X
10	X	n.a.	n.a.	X	X	n.a	n.a	n.a	n.a.	X	n.a.	n.a.	X
11	X	n.a.	X	X	X	X	X	n.a	n.a	X	n.a.	n.a.	X
12	X	n.a.	n.a.	n.a.	n.a	n.a	n.a	n.a	n.a.	X	n.a.	n.a.	n.a.
13	X	n.a.	X	X	n.a	n.a	X	n.a	n.a.	X	X	n.a.	n.a.
14	X	n.a	n.a	n.a	n.a	n.a	X	n.a	n.a	X	n.a	n.a	X
15	X	X	X	X	n.a	n.a	X	n.a	n.a.	n.a.	n.a.	n.a.	X

6. CONCLUSION

In present review, a bibliography synthesis about dynamic filtration (application, research items, trends and stakeholders) was reported. Almost 150 papers have been scrutinized, and a qualitative and quantitative analysis was conducted thanks to specific software (bibliometric methodology). It enables identifying the most important actors (or scientific clusters), as well as the evolution of "research hotspots" over the last 30 years. The application fields (empirical data) with different lab, pilot or industrial modules were exhaustively identified and discussed.

The fouling control and flux enhancement have been well documented in the literature, which confirms the high potential of shear-enhanced dynamic filtration. The lab-scale modules are mainly applied to water treatment, food processing, and bioprocess engineering. In recent publications, microalgae filtration constitutes a promising research topic but is still limited to lab and pilot scales. In industrial modules, wastewater treatment and paper mill sludge are reported. However, it is assumed that industrial applications are confined to internal practices and trade secrets. The knowledge gap to expand and scale-up DF from lab to industry should be supplemented. A brake on DF's development appears to lie in their mechanical complexity. At present, the selection of DF device and operating conditions is driven by empirical trial-result strategy. The general trend is to improve filtration performances through the control of local shear rate and pressure within the filtration cell and specifically at the membrane surface. In rotating systems, most of the research has focused on equipment improvements (MSD, SBM, CSAF) and alternative applications (microalgae, halogenated compounds, PAA-Cd). In oscillating systems (except VSEP), the applications are poorly documented in comparison with the rotating systems. Fluid velocity, pressure and shear-stress fields are rarely investigated. The shear-rate intensity is determined by the oscillating frequency as well as amplitude. Thus, the fluctuation value of shear stress is correlated with the oscillating amplitude, frequency and rheological behaviour. In the last decade, several new oscillating devices such as VERO, USVM, MMV and AVM have emerged. The frequency and amplitude of oscillation were controlled within a wide range from 5 to 60 Hz and 1.2 mm to 40 mm, respectively, with a more flexible generation of filtration driving force (Transmembrane pressure) and fouling limitation (shear stress). Dynamic filtration shows great potential with concentrated and fouling fluids, which would be restrictive criteria in conventional cross-flow filtration. However, high shear-rates may impact some sensitive suspensions, such as biomolecules (cellulosic polymer, proteins), microorganisms (Prokaryotic and eukaryotic cells) and chemical molecules (metal complexes).

Technical specifications of DF modules have been described. One major challenge was to identify all existing DF modules and to propose a rational classification. Geometric complexity put forward the need to characterize instantaneous and local hydrodynamics up to macroscopic data such as specific power consumption. However, the characterization of fluid flow within dynamic filtration modules (within filtration cell, at membrane surface) appears as crucial but still partial and delicate information to access. Different scale of hydrodynamics investigations was described. According to empirical correlations, mean shear rate and transmembrane pressure can be estimated with respect to the knowledge of core velocity coefficient and operating conditions. However, some

hydrodynamics in oscillating and/or vibrating systems needs further research. The instantaneous magnitudes of local shear-rate and pressure at the membrane surface are still not yet reported. How to realize accurate measurements stands as a challenge to be addressed. In addition, this approach could be extended to Non-Newtonian fluids, including viscoelastic and viscoplastic rheological behaviour. Finally, the main criteria to select dynamic filtration modules (critical conditions, performances, power) are introduced. Process engineers need technical synthesis to know, to evaluate in order to select DF devices and optimal operating conditions.

7. ACKNOWLEDGEMENT

The financial supports of China Scholarship Council (CSC) for Ming CHENG (grant No. 201801810069) and Xiaomin Xie (grant No. 201304490066) are gratefully acknowledged.

REFERENCE

[1] M. Cheryan, Ultrafiltration and Microfiltration Handbook, Taylor & Francis, 1998.

[2] G. Daufin, J.P. Escudier, H. Carrère, S. Bérot, L. Fillaudeau, M. Decloux, Recent and Emerging Applications of Membrane Processes in the Food and Dairy Industry, Food and Bioproducts Processing, 79 (2001) 89-102.

[3] W.H. Smith, Germination of Macrophomina phaseoli sclerotia as effected by Pinus lambertiana root exudate, Can J Microbiol, 15 (1969) 1387-1391.

[4] P. Aimar, G. Daufin, Séparations par membrane dans l'industrie alimentaire, F3250, Techniques de l'ingénieur, (2004) 1-23.

[5] L. Bachus, A. Custodio, 4 - The affinity laws, in: L. Bachus, A. Custodio (Eds.) Know and Understand Centrifugal Pumps, Elsevier Science, Oxford, 2003, pp. 39-43.

[6] G. Daufin, J.-P. Labbé, Equipment Fouling in the Dairy Application: Problem and Pretreatment, in: Z. Amjad (Ed.) Calcium Phosphates in Biological and Industrial Systems, Springer US, Boston, MA, 1998, pp. 437-463.

[7] R.J. Wakeman, E.S. Tarleton, Experiments using electricity to prevent fouling in membrane filtration, Filtration & Separation, 23 (1986) 174-176.

[8] L. Fillaudeau, M. Lalande, A Practical Method to Predict Steady-State Flux and Fouling in the Crossflow Microfiltration of Rough Beer with 1.40 μm Tubular Ceramic Membranes, Food and Bioproducts Processing, 76 (1998) 217-223.

[9] V.G.J. Rodgers, R.E. Sparks, Effect of transmembrane pressure pulsing on concentration polarization, Journal of Membrane Science, 68 (1992) 149-168.

[10] I.G. Wenten, Mechanisms and control of fouling in crossflow microfiltration, Filtration & Separation, 32 (1995) 252-253.

[11] H. Mallubhotla, G. Belfort, Flux enhancement during Dean vortex microfiltration. 8. Further diagnostics1This paper is part 8. Previous papers of the series can be found in 6, 7, 8, 9, 10, 11. Papers 3 and 7 are submitted and in preparation, respectively.1, Journal of Membrane Science, 125 (1997) 75-91.

[12] H. Mallubhotla, S. Hoffmann, M. Schmidt, J. Vente, G. Belfort, Flux enhancement during dean vortex tubular membrane nanofiltration. 10. Design, construction, and system characterization1This paper is part 10. Previous papers of the series can be found in 7, 8, 9, 10, 11, 12, 13. Papers # 7 and 3 are in press and in preparation, respectively.1, Journal of Membrane Science, 141 (1998) 183-195.

[13] H. Mallubhotla, M. Schmidt, K. Hyun Lee, G. Belfort, Flux enhancement during Dean vortex tubular membrane nanofiltration: 13. Effects of concentration and solute type1This paper is part 13. Previous papers of the series can be found in 7, 8, 9, 10, 11, 12, 13, 14, 15, 29. Paper 7 has been submitted while papers 11 and 12 are in the review process.1, Journal of Membrane Science, 153 (1999) 259-269.

[14] T. Horie, S. Shiota, T. Akagi, N. Ohmura, S. Wang, V. Eze, A. Harvey, Y. Hirata, Intensification of hollow fiber membrane cross-flow filtration by the combination of helical baffle and oscillatory flow, Journal of Membrane Science, 554 (2018) 134-139.

[15] T. Akagi, T. Horie, H. Masuda, K. Matsuda, H. Matsumoto, N. Ohmura, Y. Hirata, Improvement of separation performance by fluid motion in the membrane module with a helical baffle, Separation and Purification Technology, 198 (2017).

[16] B.B. Gupta, P. Blanpain, M.Y. Jaffrin, Permeate flux enhancement by pressure and flow pulsations in microfiltration with mineral membranes, Journal of Membrane Science, 70 (1992) 257-266.

[17] M. Mercier, C. Fonade, C. Lafforgue-Delorme, Influence of the flow regime on the efficiency of a gas-liquid two-phase medium filtration, Biotechnol. Tech., 9 (1995) 853-858.

[18] L. Borea, V. Naddeo, M.S. Shalaby, T. Zarra, V. Belgiorno, H. Abdalla, A.M. Shaban, Wastewater treatment by membrane ultrafiltration enhanced with ultrasound: Effect of membrane flux and ultrasonic frequency, Ultrasonics, 83 (2018) 42-47.
[19] M.Y. Jaffrin, L.-H. Ding, O. Akoum, A. Brou, A hydrodynamic comparison between rotating disk and vibratory dynamic filtration systems, Journal of Membrane Science, 242 (2004) 155-167.
[20] M.Y. Jaffrin, Dynamic shear-enhanced membrane filtration: A review of rotating disks, rotating membranes and vibrating systems, Journal of Membrane Science, 324 (2008) 7-25.
[21] L. Ding, M.Y. Jaffrin, J. Luo, Dynamic Filtration with Rotating Disks, and Rotating or Vibrating Membranes, (2015) 27-59.
[22] M. Chai, Y. Ye, V. Chen, Application of rotational vibration in a submerged hollow fibre membrane system for bioseparation of high concentration yeast suspensions, Journal of Membrane Science, 573 (2019) 145-156.
[23] L. Villafana-Lopez, E. Clavijo Rivera, S. Liu, E. Couallier, M. Frappart, Shear-enhanced membrane filtration of model and real microalgae extracts for lipids recovery in biorefinery context, Bioresour Technol, 288 (2019) 121539.
[24] M. Hapońska, E. Clavero, J. Salvadó, C. Torras, Application of ABS membranes in dynamic filtration for Chlorella sorokiniana dewatering, Biomass and Bioenergy, 111 (2018) 224-231.
[25] P. Mikulasek, Methods to reduce concentration polarization and fouling in membrane filtration, Collect. Czech. Chem. Commun., 59 (1994) 737-755.
[26] S. Lee, R.M. Lueptow, Rotating Membrane Filtration and Rotating Reverse Osmosis, J. Chem. Eng. Jpn., 37 (2004) 471-482.
[27] M.Y. Jaffrin, Hydrodynamic Techniques to Enhance Membrane Filtration, Annual Review of Fluid Mechanics, 44 (2012) 77-96.
[28] M.Y. Jaffrin, Dynamic filtration with rotating disks, and rotating and vibrating membranes: an update, Current Opinion in Chemical Engineering, 1 (2012) 171-177.
[29] L.H. Ding, M.Y. Jaffrin, Benefits of High Shear Rate Dynamic Nanofiltration and Reverse Osmosis: A Review, Separation Science and Technology, 49 (2014) 1953-1967.
[30] T. Zsirai, H. Qiblawey, M.J. A-Marri, S. Judd, The impact of mechanical shear on membrane flux and energy demand, Journal of Membrane Science, 516 (2016) 56-63.
[31] C. Chen, CiteSpace II: Detecting and visualizing emerging trends and transient patterns in scientific literature, Journal of the American Society for Information Science and Technology, 57 (2006) 359-377.
[32] C. Bhattacharjee, P. Bhattacharya, Ultrafiltration of black liquor using rotating disk membrane module, Separation and Purification Technology, 49 (2006) 281-290.
[33] S. Bhattacharjee, S. Datta, C. Bhattacharjee, Performance study during ultrafiltration of Kraft black liquor using rotating disk membrane module, Journal of Cleaner Production, 14 (2006) 497-504.
[34] J. Luo, L. Ding, Y. Wan, M.Y. Jaffrin, Flux decline control in nanofiltration of detergent wastewater by a shear-enhanced filtration system, Chemical Engineering Journal, 181-182 (2012) 397-406.
[35] C.M. Wisniewski, C.S. Slater, M.J. Savelski, Dynamic vibratory membrane processing for use in water recovery from soluble coffee product manufacturing wastewater, Clean Technologies and Environmental Policy, 20 (2018) 1791-1803.
[36] S. Kertész, Á. Veszprémi, Z. László, J. Csanádi, G. Keszthelyi-Szabó, C. Hodúr, Investigation of module vibration in ultrafiltration, Desalination and Water Treatment, 55 (2014) 2836-2842.
[37] M. Mertens, M.R. Bilad, A.Y. Gebreyohannes, L. Marbelia, I.F.J. Vankelecom, Membrane development for improved performance of a magnetically induced vibration system for anaerobic sludge filtration, Separation and Purification Technology, 200 (2018) 120-129.

[38] I. Ruigómez, L. Vera, E. González, G. González, J. Rodríguez-Sevilla, A novel rotating HF membrane to control fouling on anaerobic membrane bioreactors treating wastewater, Journal of Membrane Science, 501 (2016) 45-52.
[39] B. Gao, L. Liu, J. Liu, F. Yang, A photo-catalysis and rotating nano-CaCO3 dynamic membrane system with Fe-ZnIn2S4 efficiently removes halogenated compounds in water, Applied Catalysis B: Environmental, 138-139 (2013) 62-69.
[40] B. Gao, L.F. Liu, J.D. Liu, F.L. Yang, Photocatalysis and rotating dynamic membrane hybrid system with Fe-ZnIn2S4 efficiently removes 2,4,6-Tribromophenol in water: effect of dynamic membrane, in: X. Quan (Ed.) 2013 International Symposium on Environmental Science and Technology, 2013, pp. 509-514.
[41] Y. Choi, H. Oh, S. Lee, Y. Choi, T.M. Hwang, J.C. Jeon, Y.K. Choung, Removal of taste and odor model compounds (2-MIB and geosmin) with the NF membrane, Desalination and Water Treatment, 15 (2010) 141-148.
[42] A. Sarkar, D. Sarkar, M. Gupta, C. Bhattacharjee, Recovery of Polyvinyl Alcohol from Desizing Wastewater Using a Novel High-Shear Ultrafiltration Module, CLEAN - Soil Air Water, 40 (2012).
[43] G. Zakrzewska-Trznadel, M. Harasimowicz, A. Miśkiewicz, A. Jaworska, E. Dłuska, S. Wroński, Reducing fouling and boundary-layer by application of helical flow in ultrafiltration module employed for radioactive wastes processing, Desalination, 240 (2009) 108-116.
[44] C. Cojocaru, G. Zakrzewska-Trznadel, A. Miskiewicz, Removal of cobalt ions from aqueous solutions by polymer assisted ultrafiltration using experimental design approach Part 2: Optimization of hydrodynamic conditions for a crossflow ultrafiltration module with rotating part, J. Hazard. Mater., 169 (2009) 610-620.
[45] Z. Tu, L. Ding, M. Frappart, M.Y. Jaffrin, Studies on treatment of sodium dodecyl benzene sulfonate solution by high shear ultrafiltration system, Desalination, 240 (2009) 251-256.
[46] N. Moulai-Mostefa, L.H. Ding, M. Frappart, M.Y. Jaffrin, Treatment of Aqueous Ionic Surfactant Solutions by Dynamic Ultrafiltration, Separation Science and Technology, 42 (2007) 2583-2594.
[47] X. Su, W. Li, A. Palazzolo, S. Ahmed, Concentration polarization and permeate flux variation in a vibration enhanced reverse osmosis membrane module, Desalination, 433 (2018) 75-88.
[48] K.J. Hwang, S.Y. Wang, E. Iritani, N. Katagiri, Fine particle removal from seawater by using cross-flow and rotating-disk dynamic filtration, Journal of the Taiwan Institute of Chemical Engineers, 62 (2016) 45-53.
[49] D. Sarkar, S. Bardhan, A. Bandyopadhyay, M. Chakraborty, C. Bhattacharjee, Simulation of continuous stirred ultrafiltration process: an approach based on surface renewal theory, Asia-Pac. J. Chem. Eng., 7 (2012) 279-294.
[50] A. Sarkar, D. Sarkar, C. Bhattacharjee, Design and performance characterization of a new shear enhanced module with inbuilt cleaning arrangement, Journal of Chemical Technology & Biotechnology, 87 (2012) 1121-1130.
[51] D. Sarkar, C. Bhattacharjee, Modeling and analytical simulation of rotating disk ultrafiltration module, Journal of Membrane Science, 320 (2008) 344-355.
[52] S. Ri, Z. Xu, Y. Zhou, G.e. Chen, Y. Kim, Experimental Study on Revolving Cross-flow Microfiltration of Highly Viscous Liquids, Chinese Journal of Chemical Engineering, 16 (2008) 961-964.
[53] H.S. Marke, M.P. Breil, E.B. Hansen, M. Pinelo, U. Krühne, Investigation of the velocity factor in a rotational dynamic microfiltration system, Separation and Purification Technology, 220 (2019) 69-77.
[54] S. Lee, R.M. Lueptow, Control of scale formation in reverse osmosis by membrane rotation, Desalination, 155 (2003) 131-139.

[55] X. Su, W. Li, A. Palazzolo, S. Ahmed, Permeate flux increase by colloidal fouling control in a vibration enhanced reverse osmosis membrane desalination system, Desalination, 453 (2019) 22-36.
[56] M. Frappart, M.Y. Jaffrin, L.H. Ding, V. Espina, Effect of vibration frequency and membrane shear rate on nanofiltration of diluted milk, using a vibratory dynamic filtration system, Separation and Purification Technology, 62 (2008) 212-221.
[57] W. Zhang, L. Ding, Investigation of membrane fouling mechanisms using blocking models in the case of shear-enhanced ultrafiltration, Separation and Purification Technology, 141 (2015) 160-169.
[58] M. Frappart, O. Akoum, L. Ding, M. Jaffrin, Treatment of dairy process waters modelled by diluted milk using dynamic nanofiltration with a rotating disk module, Journal of Membrane Science, 282 (2006) 465-472.
[59] O. Akoum, M.Y. Jaffrin, L.H. Ding, M. Frappart, Treatment of dairy process waters using a vibrating filtration system and NF and RO membranes, Journal of Membrane Science, 235 (2004) 111-122.
[60] M. Frappart, M. Jaffrin, L.H. Ding, Reverse osmosis of diluted skim milk: Comparison of results obtained from vibratory and rotating disk modules, Separation and Purification Technology, 60 (2008) 321-329.
[61] S. Ladeg, Z. Zhu, N. Moulai-Mostefa, L. Ding, M.Y. Jaffrin, CFD Simulation of the Distribution of Pressure and Shear Rate on the Surface of Rotating Membrane Equipped with Vanes for the Ultrafiltration of Dairy Effluent, Arabian Journal for Science and Engineering, 43 (2017) 2237-2245.
[62] W. Zhang, L. Ding, M.Y. Jaffrin, B. Tang, Membrane cleaning assisted by high shear stress for restoring ultrafiltration membranes fouled by dairy wastewater, Chemical Engineering Journal, 325 (2017) 457-465.
[63] S. Lee, R.M. Lueptow, Experimental verification of a model for rotating reverse osmosis, Desalination, 146 (2002) 353-359.
[64] M. Ebrahimi, O. Schmitz, S. Kerker, F. Liebermann, P. Czermak, Dynamic cross-flow filtration of oilfield produced water by rotating ceramic filter discs, Desalination and Water Treatment, 51 (2013) 1762-1768.
[65] L. Li, L. Ding, Z. Tu, Y. Wan, D. Clausse, J.-L. Lanoisellé, Recovery of linseed oil dispersed within an oil-in-water emulsion using hydrophilic membrane by rotating disk filtration system, Journal of Membrane Science, 342 (2009) 70-79.
[66] N. Moulai-Mostefa, O. Akoum, M. Nedjihoui, L. Ding, M.Y. Jaffrin, Comparison between rotating disk and vibratory membranes in the ultrafiltration of oil-in-water emulsions, Desalination, 206 (2007) 494-498.
[67] N. Moulai-Mostefa, M. Frappart, O. Akoum, L. Ding, M.Y. Jaffrin, Separation of water from metal working emulsions by ultrafiltration using vibratory membranes, J Hazard Mater, 177 (2010) 978-982.
[68] T. Murase, T. Ohn, K. Kamimura, Dynamic microfiltration of dilute O/W emulsion in rotating cylindrical membrane filter, Kag. Kog. Ronbunshu, 22 (1996) 120-126.
[69] T. Murase, A.-W. Yosufu, Microfiltration-Rate Increase of O/W Emulsion by Use of Rotating Membrane Filter with Additional Suspended Solids, Kag. Kog. Ronbunshu, 23 (1997) 452-454.
[70] A. Ullah, J. Ahmad, H. Khan, S.W. Khan, F. Zamani, S.W. Hasan, V.M. Starov, J.W. Chew, Membrane oscillation and slot (pore) blocking in oil-water separation, Chem. Eng. Res. Des., 142 (2019) 111-120.
[71] T. Li, A.W.-K. Law, M. Cetin, A.G. Fane, Fouling control of submerged hollow fibre membranes by vibrations, Journal of Membrane Science, 427 (2013) 230-239.

[72] T. Murase, C. Pradistsuwana, E. Iritani, K. Kano, Dynamic microfiltration of dilute slurries with a rotating ceramic membrane, Journal of Membrane Science, 62 (1991) 187-199.
[73] K.-J. Hwang, S.-E. Wu, Y.-L. Hsueh, Analysis on the nonuniformity of cake formation in rotating-disk dynamic microfiltration, Separation and Purification Technology, 198 (2018) 16-24.
[74] T. Murase, D.-W. Yang, E. Iritani, Microfiltration Characteristics of High-Viscosity Slurries in Rotating Dynamic Filter, Kag. Kog. Ronbunshu, 18 (1992) 708-713.
[75] K. Takata, K. Tanida, Structure of shear-enhanced flow on membrane surface with horizontal vibration and its effect on filtration performance, Chemical Engineering Research and Design, 134 (2018) 130-139.
[76] R.B. Aim, S. Vigneswaran, H. Prasanthi, V. Jegatheesan, Influence of particle size and size distribution in granular bed filtration and dynamic microfiltration, Water Sci. Technol., 36 (1997) 207-215.
[77] L. Ding, M. Jaffrin, M. Mellal, G. He, Investigation of performances of a multishaft disk (MSD) system with overlapping ceramic membranes in microfiltration of mineral suspensions, Journal of Membrane Science, 276 (2006) 232-240.
[78] Z. Tu, L. Ding, Microfiltration of mineral suspensions using a MSD module with rotating ceramic and polymeric membranes, Separation and Purification Technology, 73 (2010) 363-370.
[79] R. Bouzerar, L. Ding, M.Y. Jaffrin, Local permeate flux–shear–pressure relationships in a rotating disk microfiltration module: implications for global performance, Journal of Membrane Science, 170 (2000) 127-141.
[80] G. He, L.H. Ding, P. Paullier, M.Y. Jaffrin, Experimental study of a dynamic filtration system with overlapping ceramic membranes and non-permeating disks rotating at independent speeds, Journal of Membrane Science, 300 (2007) 63-70.
[81] M. Loginov, N.I. Lebovka, O. Larue, L.H. Ding, E. Vorobiev, Dead-End Dynamic Filtration of Highly Concentrated CaCO3 Suspensions in the Presence of a Dispersant, Chem. Eng. Technol., 33 (2010) 1260-1268.
[82] D.E. Hadzismajlovic, C.D. Bertram, Flux enhancement in laminar crossflow microfiltration using a collapsible-tube pulsation generator1Presented in part at IMSTEC '96 (Intl. Membr. Sci. & Technol. Conf., Sydney, Australia, 12–14 Nov. 1996).1, Journal of Membrane Science, 142 (1998) 173-189.
[83] J.Y. Park, C.K. Choi, J.J. Kim, A study on dynamic separation of silica slurry using a rotating membrane filter 1. Experiments and filtrate fluxes, Journal of Membrane Science, 97 (1994) 263-273.
[84] S.-E. Wu, K.-J. Hwang, T.-W. Cheng, K.-L. Tung, E. Iritani, N. Katagiri, Structural design of a rotating disk dynamic microfilter in improving filtration performance for fine particle removal, Journal of the Taiwan Institute of Chemical Engineers, 94 (2019) 43-52.
[85] C. Kyun Choi, J. Yong Park, W. Cheol Park, J. Jin Kim, A study on dynamic separation of silica slurry using a rotating membrane filter: 2. Modelling of cake formation, Journal of Membrane Science, 157 (1999) 177-187.
[86] R. Ben Aim, M.G. Liu, S. Vigneswaran, Recent Development of Membrane Processes for Water and Waste Water Treatment, Water Sci. Technol., 27 (1993) 141-149.
[87] R. Bouzerar, M.Y. Jaffrin, A. Lefevre, P. Paullier, Concentration of ferric hydroxide suspensions in saline medium by dynamic cross-flow filtration, Journal of Membrane Science, 165 (2000) 111-123.
[88] R. Bouzerar, P. Paullier, M.Y. Jaffrin, Concentration of mineral suspensions and industrial effluents using a rotating disk dynamic filtration module, Desalination, 158 (2003) 79-85.
[89] P. Ji, A. Motin, W. Shan, A. Bénard, M.L. Bruening, V.V. Tarabara, Dynamic crossflow filtration with a rotating tubular membrane: Using centripetal force to decrease fouling by buoyant particles, Chemical Engineering Research and Design, 106 (2016) 101-114.

[90] L. Ding, O. Al-Akoum, A. Abraham, M.Y. Jaffrin, Milk protein concentration by ultrafiltration with rotating disk modules, Desalination, 144 (2002) 307-311.
[91] O. Al-Akoum, L. Ding, R. Chotard-Ghodsnia, M.Y. Jaffrin, G. Gésan-Guiziou, Casein micelles separation from skimmed milk using a VSEP dynamic filtration module, Desalination, 144 (2002) 325-330.
[92] O. Akoum, M.Y. Jaffrin, L.-H. Ding, Concentration of total milk proteins by high shear ultrafiltration in a vibrating membrane module, Journal of Membrane Science, 247 (2005) 211-220.
[93] V. Espina, M. Jaffrin, M. Frappart, L. Ding, Separation of casein micelles from whey proteins by high shear microfiltration of skim milk using rotating ceramic membranes and organic membranes in a rotating disk module, Journal of Membrane Science, 325 (2008) 872-879.
[94] V. Espina, M.Y. Jaffrin, M. Frappart, L.H. Ding, Separation of casein from whey proteins by dynamic filtration, Desalination, 250 (2010) 1109-1112.
[95] P. Meyer, A. Mayer, U. Kulozik, High concentration of skim milk proteins by ultrafiltration: Characterisation of a dynamic membrane system with a rotating membrane in comparison with a spiral wound membrane, International Dairy Journal, 51 (2015) 75-83.
[96] J. Schäfer, R. Bast, Z. Atamer, S. Nöbel, R. Kohlus, J. Hinrichs, Concentration of skim milk by means of dynamic filtration using overlapping rotating ceramic membrane disks, International Dairy Journal, 78 (2018) 11-19.
[97] V.S. Espina, M.Y. Jaffrin, L.H. Ding, Comparison of rotating ceramic membranes and polymeric membranes in fractionation of milk proteins by microfiltration, Desalination, 245 (2009) 714-722.
[98] V. Espina, M.Y. Jaffrin, L. Ding, Extraction and Separation of α-lactalbumin and β-Lactoglobulin from Skim Milk by Microfiltration and Ultrafiltration at High Shear Rates: A Feasibility Study, Separation Science and Technology, 44 (2009) 3832-3853.
[99] V. Espina, M.Y. Jaffrin, L. Ding, B. Cancino, Fractionation of pasteurized skim milk proteins by dynamic filtration, Food Research International, 43 (2010) 1335-1346.
[100] V. Espina, M.Y. Jaffrin, P. Paullier, L.H. Ding, Comparison of permeate flux and whey protein transmission during successive microfiltration and ultrafiltration of UHT and pasteurized milks, Desalination, 264 (2010) 151-159.
[101] O. Akoum, D. Richfield, M.Y. Jaffrin, L.H. Ding, P. Swart, Recovery of trypsin inhibitor and soy milk protein concentration by dynamic filtration, Journal of Membrane Science, 279 (2006) 291-300.
[102] L. Fillaudeau, B. Boissier, A. Moreau, P. Blanpain-Avet, S. Ermolaev, N. Jitariouk, Investigation of rotating and vibrating filtration for clarification of rough beer, Journal of Food Engineering, 80 (2007) 206-217.
[103] Y.E. Rayess, Y. Manon, N. Jitariouk, C. Albasi, M.M. Peuchot, A. Devatine, L. Fillaudeau, Wine clarification with Rotating and Vibrating Filtration (RVF): Investigation of the impact of membrane material, wine composition and operating conditions, Journal of Membrane Science, 513 (2016) 47-57.
[104] Z. Zhu, H. Mhemdi, L. Ding, O. Bals, M.Y. Jaffrin, N. Grimi, E. Vorobiev, Dead-End Dynamic Ultrafiltration of Juice Expressed from Electroporated Sugar Beets, Food and Bioprocess Technology, 8 (2014) 615-622.
[105] W. Zhang, N. Grimi, M.Y. Jaffrin, L. Ding, Leaf protein concentration of alfalfa juice by membrane technology, Journal of Membrane Science, 489 (2015) 183-193.
[106] W. Zhang, L. Ding, N. Grimi, M.Y. Jaffrin, B. Tang, Application of UF-RDM (Ultafiltration Rotating Disk Membrane) module for separation and concentration of leaf protein from alfalfa juice: Optimization of operation conditions, Separation and Purification Technology, 175 (2017) 365-375.

[107] Z.Z. Zhu, X. Luo, F.F. Yin, S.Y. Li, J.R. He, Clarification of Jerusalem Artichoke Extract Using Ultra-filtration: Effect of Membrane Pore Size and Operation Conditions, Food and Bioprocess Technology, 11 (2018) 864-873.
[108] M. Frappart, A. Massé, M.Y. Jaffrin, J. Pruvost, P. Jaouen, Influence of hydrodynamics in tangential and dynamic ultrafiltration systems for microalgae separation, Desalination, 265 (2011) 279-283.
[109] S.D. Ríos, J. Salvadó, X. Farriol, C. Torras, Antifouling microfiltration strategies to harvest microalgae for biofuel, Bioresour. Technol., 119 (2012) 406-418.
[110] S.D. Rios, E. Clavero, J. Salvadó, X. Farriol, C. Torras, Dynamic Microfiltration in Microalgae Harvesting for Biodiesel Production, Industrial & Engineering Chemistry Research, 50 (2011) 2455-2460.
[111] C. Nurra, E. Clavero, J. Salvado, C. Torras, Vibrating membrane filtration as improved technology for microalgae dewatering, Bioresour Technol, 157 (2014) 247-253.
[112] K.J. Hwang, S.J. Lin, Filtration flux-shear stress-cake mass relationships in microalgae rotating-disk dynamic microfiltration, Chemical Engineering Journal, 244 (2014) 429-437.
[113] C. Nurra, C. Torras, E. Clavero, S. Rios, M. Rey, E. Lorente, X. Farriol, J. Salvado, Biorefinery concept in a microalgae pilot plant. Culturing, dynamic filtration and steam explosion fractionation, Bioresour Technol, 163 (2014) 136-142.
[114] K. Kim, J.-Y. Jung, J.-H. Kwon, J.-W. Yang, Dynamic microfiltration with a perforated disk for effective harvesting of microalgae, Journal of Membrane Science, 475 (2015) 252-258.
[115] K.-J. Hwang, S.-E. Wu, Disk structure on the performance of a rotating-disk dynamic filter: A case study on microalgae microfiltration, Chemical Engineering Research and Design, 94 (2015) 44-51.
[116] C.S. Slater, M.J. Savelski, P. Kostetskyy, M. Johnson, Shear-enhanced microfiltration of microalgae in a vibrating membrane module, Clean Technologies and Environmental Policy, 17 (2015) 1743-1755.
[117] K. Kim, J.-Y. Jung, H. Shin, S.-A. Choi, D. Kim, S.C. Bai, Y.K. Chang, J.-I. Han, Harvesting of Scenedesmus obliquus using dynamic filtration with a perforated disk, Journal of Membrane Science, 517 (2016) 14-20.
[118] E. Lorente, M. Haponska, E. Clavero, C. Torras, J. Salvado, Microalgae fractionation using steam explosion, dynamic and tangential cross-flow membrane filtration, Bioresour Technol, 237 (2017) 3-10.
[119] J.Y. Jung, K. Kim, S.A. Choi, H. Shin, D. Kim, S.C. Bai, Y.K. Chang, J.I. Han, Dynamic filtration with a perforated disk for dewatering of Tetraselmis suecica, Environ Technol, 38 (2017) 3102-3108.
[120] J. Ye, Q. Zhou, X.Z. Zhang, Q. Hu, Microalgal dewatering using a polyamide thin film composite forward osmosis membrane and fouling mitigation, Algal Res., 31 (2018) 421-429.
[121] E. Lorente, M. Haponska, E. Clavero, C. Torras, J. Salvado, Steam Explosion and Vibrating Membrane Filtration to Improve the Processing Cost of Microalgae Cell Disruption and Fractionation, Processes, 6 (2018).
[122] M. Hapońska, E. Clavero, J. Salvadó, X. Farriol, C. Torras, Pilot scale dewatering of Chlorella sorokiniana and Dunaliella tertiolecta by sedimentation followed by dynamic filtration, Algal Research, 33 (2018) 118-124.
[123] Y. Zhang, X. Li, R. Xu, C. Ma, X. Wang, Q. Fu, Algal fouling control in a hollow fiber module during ultrafiltration by angular vibrations, Journal of Membrane Science, 569 (2019) 200-208.
[124] M. Mateus, J.M.S. Cabral, Steroid recovery by a rotary membrane system, Biotechnol. Tech., 5 (1991) 43-48.
[125] S.S. Lee, A. Burt, G. Russotti, B. Buckland, Microfiltration of recombinant yeast cells using a rotating disk dynamic filtration system, Biotechnol. Bioeng., 48 (1995) 386-400.

[126] O.A. Akoum, M.Y. Jaffrin, L. Ding, P. Paullier, C. Vanhoutte, An hydrodynamic investigation of microfiltration and ultrafiltration in a vibrating membrane module, Journal of Membrane Science, 197 (2002) 37-52.
[127] A. Brou, L. Ding, P. Boulnois, M.Y. Jaffrin, Dynamic microfiltration of yeast suspensions using rotating disks equipped with vanes, Journal of Membrane Science, 197 (2002) 269-282.
[128] A. Adach, S. Wroński, M. Buczkowski, W. Starosta, B. Sartowska, Mechanism of microfiltration on the rotating track membrane, Separation and Purification Technology, 26 (2002) 33-41.
[129] S. Beier, M. Guerra, A. Garde, G. Jonsson, Dynamic microfiltration with a vibrating hollow fiber membrane module: Filtration of yeast suspensions, Journal of Membrane Science, 281 (2006) 281-287.
[130] S.P. Beier, G. Jonsson, Critical flux determination by flux-stepping, AIChE Journal, 56 (2009) 1739-1747.
[131] H.G. Gomaa, S. Rao, A.M. Al-Taweel, Intensification of membrane microfiltration using oscillatory motion, Separation and Purification Technology, 78 (2011) 336-344.
[132] A. Kola, Y. Ye, A. Ho, P. Le-Clech, V. Chen, Application of low frequency transverse vibration on fouling limitation in submerged hollow fibre membranes, Journal of Membrane Science, 409-410 (2012) 54-65.
[133] H.G. Gomaa, R. Sabouni, Energetic consideration and flux characteristics of roughed-surface membrane in presence of reversing shear, Chemical Engineering Research and Design, 92 (2014) 1771-1780.
[134] A. G Giorges, J. Pierson, Flow Dynamic Effect in Cake Shape and Resistance in Membrane Filtration, 2011.
[135] A. Brou, M.Y. Jaffrin, L.H. Ding, J. Courtois, Microfiltration and ultrafiltration of polysaccharides produced by fermentation using a rotating disk dynamic filtration system, Biotechnol Bioeng, 82 (2003) 429-437.
[136] C. Harscoat, M.Y. Jaffrin, R. Bouzerar, J. Courtois, Influence of fermentation conditions and microfiltration processes on membrane fouling during recovery of glucuronane polysaccharides from fermentation broths, Biotechnol. Bioeng., 65 (1999) 500-511.
[137] M. Mellal, M.Y. Jaffrin, L.H. Ding, C. Delattre, P. Michaud, J. Courtois, Separation of oligoglucuronans of low degrees of polymerization by using a high shear rotating disk filtration module, Separation and Purification Technology, 60 (2008) 22-29.
[138] J.H. Vogel, K.-H. Kroner, Controlled shear filtration: A novel technique for animal cell separation, Biotechnol. Bioeng., 63 (1999) 663-674.
[139] J. Cole, J.D. Brantley, Dynamic membrane filtration in cell and protein production, Biopharm-Technol. Bus. Biopharm., 9 (1996) 66-&.
[140] L.R. Castilho, F.B. Anspach, CFD-aided design of a dynamic filter for mammalian cell separation, Biotechnol. Bioeng., 83 (2003) 514-524.
[141] D. Sarkar, D. Datta, D. Sen, C. Bhattacharjee, Simulation of continuous stirred rotating disk-membrane module: An approach based on surface renewal theory, Chemical Engineering Science, 66 (2011) 2554-2567.
[142] A. Sarkar, S. Moulik, D. Sarkar, A. Roy, C. Bhattacharjee, Performance characterization and CFD analysis of a novel shear enhanced membrane module in ultrafiltration of Bovine Serum Albumin (BSA), Desalination, 292 (2012) 53-63.
[143] M. Naskar, K. Rana, D. Chatterjee, T. Dhara, R. Sultana, D. Sarkar, Design, performance characterization and hydrodynamic modeling of intermeshed spinning basket membrane (ISBM) module, Chemical Engineering Science, 206 (2019) 446-462.
[144] J. Gursch, R. Hohl, G. Toschkoff, D. Dujmovic, J. Brozio, M. Krumme, N. Rasenack, J. Khinast, Continuous Processing of Active Pharmaceutical Ingredients Suspensions via Dynamic Cross-Flow Filtration, J. Pharm. Sci., 104 (2015) 3481-3489.

[145] Y.-F. Maa, C.C. Hsu, Investigation on fouling mechanisms for recombinant human growth hormone sterile filtration, J. Pharm. Sci., 87 (1998) 808-812.
[146] L. Fernandez-Cerezo, A. Rayat, A. Chatel, J.M. Pollard, G.J. Lye, M. Hoare, An ultra scale-down method to investigate monoclonal antibody processing during tangential flow filtration using ultrafiltration membranes, Biotechnol. Bioeng., 116 (2019) 581-590.
[147] U. Frenander, A.S. JÖNsson, Cell harvesting by cross-flow microfiltration using a shear-enhanced module, Biotechnol. Bioeng., 52 (1996) 397-403.
[148] Spin Tek- Model ST- ll- Rotary Membrane system, in, https://www.environmental-expert.com/products/spintek-model-st-ii-rotary-membrane-system-97370.
[149] M.M. Dal-Cin, C.N. Lick, A. Kumar, S. Lealess, Dispersed phase back transport during ultrafiltration of cutting oil emulsions with a spinning membrane disc geometry1Issued as NRCC No. 41962.1, Journal of Membrane Science, 141 (1998) 165-181.
[150] J. Bendick, B. Reed, P. Morrow, T. Carole, Using a high shear rotary membrane system to treat shipboard wastewaters: Experimental disc diameter, rotation and flux relationships, Journal of Membrane Science, 462 (2014) 178-184.
[151] J. Bendick, B. Reed, P. Morrow, T. Carole, Effect of Backpulsing and Continuous Surface Cleaning on High-Shear Rotary Membrane System Permeate Flux Performance for Naval Shipboard Wastewaters, Journal of Environmental Engineering, 140 (2014) 04014004.
[152] B.E. Reed, W. Lin, R. Viadero, J. Young, Treatment of Oily Wastes Using High-Shear Rotary Ultrafiltration, Journal of Environmental Engineering, 123 (1997) 1234-1242.
[153] R. Viadero, R. Jr, B. Reed, Study of series resistances in high-shear rotary ultrafiltration, Journal of Membrane Science, 162 (1999) 199-211.
[154] R.C.V. Jr, B.E. Reed, Rotation and Concentration Effects in High-Shear Ultrafiltration, Journal of Environmental Engineering, 125 (1999) 638-646.
[155] R.C. Viadero, D.A. Masciola, B.E. Reed, R.L. Vaughan, Two-phase limiting flux in high-shear rotary ultrafiltration of oil-in-water emulsions, Journal of Membrane Science, 175 (2000) 85-96.
[156] F. Liebermann, Dynamic cross flow filtration with Novoflow's single shaft disk filters, Desalination, 250 (2010) 1087-1090.
[157] Modular Spin Disk Filter MSDF, in, https://divaenvitec.com/divaenvitec/products/modular-spin-disk-filter-msdf.
[158] Rotating disk filter, in, https://www.igb.fraunhofer.de/en/research/water-technologies/wastewater-treatment/water-purification-and-bioreactor-concepts/cost-optimized-filtration.html.
[159] ROCKET CERAMIC FILTER, in, http://www.vinimat.fr/produit/3/2/83/filtre-ceramique-rocket.html.
[160] R. Alnaizy, A. Aidan, H. Luo, Performance assessment of a pilot-size vacuum rotation membrane bioreactor treating urban wastewater, Applied Water Science, 1 (2011) 103-110.
[161] HUBER Memmbrane Filtration VRM, in, https://www.huber.de/products/membrane-filtration-mbr/huber-membrane-filtration-vrmr.html.
[162] M.Y. Jaffrin, G. He, L.H. Ding, P. Paullier, Effect of membrane overlapping on performance of multishaft rotating ceramic disk membranes, Desalination, 200 (2006) 269-271.
[163] D. Sarkar, A. Sarkar, A. Roy, C. Bhattacharjee, Performance characterization and design evaluation of spinning basket membrane (SBM) module using computational fluid dynamics (CFD), Separation and Purification Technology, 94 (2012) 23-33.
[164] L. Liu, B. Gao, J. Liu, F. Yang, Rotating a helical membrane for turbulence enhancement and fouling reduction, Chemical Engineering Journal, 181-182 (2012) 486-493.
[165] G. Rock, P. Tittley, N. McCombie, Plasma collection using an automated membrane device, Transfusion, 26 (1986) 269-271.

[166] A. Salama, Investigation of the problem of filtration of oily-water systems using rotating membranes: A multicontinuum study, Colloids and Surfaces A: Physicochemical and Engineering Aspects, 541 (2018) 175-187.
[167] K.H. Kroner, V. Nissinen, Dynamic filtration of microbial suspensions using an axially rotating filter, Journal of Membrane Science, 36 (1988) 85-100.
[168] R. Bouzerar, M. Jaffrin, L.-H. Ding, P. Paullier, Influence of Geometry and Angular Velocity on Performance of a Rotating Disk Filter, AIChE Journal, 46 (2000) 257-265.
[169] L. Ding, W. Zhang, A. Ould-Dris, M.Y. Jaffrin, B. Tang, Concentration of Milk Proteins for Producing Cheese Using a Shear-Enhanced Ultrafiltration Technique, Industrial & Engineering Chemistry Research, 55 (2016) 11130-11138.
[170] J. Luo, L. Ding, Y. Wan, P. Paullier, M.Y. Jaffrin, Application of NF-RDM (nanofiltration rotating disk membrane) module under extreme hydraulic conditions for the treatment of dairy wastewater, Chemical Engineering Journal, 163 (2010) 307-316.
[171] J. Luo, W. Cao, L. Ding, Z. Zhu, Y. Wan, M.Y. Jaffrin, Treatment of dairy effluent by shear-enhanced membrane filtration: The role of foulants, Separation and Purification Technology, 96 (2012) 194-203.
[172] J. Luo, L. Ding, Y. Wan, P. Paullier, M.Y. Jaffrin, Fouling behavior of dairy wastewater treatment by nanofiltration under shear-enhanced extreme hydraulic conditions, Separation and Purification Technology, 88 (2012) 79-86.
[173] Z. Zhu, J. Luo, L. Ding, O. Bals, M.Y. Jaffrin, E. Vorobiev, Chicory juice clarification by membrane filtration using rotating disk module, Journal of Food Engineering, 115 (2013) 264-271.
[174] J. Luo, L. Ding, Influence of pH on treatment of dairy wastewater by nanofiltration using shear-enhanced filtration system, Desalination, 278 (2011) 150-156.
[175] Z. Zhu, S. Ladeg, L. Ding, O. Bals, M.-M. Nadji, M.Y. Jaffrin, E. Vorobiev, Study of rotating disk assisted dead-end filtration of chicory juice and its performance optimization, Industrial Crops and Products, 53 (2014) 154-162.
[176] J. Luo, L. Ding, Y. Wan, M.Y. Jaffrin, Threshold flux for shear-enhanced nanofiltration: Experimental observation in dairy wastewater treatment, Journal of Membrane Science, 409-410 (2012) 276-284.
[177] Z. Zhu, H. Mhemdi, W. Zhang, L. Ding, O. Bals, M.Y. Jaffrin, N. Grimi, E. Vorobiev, Rotating Disk-Assisted Cross-Flow Ultrafiltration of Sugar Beet Juice, Food and Bioprocess Technology, 9 (2015) 493-500.
[178] L.-H. Ding, O. Akoum, A. Abraham, M.Y. Jaffrin, High shear skim milk ultrafiltration using rotating disk filtration systems, AIChE Journal, 49 (2003) 2433-2441.
[179] J. Luo, Z. Zhu, L. Ding, O. Bals, Y. Wan, M.Y. Jaffrin, E. Vorobiev, Flux behavior in clarification of chicory juice by high-shear membrane filtration: Evidence for threshold flux, Journal of Membrane Science, 435 (2013) 120-129.
[180] L. Chen, Y. Qiu, Removal of Cd (II) from dilute aqueous solutions by complexation–ultrafiltration using rotating disk membrane and the shear stability of PAA–Cd complex, Chinese Journal of Chemical Engineering, 27 (2019) 519-527.
[181] S.Y. Tang, Y.R. Qiu, Removal of Zn (II) by complexation-ultrafiltration using rotating disk membrane and the shear stability of PAA-Zn complex, Korean J. Chem. Eng., 35 (2018) 2078-2085.
[182] F. Meyer, I. Gehmlich, R. Guthke, A. Górak, W.A. Knorre, Analysis and simulation of complex interactions during dynamic microfiltration of Escherichia coli suspensions, Biotechnol. Bioeng., 59 (1998) 189-202.
[183] T.R. Bentzen, N. Ratkovich, S. Madsen, J.C. Jensen, S.N. Bak, M.R. Rasmussen, Analytical and numerical modelling of Newtonian and non-Newtonian liquid in a rotational cross-flow MBR, Water Sci Technol, 66 (2012) 2318-2327.

[184] FMX: Anti-Fouling Membrane Filtration System, in, https://bkt21.com/fmx-technology-index.
[185] LIFE 18™- disk separator, in, https://www.miltenyibiotec.com/FR-en/products/therasorb-therapeutic-apheresis/disposables/disposables-for-life-18/life-18tm-disk-separator.html#330-000-038.
[186] P. Francis, D.M. Martinez, F. Taghipour, B.D. Bowen, C.A. Haynes, Optimizing the rotor design for controlled-shear affinity filtration using computational fluid dynamics, Biotechnol Bioeng, 95 (2006) 1207-1217.
[187] R. Bott, T. Langeloh, E. Ehrfeld, Dynamic cross flow filtration, Chemical Engineering Journal, 80 (2000) 245-249.
[188] J. Nuortila-Jokinen, A. Kuparinen, M. Nyström, Tailoring an economical membrane process for internal purification in the paper industry, Desalination, 119 (1998) 11-19.
[189] T. Huuhilo, P. Väisänen, J. Nuortila-Jokinen, M. Nyström, Influence of shear on flux in membrane filtration of integrated pulp and paper mill circulation water, Desalination, 141 (2001) 245-258.
[190] M. Mänttäri, J. Nuortila-Jokinen, M. Nyström, Evaluation of nanofiltration membranes for filtration of paper mill total effluent, Filtration & Separation, 34 (1997) 275-280.
[191] M. Mänttäri, K. Viitikko, M. Nyström, Nanofiltration of biologically treated effluents from the pulp and paper industry, Journal of Membrane Science, 272 (2006) 152-160.
[192] J. Nuortila-Jokinen, M. Nyström, Comparison of membrane separation processes in the internal purification of paper mill water, Journal of Membrane Science, 119 (1996) 99-115.
[193] L. Fillaudeau, B. Boissier, S. Ermolaev, N. Jitariouk, Etude hydrodynamique d'un module de filtration dynamique, Ind. Alim. Agri., 124 (2007) 8-16.
[194] X.M. Xie, C. Andre, N. Dietrich, P. Schmitz, L. Fillaudeau, Flow investigation in an innovating dynamic filtration module using tracing methods, Separation and Purification Technology, 227 (2019).
[195] X. Xie, C. Le Men, N. Dietrich, P. Schmitz, L. Fillaudeau, Local hydrodynamic investigation by PIV and CFD within a Dynamic filtration unit under laminar flow, Separation and Purification Technology, 198 (2018) 38-51.
[196] X. Xie, N. Dietrich, L. Fillaudeau, C. Le Men, P. Schmitz, A. Liné, Local hydrodynamics investigation within a dynamic filtration unit under laminar flow, Chemical Engineering Research and Design, 132 (2018) 954-965.
[197] N. Jitariouk, Apparatus, system and method for separating liquids, in, Google Patents, 2003.
[198] RVF-filtration, in, http://rvf-filtration.com/.
[199] H. Balavi, Y. Boluk, Dynamic filtration of drilling fluids and fluid loss under axially rotating crossflow filtration, Journal of Petroleum Science and Engineering, 163 (2018) 611-615.
[200] A. Zouboulis, E. Peleka, A. Ntolia, Treatment of Tannery Wastewater with Vibratory Shear-Enhanced Processing Membrane Filtration, Separations, 6 (2019) 20.
[201] Vibratory Shear Enhanced Processing VSEP, in, https://www.vsep.com/product/series-i/.
[202] J. Postlethwaite, S.R. Lamping, G.C. Leach, M.F. Hurwitz, G.J. Lye, Flux and transmission characteristics of a vibrating microfiltration system operated at high biomass loading, Journal of Membrane Science, 228 (2004) 89-101.
[203] Vibrating Membrane Filtration (VMF) Pallsep Systems, in, https://shop.pall.com/us/en/biotech/tangential-flow-filtration/automated-systems/zidgri78lfv?CategoryName=BP0703&CatalogID=Biopharmaceuticals&tracking=searchterm:PallSep+Biotech+PS400.
[204] H.G. Gomaa, S. Rao, Analysis of flux enhancement at oscillating flat surface membranes, Journal of Membrane Science, 374 (2011) 59-66.
[205] H. Gomaa, A.M. Al Taweel, Dynamic analysis of mass transfer at vertically oscillating surfaces, Chemical Engineering Journal, 102 (2004) 71-82.

[206] H.G. Gomaa, Flux characteristics at oscillating membrane equipped with turbulent promoters, Chemical Engineering Journal, 191 (2012) 541-547.
[207] H.G. Gomaa, S. Rao, M.A. Taweel, Flux enhancement using oscillatory motion and turbulence promoters, Journal of Membrane Science, 381 (2011) 64-73.
[208] F. Zhao, Y. Zhang, H. Chu, S. Jiang, Z. Yu, M. Wang, X. Zhou, J. Zhao, A uniform shearing vibration membrane system reducing membrane fouling in algae harvesting, Journal of Cleaner Production, 196 (2018) 1026-1033.
[209] M. Mertens, M. Quintelier, I.F.J. Vankelecom, Magnetically induced membrane vibration (MMV) system for wastewater treatment, Separation and Purification Technology, 211 (2019) 909-916.
[210] M.R. Bilad, G. Mezohegyi, P. Declerck, I.F. Vankelecom, Novel magnetically induced membrane vibration (MMV) for fouling control in membrane bioreactors, Water Res, 46 (2012) 63-72.
[211] Z. Zhao, M. Mertens, Y. Li, K. Muylaert, I.F.J. Vankelecom, A highly efficient and energy-saving magnetically induced membrane vibration system for harvesting microalgae, Bioresour Technol, 300 (2020) 122688.
[212] Y. Li, M.R. Bilad, I.F.J. Vankelecom, Application of a magnetically induced membrane vibration (MMV) system for lignocelluloses hydrolysate filtration, Journal of Membrane Science, 452 (2014) 165-170.
[213] M.R. Bilad, V. Discart, D. Vandamme, I. Foubert, K. Muylaert, I.F. Vankelecom, Harvesting microalgal biomass using a magnetically induced membrane vibration (MMV) system: filtration performance and energy consumption, Bioresour Technol, 138 (2013) 329-338.
[214] F. Zhao, H. Chu, Y. Zhang, S. Jiang, Z. Yu, X. Zhou, J. Zhao, Increasing the vibration frequency to mitigate reversible and irreversible membrane fouling using an axial vibration membrane in microalgae harvesting, Journal of Membrane Science, 529 (2017) 215-223.
[215] F. Zhao, H. Chu, X. Tan, L. Yang, Y. Su, X. Zhou, J. Zhao, Y. Zhang, Using axial vibration membrane process to mitigate membrane fouling and reject extracellular organic matter in microalgae harvesting, Journal of Membrane Science, 517 (2016) 30-38.
[216] F. Zhao, H. Chu, Y. Su, X. Tan, Y. Zhang, L. Yang, X. Zhou, Microalgae harvesting by an axial vibration membrane: The mechanism of mitigating membrane fouling, Journal of Membrane Science, 508 (2016) 127-135.
[217] R. Holdich, K. Schou, M. Dragosavac, S. Kellet, H. Bandulasena, A comparison of azimuthal and axial oscillation microfiltration using surface and matrix types of microfilters with a cake-slurry shear plane exhibiting non-Newtonian behaviour, Journal of Membrane Science, 550 (2018) 357-364.
[218] G. Genkin, T. Waite, A. Fane, S. Chang, The effect of vibration and coagulant addition on the filtration performance of submerged hollow fibre membranes, Journal of Membrane Science, 281 (2006) 726-734.
[219] S. Beier, G. Jonsson, Separation of enzymes and yeast cells with a vibrating hollow fiber membrane module, Separation and Purification Technology, 53 (2007) 111-118.
[220] S. Prip Beier, G. Jonsson, A vibrating membrane bioreactor (VMBR): Macromolecular transmission—influence of extracellular polymeric substances, Chemical Engineering Science, 64 (2009) 1436-1444.
[221] B. Wu, Y. Zhang, Z. Mao, W.S. Tan, Y.Z. Tan, J.W. Chew, T.H. Chong, A.G. Fane, Spacer vibration for fouling control of submerged flat sheet membranes, Separation and Purification Technology, 210 (2019) 719-728.
[222] M. Chai, Y. Ye, V. Chen, Separation and concentration of milk proteins with a submerged membrane vibrational system, Journal of Membrane Science, 524 (2017) 305-314.

[223] J.C. Kim, F. Garzotto, D.N. Cruz, A. Clementi, F. Nalesso, J.H. Kim, E. Kang, H.C. Kim, C. Ronco, Computational modeling of effects of mechanical shaking on hemodynamics in hollow fibers, Int. J. Artif. Organs, 35 (2012) 301-307.
[224] J. Kim, F. Garzotto, D. Cruz, C. Goh, F. Nalesso, J. Kim, E. Kang, H.C. Kim, C. Ronco, Enhancement of Solute Removal in a Hollow-Fiber Hemodialyzer by Mechanical Vibration, Blood purification, 31 (2011) 227-234.
[225] L. Qin, Z. Fan, L. Xu, G. Zhang, G. Wang, D. Wu, X. Long, Q. Meng, A submerged membrane bioreactor with pendulum type oscillation (PTO) for oily wastewater treatment: membrane permeability and fouling control, Bioresour Technol, 183 (2015) 33-41.
[226] O.T. Komesli, C.F. Gökçay, Investigation of sludge viscosity and its effects on the performance of a vacuum rotation membrane bioreactor, Environ. Technol., 35 (2014) 645-652.
[227] T.K. Sherwood, P.L.T. Brian, R.E. Fisher, Desalination by Reverse Osmosis, Industrial & Engineering Chemistry Fundamentals, 6 (1967) 2-12.
[228] C. Torras, J. Pallares, R. Garcia-Valls, M.Y. Jaffrin, Numerical simulation of the flow in a rotating disk filtration module, Desalination, 235 (2009) 122-138.
[229] M. Mellal, L. Hui Ding, M. Y. Jaffrin, C. Delattre, P. Michaud, J. Courtois, Separation and Fractionation of Oligouronides by Shear-Enhanced Filtration, Separation Science and Technology, 42 (2007) 349-361.
[230] S.-Y. Tang, D.-Y. Wu, Y.-R. Qiu, Computation fluid dynamic simulation and experimental validation of shear induce dissociation coupling ultrafiltration technology for the treatment of lead contained wastewater, Separation and Purification Technology, 241 (2020) 116750.
[231] M. Mänttäri, J. Nuortila-Jokinen, M. Nyström, Influence of filtration conditions on the performance of NF membranes in the filtration of paper mill total effluent, Journal of Membrane Science, 137 (1997) 187-199.
[232] W. Li, X. Su, A. Palazzolo, S. Ahmed, E. Thomas, Reverse osmosis membrane, seawater desalination with vibration assisted reduced inorganic fouling, Desalination, 417 (2017) 102-114.
[233] S. Chandrasekhar, S. Chandrasekhar, L. Lee, The stability of spiral flow between rotating cylinders, Proceedings of the Royal Society of London. Series A. Mathematical and Physical Sciences, 265 (1962) 188-197.
[234] D. Cébron, P. Maubert, M. Le Bars, Tidal instability in a rotating and differentially heated ellipsoidal shell, Geophysical Journal International, 182 (2010) 1311-1318.
[235] J. Murkes, C.G. Carlsson, Crossflow filtration: Theory and practice, (1988).
[236] S. Rosenblat, Flow between torsionally oscillating disks, Journal of Fluid Mechanics, 8 (2006) 388-399.
[237] M. Mori, I. Seyssiecq, N. Roche, Rheological measurements of sewage sludge for various solids concentrations and geometry, Process Biochemistry, 41 (2006) 1656-1662.
[238] M.C. Porter, Concentration Polarization with Membrane Ultrafiltration, Product R&D, 11 (1972) 234-248.
[239] E.M.V. Hoek, A.S. Kim, M. Elimelech, Influence of Crossflow Membrane Filter Geometry and Shear Rate on Colloidal Fouling in Reverse Osmosis and Nanofiltration Separations, Environmental Engineering Science, 19 (2002) 357-372.
[240] W.F. Blatt, A. Dravid, A.S. Michaels, L. Nelsen, Solute Polarization and Cake Formation in Membrane Ultrafiltration: Causes, Consequences, and Control Techniques, in: J.E. Flinn (Ed.) Membrane Science and Technology: Industrial, Biological, and Waste Treatment Processes, Springer US, Boston, MA, 1970, pp. 47-97.
[241] C.K. Colton, Permeability and transport studies in batch and flow dialyzers with applications to hemodialysis, PhD theses, Dept. Chem. Eng. M.I.T., (1969).
[242] Y. Manon, L. Fillaudeau, D. Anne-Archard, J.-L. Uribelarrea, C. Molina-Jouve, On-line rheology of cell cultures in a bioreactor, in: 8.World Congress of Chemical Engineering (WCCE8), Montreal, Canada, 2009, pp. np.

[243] L.O. Wilson, N.L. Schryer, Flow between a stationary and a rotating disk with suction, Journal of Fluid Mechanics, 85 (2006) 479-496.
[244] R. Bouzerar, Filtration dynamique dans un module plan à disque rotatif : Application à des suspensions minérales, in, 1999, pp. 181 p.
[245] K. Atsumi, T. Makino, K. Kato, T. Murase, E. Iritani, P. Chidphong, M. Shirato, Frictional resistance of grooved rotor in cylindrical dynamic filter chamber without permeation or throughflow, Kag. Kog. Ronbunshu, 14 (1988) 14-19.
[246] R. Adrian, Bibliography of Particle Image Velocimetry Using Imaging Methods: 1917–1995, DLR Deutsches Zentrum fur Luft- und Raumfahrt e.V. - Forschungsberichte, (2011).
[247] T. Yoshizawa, Handbook of optical metrology: Principles and Applications, CRC Press, 2017.
[248] C.P. Gendrich, M.M. Koochesfahani, D.G. Nocera, Molecular tagging velocimetry and other novel applications of a new phosphorescent supramolecule, Experiments in Fluids, 23 (1997) 361-372.
[249] R.W. Johnson, Handbook of fluid dynamics, Crc Press, 2016.
[250] A. Cenedese, G. Doglia, G.P. Romano, G. De Michele, G. Tanzini, LDA and PIV velocity measurements in free jets, Experimental Thermal and Fluid Science, 9 (1994) 125-134.
[251] L.E. Drain, The laser Doppler technique, John Wiley, 1980.
[252] J. Kilander, A. Rasmuson, Energy dissipation and macro instabilities in a stirred square tank investigated using an LE PIV approach and LDA measurements, Chemical Engineering Science, 60 (2005) 6844-6856.
[253] L. Böhm, S. Jankhah, J. Tihon, P. Berube, M. Kraume, Application of the Electrodiffusion Method to Measure Wall Shear Stress: Integrating Theory and Practice, Chem. Eng. Technol., 37 (2014) 1-14.
[254] J.E. Mitchell, T.J. Hanratty, A study of turbulence at a wall using an electrochemical wall shear-stress meter, Journal of Fluid Mechanics, 26 (1966) 199.
[255] S. Toyama, Y. Tanaka, S. Shirogane, T. Nakamura, T. Umino, R. Uehara, T. Okamoto, H. Igarashi, Development of Wearable Sheet-Type Shear Force Sensor and Measurement System that is Insusceptible to Temperature and Pressure, Sensors (Basel), 17 (2017) 1752.
[256] J. Günther, D. Hobbs, C. Albasi, C. Lafforgue, A. Cockx, P. Schmitz, Modeling the effect of packing density on filtration performances in hollow fiber microfiltration module: A spatial study of cake growth, Journal of Membrane Science, 389 (2012) 126-136.
[257] L. Oxarango, P. Schmitz, M. Quintard, Laminar flow in channels with wall suction or injection: a new model to study multi-channel filtration systems, Chemical Engineering Science, 59 (2004) 1039-1051.
[258] M. Linkès, P. Fede, J. Morchain, P. Schmitz, Numerical investigation of subgrid mixing effects on the calculation of biological reaction rates, Chemical Engineering Science, 116 (2014) 473-485.
[259] Z. Kovács, Continuous Diafiltration: Cocurrent and Countercurrent Modes, Springer Berlin Heidelberg, 2016.
[260] X. Xie, Investigation of local and global hydrodynamics of a dynamic filtration module (RVF technology) for intensification of industrial bioprocess, in, 2017.
[261] O. Akoum, D. Richfield, M. Jaffrin, L. Ding, P. Swart, Recovery of trypsin inhibitor by soy milk ultrafiltration using a rotating disk system, Desalination, 191 (2006) 438-445.